Rare-earth doped polymer waveguides and light emitting diodes

CIP-DATA KONINKLIJKE BIBLIOTHEEK, DEN HAAG

Slooff, Lenneke Hendrika

Rare-earth doped polymer waveguides and light emitting diodes
Lenneke Hendrika Slooff
Thesis Utrecht University- With ref.-With summary in Dutch
ISBN: 90-393-2537-5
Subject headings: rare-earth/polymer/optical waveguide/amplifier/LED

Rare-earth doped polymer waveguides and light emitting diodes

Zeldzaam-aard gedoteerde polymeer lichtgeleiders en licht emitterende diodes

(met een samenvatting in het Nederlands)

Proefschrift

ter verkrijging van de graad van doctor aan de Universiteit Utrecht op gezag van de Rector Magnificus, Prof. Dr. H. O. Voorma, ingevolge het besluit van het College voor Promoties in het openbaar te verdedigen op vrijdag 17 november 2000 des ochtends te 10.30 uur

door

Lenneke Hendrika Slooff

Geboren op 18 augustus 1972 te Uithoorn

Promotor: Prof. Dr. A. Polman
Faculteit der Natuur- en Sterrenkunde, Universiteit Utrecht
FOM-Instituut voor Atoom- en Molecuulfysica, Amsterdam

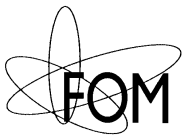

The work described in this thesis was performed at the FOM-Institute for Atomic and Molecular Physics, Kruislaan 407, 1098 SJ Amsterdam, The Netherlands. It is part of the research program of the Foundation for Fundamental Research on Matter (FOM), and was made possible by financial support from the Dutch Organization for the Advancement of Research (NWO), and the ESPRIT basic research program SCOOP of the European Union.

Elk weten komt uit ervaring voort
-Kant-

Contents

1 Introduction

The era of optical telecommunication started in the late 1980's with the introduction of high-quality optical fibers. From that moment on, optical fibers have increasingly replaced the traditional coax cable for long distance telecommunication, and transmission speeds of over 1 Tbit/s can now be achieved over one single optical fiber. This enormous success can be attributed to two major developments. The first one is the reduction of transmission losses in optical fibers to about 0.2 dB/km (at a wavelength of 1550 nm). The second is the development of the erbium-doped fiber amplifier, which can amplify the optical signal without electronic conversion, thus enabling high bit rates. These fiber amplifiers are typically 50 m long, which is no problem in long-range applications. However, for complex high-density circuitry, such as will be used in future fiber-to-the-home applications, they are impractical. This asks for the development of integrated planar optical amplifiers.

1.1 Integrated optics

In optical telecommunication systems, light is used to transport information between different users. To manipulate the optical signals on a local scale, devices like splitters, couplers, multiplexers, and amplifiers are needed. Such devices can be readily made and integrated on one planar substrate, a technology called integrated optics. The basic element in a photonic integrated circuit is the planar optical waveguide (see Fig. 1.1). It consists of a high refractive index guiding layer with a ridge geometry, sandwiched between two lower-index cladding layers. The telecommunication signal travels through the guiding layer and is confined in the transverse directions as a result of total internal reflection at the interface between core and cladding.

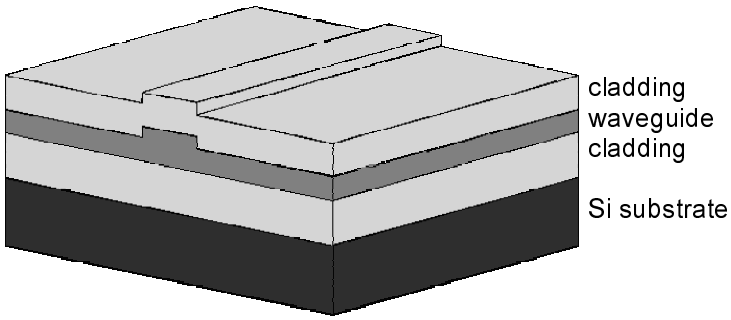

Figure 1.1 Channel waveguide structure for integrated optics applications. A high refractive index guiding layer is embedded between low-index cladding layers. The multilayer structure can e.g. be made on top of a silicon substrate.

Optical losses in the waveguide (absorption, scattering), coupling losses, or intrinsic intensity loss in optical splitters, call for the integration of optical amplifiers in photonic integrated circuits. These can be made by doping the guiding layer with an active element that (if pumped properly) gives rise to the optical gain. This thesis will discuss the optical properties of polymer optical amplifiers doped with rare-earth ions as the active element.

1.2 Rare-earth ions as the active element

Trivalent rare-earth ions are well known for their special optical properties, which result from the fact that the electrons of the partially filled 4*f*-shell are shielded from the surrounding completely filled 5*s* and 5*p* shells. The energy levels of the 4*f*-shell have equal parity, and hence electric dipole transitions are forbidden. In a solid, the slight mixing with odd-parity wavefunctions makes the transition slightly allowed. The absorption and emission cross sections are therefore small, and the luminescence lifetimes can be quite long (ms). The influence of the electric field around the ion removes the degeneracy of the 4*f*-levels, resulting in a Stark-splitting of the energy levels. However, due to the shielding by the outer lying shells, the magnitude of the splitting is small, resulting in relatively narrow emission lines, of which the wavelength is almost independent of the host material.

The energy levels of the 4*f*-shell arise from spin-spin and spin-orbit interactions[1] and are often denoted using Russel-Saunders notation $^{2S+1}L_J$, in which S is the total spin-impulse momentum, L the total orbital angular momentum, and J the total angular momentum. There exist 14 rare-earth elements, that all have a different number of electrons in the incompletely filled 4*f*-shell. As a result, each rare-earth ion has its own specific energy levels, and hence typical luminescence lines. The rare-earth ions erbium (Er) and

neodymium (Nd) have transitions at 1.53 μm and 1.34 μm respectively, which are two standard wavelengths used in optical telecommunication.

In order to achieve optical gain using these rare-earth ions, the ion is first excited from the ground state into a higher lying state. From there it can decay to the luminescent state from which it can return to a lower lying state by emission of a photon. If the pump rate is high enough, population inversion between the two levels involved in the emission builds up. A telecommunication signal can then induce stimulated emission in the rare-earth ion resulting in amplification of the signal.

1.3 The host material

As already mentioned, the choice of host material in rare-earth doped optical waveguide amplifiers does not influence the position of the energy levels of the rare-earth ions. Therefore, in principle any material that has little absorption at the pump and emission wavelengths can be used. Many different rare-earth doped inorganic materials have been studied, like e.g. pure SiO_2, silicate and phosphate glasses, $LiNbO_3$, and Al_2O_3,[2] and in some cases optical gain has been achieved. Only recently, the use of polymers in optical waveguide amplifiers is being considered.

The growing interest in polymers for use in integrated optics stems from the potential of mass production of low-cost devices on planar substrates, combined with the wide range of optical properties available for specific applications. Polymers developed for use in optical telecommunication applications include acrylates, polyimides, and olefins.[3] The refractive index of these polymers can be tuned with an accuracy of less than 0.0001 by blending and co-polymerization.

Low optical absorption is one of the major requirements for the host material. In polymers, optical absorption is caused by both molecular or polymeric electronic excited states, and by fundamental and overtone vibrations of molecular bonds. The most important absorptions in the optical telecommunication window are due to vibrational states of O-H and C-H bonds. Since the energy of the vibration is inversely related to the reduced mass, substitution of the hydrogen atoms by deuterium, fluorine, or chlorine reduces the energy of the fundamental vibration, shifting the absorption out of the telecommunication window. For example, a fluorinated polymer waveguide can have losses below 0.2 dB/cm at 1.5 μm,[3] which is well acceptable for integrated optics devices with cm length scales.

Polymer waveguide structures can be made by several techniques. Photosensitive polymers can be used that are made by adding photosensitive polymerisation initiators to the monomer mixtures. The patterning of the device is then done by illumination with ultraviolet light through a mask, or by direct

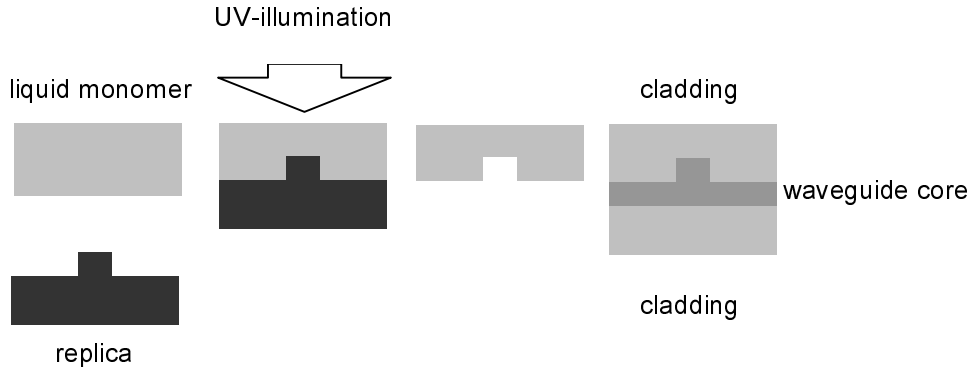

Figure 1.2 Schematic presentation of the soft embossing process for the fabrication of polymer waveguides.

laser writing. In both cases, the light induces a polymerisation reaction in the exposed region. The unreacted material can be removed using a conventional wet etch process. Polymer waveguides can also be defined using standard reactive ion etching techniques, that are known to yield well-defined structures with small side-wall roughness. More recently, the soft embossing technique has been developed (see Fig. 1.2). It employs an ultraviolet-transparent replica of the waveguide structure, which is impressed into the liquid monomer which is then illuminated with ultraviolet light. After the polymerisation reaction, the replica is removed. Waveguides are then formed by spin-coating the guiding layer onto this imprinted cladding layer thus defining a ridge structure, whereupon a second cladding layer is deposited.

1.4 This thesis

Rare-earth ions are insoluble in a polymer film. This makes the fabrication of rare-earth doped polymer waveguides much more complicated than that of inorganic waveguides. In the latter case the rare-earth ions can be incorporated rather easily using e.g. ion implantation, melting or deposition. In this thesis we have taken up the challenge to solve the doping problem in polymers using a variety of techniques. Chapter 2 introduces an Er-doped organic polydentate cage complex, which encapsulates the rare-earth ion and makes it dissolvable into a polymer matrix. The optical properties of these complexes in solution are studied, and it is found that the emission bandwidth is very large. However, vibrational coupling to O-H and C-H bonds in the solvent partly quenches the optical transition. In Chapter 3 the optical properties of a lissamine-functionalised organic Nd complex doped into a polycarbonate waveguide are

studied. Upon optical excitation, the highly absorbing lissamine becomes excited, whereupon Dexter energy transfer to the Nd^{3+} ion occurs. The effective absorption cross section of this process is four orders of magnitude higher than that for direct optical excitation of the Nd. The lissamine sensitiser is not stable under illumination. This is studied in more detail in Chapter 4, in which a model is proposed to describe the observed time-dependence of the lissamine and Nd luminescence intensities. The highly absorbing sensitiser makes the standard butt-end coupling of the pump light into a waveguide amplifier impractical. For this reason a new waveguide configuration is introduced in Chapter 5, which gradually couples pump light from one waveguide into a parallel-placed signal guide. In this way the pump power can be used more efficiently. The coupled mode theory for this design is described.

To solve the quenching problem of the rare-earth transition, a nano-composite material is developed, that takes advantage of the good optical properties of silica as a host for the rare-earth ion, and the polymer as a waveguide material. In this composite, Er-doped silica colloids are embedded in a polymer waveguide. First, the optical properties of Er-doped silica films, made by an acid-catalysed chemical reaction are studied in Chapter 6, in order to study if the optical properties of Er ions in a material made using wet chemistry are similar to that in e.g. a glass fiber. A high luminescence quantum efficiency can be achieved if the proper annealing procedure is chosen. Next, SiO_2 colloids are fabricated using base-catalysed wet chemical synthesis, and implanted with Er ions. Chapter 7 reports the properties of these Er-doped silica spheres. Very long luminescence lifetimes are found, which is partly attributed to the low local optical density of states in these colloids as described in Chapter 8. In Chapter 9 it is shown that rare-earth doped polymers can also be excited electrically. Near-infrared electroluminescence is observed for a lissamine-sensitised Nd complex doped polymer light emitting diode. It is found that the sensitiser plays a crucial role in the energy transfer process. Finally, Chapter 10 discusses the various technological requirements that must be met to fabricate an optically or electrically pumped rare-earth doped polymer-based planar optical amplifier.

To summarise, we solve in this thesis the problem of doping rare-earth ions into polymers by developing an organic complex encapsulating the rare-earth ion. The quenching by C-H bonds in the complex leads to the development of sensitised complexes and a silica colloid/polymer nano-composite material. A new pumping mechanism designed to pump the strongly absorbing sensitiser is more efficiently. And finally it will be shown that Nd can be electrically excited by doping the sensitised organic complexes into a semiconducting polymer.

References

[1] S. Hüffner, Optical Spectra of Transparent Rare-Earth Compounds (Academic, New York, 1978)
[2] for a review see: P. G. Kik, and A. Polman, MRS Bulletin **23**, 48 (1998)
[3] for a review see: L. Eldada, and L. W. Shacklette, IEEE J. Selected topics in Quantum Electr. **6**, 54 (2000)

2 Optical properties of erbium-doped organic polydentate cage complexes

Optical properties of different erbium-doped polydentate hemispherand organic cage complexes are studied, for use in polymer-based planar optical amplifiers. Room temperature 1.54 μm photoluminescence is observed, due to an intra-4f transition in the erbium (Er) ion. The Er^{3+} ion is directly excited (at 488 nm) into one of the 4f manifolds, or indirectly (at 287 nm) via the aromatic part of the cage. The luminescence spectrum is 70 nm wide (full width at half maximum), the highest known for any Er^{3+}-doped material. The absorption cross section at 1.54 μm is 1.1×10^{-20} cm^2, higher than in most other Er^{3+}-doped materials. Measurements were performed on complexes in KBr tablets, in which the complex is in the form of small crystallites, or dissolved in dimethylformamide and butanol-OD. In KBr the luminescence lifetime < 0.5 μs, possibly due to concentration quenching effects. In butanol-OD solution, the lifetime is 0.8 μs, still well below the radiative lifetime of 4 ms estimated from the measured absorption cross sections. It is shown that quenching by C-H bonds is not the major quenching mechanism of the Er^{3+} luminescence, and that temperature quenching is very small. Therefore, an alternative quenching mechanism must take place, presumably due to the presence of O-H groups on the Er^{3+} complex. Finally a calculation is made of the gain performance of a planar polymer waveguide amplifier based on these Er^{3+} complexes, resulting in a threshold pump power of 1.4 mW and a typical gain of 1.7 dB/cm.

2.1 Er-doped organic complexes

Erbium (Er) doped materials have attracted a lot of attention, because of their potential applications in optoelectronics.[1-3] In its trivalent state the Er^{3+} ion shows an intra 4*f*-shell transition from its first excited state ($^4I_{13/2}$) to the ground state ($^4I_{15/2}$), which occurs at a wavelength of 1.54 μm. In the free Er^{3+} ion optical intra 4*f*-shell transitions are parity forbidden. Incorporated in a solid host however, the crystal field of the host induces mixing of states, which makes some of the transitions allowed. These optical transitions are rather sharp, due to the fact that the partially filled 4*f*-shell is shielded by filled 5*s* and 5*p* shells. The luminescence lifetime of the first excited state can be as long as several milliseconds.[4-6] These features make Er-doped materials very attractive for lasers and optical amplifiers operating at 1.54 μm, one of the standard telecommunication wavelengths.

Er-doped planar optical amplifiers have already been demonstrated using silica,[7-12] Al_2O_3[13] and $LiNbO_3$[14,15] hosts. However, as polymer waveguides are becoming more important, both as fibers and in thin film configurations, it is interesting to study the doping of planar polymer waveguides with Er, and to investigate if optical amplification can be achieved. Such polymer amplifiers could then be integrated in existing optical polymer devices such as splitters, switches and multiplexers[16] with low coupling losses.

The inorganic Er-salts cannot be dispersed directly into an organic matrix. To avoid this problem, the Er^{3+} ion must first be encapsulated by an organic ligand. The resulting complex can then be dispersed in a polymer film. The ligand has to be designed such that it provides enough co-ordination sites to bind the Er^{3+} ion and to form a stable complex. Furthermore it may serve to shield the Er^{3+} ion from impurities in the surrounding matrix that may quench the luminescence. For example, O-H is known to quench the luminescence due to coupling of the excited state of the ion to vibrational modes of the O-H bond.[17-19]

In this Chapter we study the optical properties of different Er-doped polydentate hemisperands, which form an overall neutral complex in which the Er^{3+} ion is encapsulated in a cage-like ligand configuration. Clear, room temperature photoluminescence at 1.54 μm is observed for these complexes with a luminescence lifetime up to 0.8 μs. Selective deuteration experiments are carried out to study the possible quenching effect of C-H bonds. Exchanging C-H for C-D has shown to be beneficial for Eu^{3+}.[20]

Two different types of excitation are studied: direct excitation in one of the Er^{3+} manifolds using a 488 nm Ar laser, and excitation via the organic ligand using a 337 nm N_2 laser, followed by energy transfer to the Er^{3+} ion (see Fig. 2.1). The temperature quenching of the luminescence and the optical

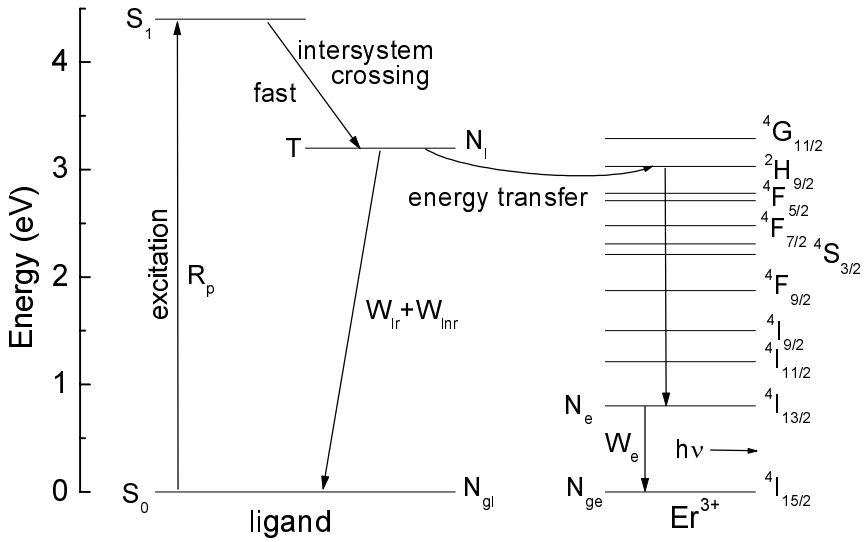

Figure 2.1 Schematic diagram of the ligand-Er^{3+} system. The complex is first excited from the singlet S_0 ground state to the singlet S_1 state (exact position not known, but higher than 3.2 eV), followed by fast relaxation to the triplet T state. From there, energy transfer to the Er^{3+} 4*f* levels may take place. From these levels, rapid relaxation to the $^4I_{13/2}$ takes place. Finally the Er^{3+} may decay to the $^4I_{15/2}$ ground manifold by emission of a 1.54 μm photon. The various symbols are discussed in the text.

absorption cross sections are discussed, and finally a performance estimate for a planar optical amplifier based on these Er-doped complexes is made.

2.2 Experiment

Three different Er^{3+} complexes were prepared in a multi-step synthesis, as discussed in detail in Ref. 20, and characterised by fast atom bombardment mass spectrometry (FAB-MS), infrared spectroscopy (FT-IR), and elemental analysis. Figure 2.2(a) shows a schematic picture of a cyclic Er^{3+} complex in which the first co-ordination sphere consists of either C-H bonds (cyc-H), or C-D bonds (cyc-D). An acyclic Er^{3+} complex (acyc-H), sketched in Fig. 2.2(b), was also studied: it is open at the top and contains 2 $O(CH_2)_3CH_3$ groups. This is different than the cyclic complex which is closed at the top, with one $C_{18}H_{37}$ chain attached to the trivalent nitrogen atom. A three-dimensional representation of the cyclic complex is shown in Fig. 2.2(c).

After synthesis, the Er^{3+} complex solutions were dried, mixed with KBr and then pressed to 1 mm thick tablets with a diameter of 1.2 cm. The Er concentration is 1.0 wt.%. This concentration does not take into account the (unknown) amount of water which may remain in the tablets as a result of the

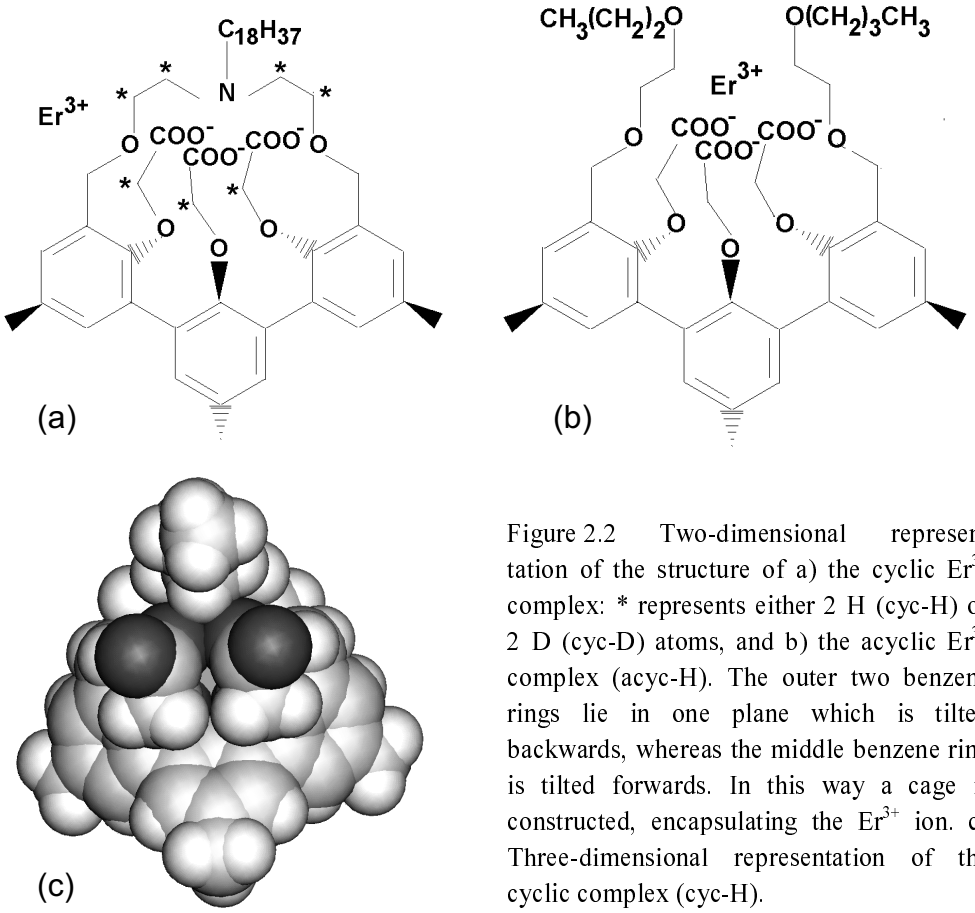

Figure 2.2 Two-dimensional representation of the structure of a) the cyclic Er^{3+} complex: * represents either 2 H (cyc-H) or 2 D (cyc-D) atoms, and b) the acyclic Er^{3+} complex (acyc-H). The outer two benzene rings lie in one plane which is tilted backwards, whereas the middle benzene ring is tilted forwards. In this way a cage is constructed, encapsulating the Er^{3+} ion. c) Three-dimensional representation of the cyclic complex (cyc-H).

preparation process. To exclude the effect of quenching due to O-H in the host, some measurements were performed on solutions in deuterated butanol (> 98 %) at a complex concentration of 10^{-4} M or dimethylformamide (DMF) at a concentration of 2×10^{-3} M. In both solvents acyc-H dissolved rather well, but the solutions with the cyclic complexes appeared somewhat turbid, indicating that not all the material had dissolved.

Photoluminescence (PL) measurements were performed using the 488 nm line of an Ar ion pump laser at a power of 100 mW for excitation. The laser beam was modulated with a mechanical chopper or an acousto-optic modulator at frequencies of 20 and 40 Hz. For the temperature dependent measurements, the samples were mounted in a closed-cycle helium cryostat, enabling measurements at temperatures ranging from 15 K to room temperature. The KBr tablets were first mounted onto a piece of crystalline silicon. The PL signal was focused into a monochromator and detected with a liquid-nitrogen cooled Ge detector, using standard lock-in techniques. The spectral resolution was 6 nm. Luminescence lifetime measurements were performed by monitoring the luminescence decay after excitation with a 0.5 ns pulsed N_2 laser (λ_{exc} = 337 nm, pulse energy 20 μJ,

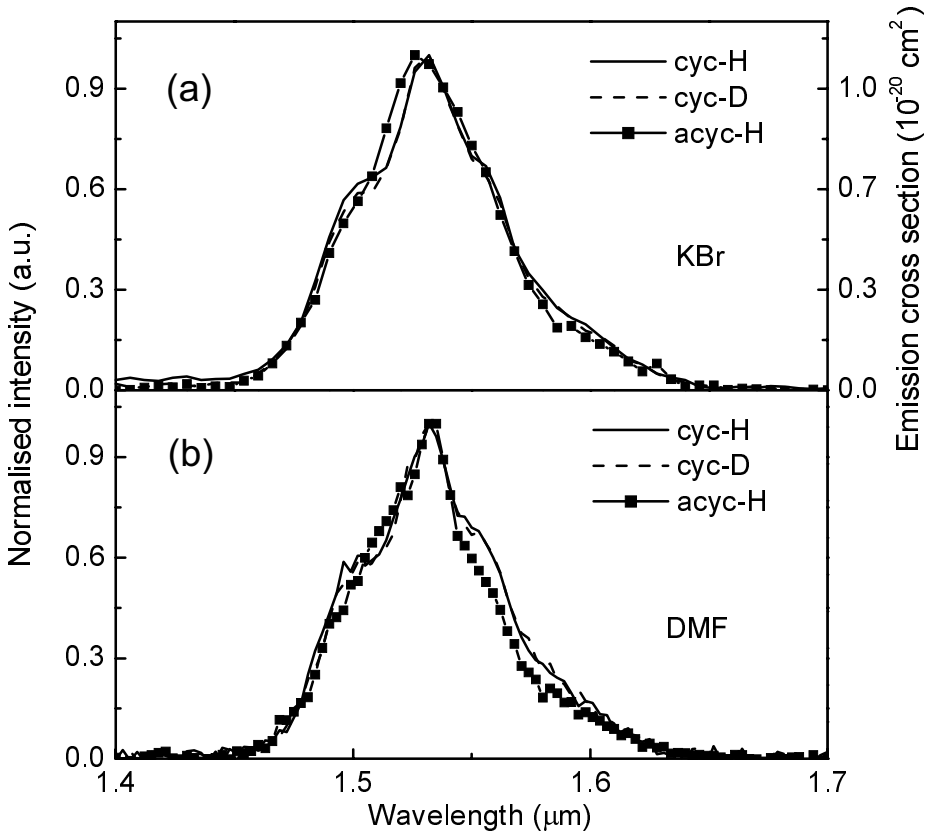

Figure 2.3 Normalised room temperature PL spectra of Er^{3+} complexes in (a) KBr tablets and (b) DMF, at a pump wavelength of 488 nm (power 100 mW).

10 Hz repetition rate). Decay signals were recorded using a cooled Ge detector with a time resolution of 0.3 μs. The signals were averaged using a digitising oscilloscope. All decay curves were analysed by deconvolution of the measured detector response.

Reflection and transmission measurements were performed using a spectrometer measuring the reflected and transmitted intensities with an integrating sphere. The spectral resolution was 0.3 nm.

2.3 Optical characterisation

Figure 2.3(a) shows normalised room-temperature PL spectra for the three complexes in KBr after excitation at 488 nm into the $^4F_{7/2}$ level (see Fig. 2.1). The peak around 1.54 μm is typical for Er^{3+} luminescence and is due to the transitions from the first excited state ($^4I_{13/2}$) to the ground state ($^4I_{15/2}$) manifolds. The full width at half-maximum (FWHM) of all spectra is 70 nm. To our knowledge this is much wider than for any other Er-doped material: Er-

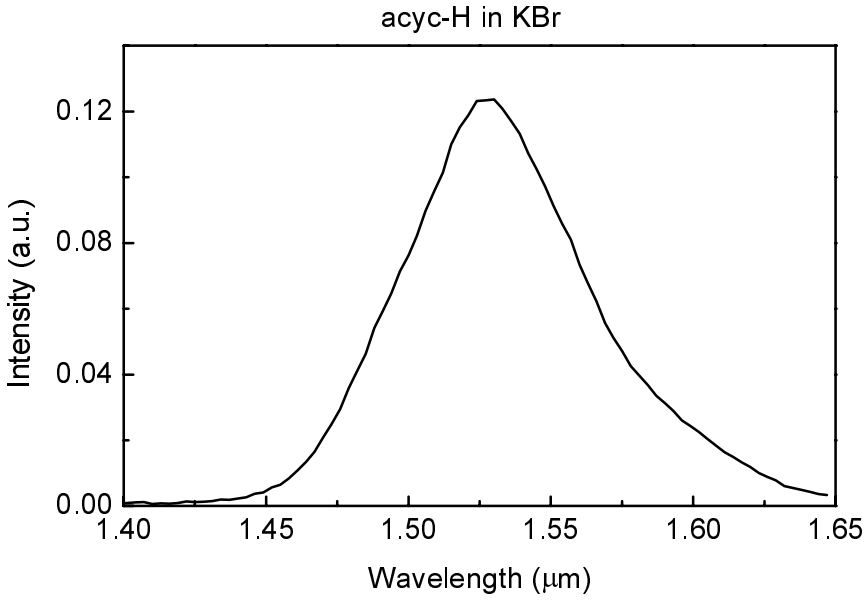

Figure 2.4 Room temperature spectrum of acyc-H in KBr after excitation via the ligand at 337 nm (pulse energy 20 μJ).

implanted SiO_2 (11 nm FWHM),[22] phosphosilicate glass (25 nm FWHM),[21] sodalime silicate glass (19 nm FWHM),[5] Al_2O_3 (55 nm FWHM),[6] and fluorohafnate glass (FWHM 64 nm).[4] Such a broad spectrum enables a wide gain bandwidth for optical amplification.

No comparison of the absolute PL intensities could be made for the three complexes, as the intensity varies over the KBr tablets (a factor 2-3). The spectral shapes measured for the two cyclic complexes are identical, and slightly different from that for the acyclic complex. This difference is attributed to a small difference in local environment for the two types of complexes. Figure 2.3(b) shows the normalised room-temperature PL spectra for the Er^{3+} complexes in DMF. Again, the shape of the spectra observed for cyc-H and cyc-D are similar, but slightly different than that of acyc-H.

Figure 2.4 shows the room-temperature PL spectrum of acyc-H in KBr after excitation at 337 nm (pulse energy 20 μJ). The 337 nm pump light is absorbed in the tail of the absorption band of the aromatic rings of the ligand. Energy transfer to the Er^{3+} ion then leads to excitation of the Er^{3+} resulting in the observed 1.54 μm luminescence.

Extinction spectra of the complexes in KBr are shown in Fig. 2.5. The absorption lines of the Er^{3+} ion are clearly visible and indicated in the figure (the level notation is given in Fig. 2.1). The steadily increasing background in the wavelength range down to 450 nm is attributed to scattering in the KBr tablets.

Using measured reflection data (not shown) and taking into account the known average areal density of Er in the samples (acyc-H: 8.54×10^{18} cm^{-2},

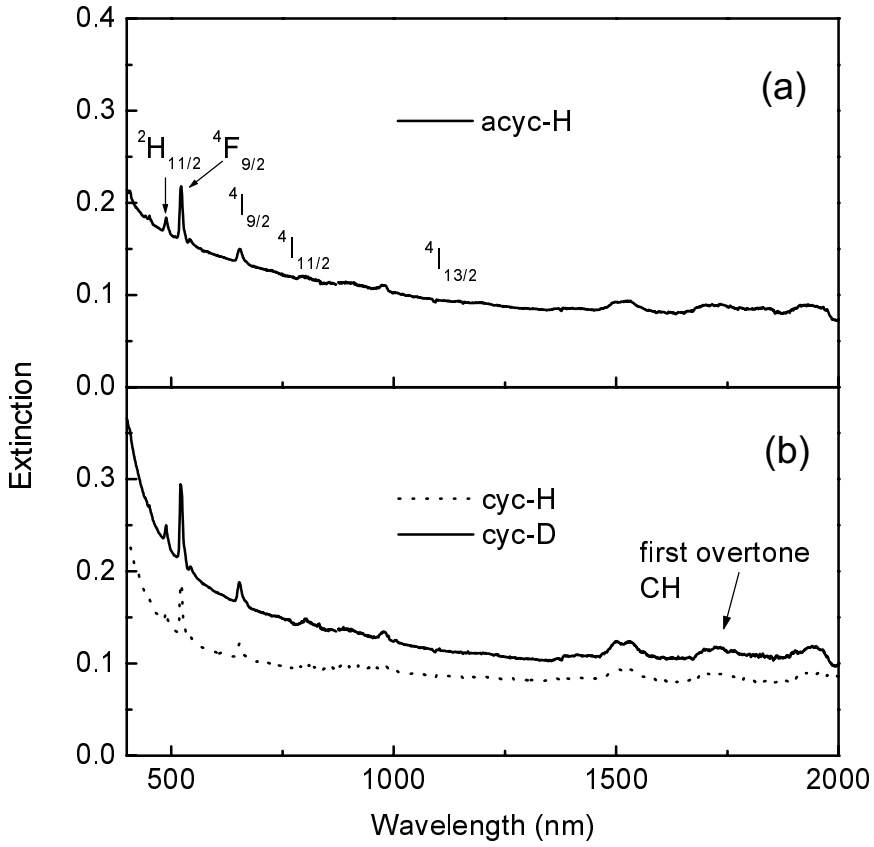

Figure 2.5 Extinction spectra of the three Er^{3+} complexes in KBr, based on transmission measurements. (a) acyc-H, (b) cyc-H and cyc-D. The absorption peaks are indicated by the level notation of the absorption band.

cyc-H: 8.21×10^{18} cm^{-2}, cyc-D: 9.04×10^{18} cm^{-2}), the 1.5 μm absorption cross sections for the $^4I_{15/2} \rightarrow {}^4F_{7/2}$ transition can be derived: $(0.62\pm0.05)\times10^{-20}$ cm^2 for acyc-H, $(1.1\pm0.4)\times10^{-20}$ cm^2 for cyc-H and $(0.93\pm0.05)\times10^{-20}$ cm^2 for cyc-D. These absorption cross sections are 1-5 times higher than the 1.5 μm cross section of Er-doped glasses,[4,22] and for Er-implanted Al_2O_3.[23] This may be related to differences in average electron distribution around the Er^{3+} ion for organic complexes compared to inorganic hosts. In practice the peak absorption and emission cross sections for Er^{3+} are nearly the same. Under this assumption and using the cross section derived above, the PL spectra of Fig. 2.3 can be converted to emission cross section spectra (see the right-hand vertical scale of Fig. 2.3(a)). From this spectrum the radiative lifetime τ can be calculated:

$$\frac{1}{\tau} = \frac{8\pi n^2}{c^2} \int \nu^2 \sigma_e(\nu) d\nu, \qquad (2.1)$$

with n the refractive index, c the speed of light and ν the optical frequency.

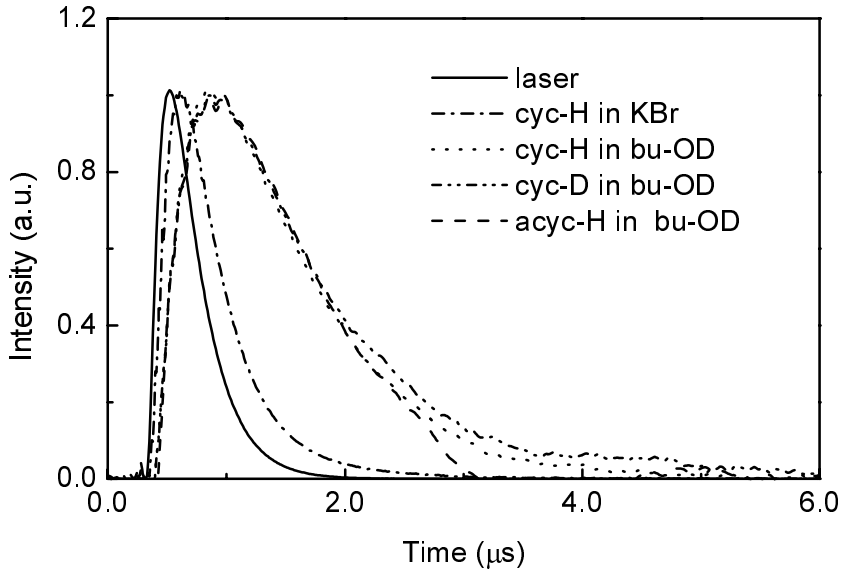

Figure 2.6 Room temperature decay measurements for the Er-doped organic complexes in KBr and butanol-OD, excited at 337 nm at a pulse energy of 20 μJ.

Table 2.1 Summary of the total Er areal density and the corresponding PL intensities for the Er^{3+} complexes in KBr and DMF.

	Er areal density (cm^{-2})	**relative PL intensity**
acyc-H (KBr)	8.5×10^{18}	142-193
acyc-H (DMF)	1.3×10^{18}	113
cyc-H (KBr)	8.2×10^{18}	210-410
cyc-H (DMF)	1.2×10^{18}	66
cyc-D (KBr)	9.0×10^{18}	178-242
cyc-D (DMF)	1.2×10^{18}	66

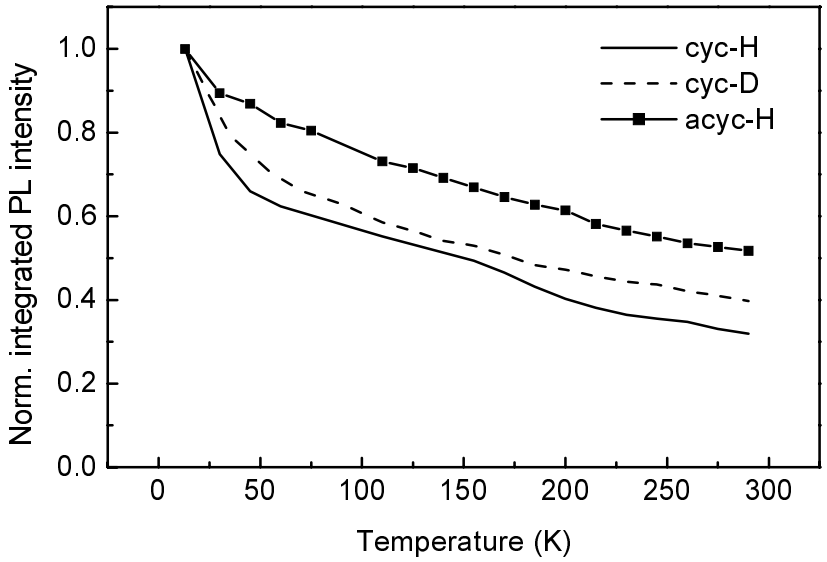

Figure 2.7 Temperature dependence of the integrated 1.54 μm PL intensity of the Er^{3+} complexes in KBr (pump power 100 mW, excitation wavelength 488 nm).

Evaluating Eq. 2.1 yields a radiative lifetime of about 4 ms for these Er^{3+} complexes.

Luminescence decay measurements for cyc-H in KBr and the three Er^{3+} complexes in butanol-OD are shown in Fig. 2.6. Deconvolution of the decay curve of cyc-H in KBr results in a luminescence lifetime of 0.5 μs. In butanol-OD the lifetimes for the three complexes are all around 0.8 μs. These lifetimes are much shorter than the radiative lifetime of 4 ms calculated from Eq. 2.1. This indicates that significant quenching of the Er^{3+} luminescence takes place.

Table 2.1 summarises the total Er areal density and the PL intensity for the KBr tablets and DMF solutions. For all complexes the areal density is typically a factor 7 higher in KBr than in the DMF solutions, but the luminescence intensity is only a factor 1.5 - 6 higher. This suggests that more luminescence quenching takes place in the KBr tablets than in the DMF solutions. A possible explanation for this difference is a concentration quenching effect: due to the mixed crystallite nature of the tablets, local concentrations of Er^{3+} may be higher than the calculated average density. Due to the local high concentration, energy transfer from one Er^{3+} ion to another can occur and the excitation can migrate among these clustered regions, followed by quenching at a defect site in the tablet. As a result the PL intensity will be lower and the luminescence lifetime shorter in the KBr tablets. In a solution where all the complexes are quite homogeneously dispersed, no concentration quenching will occur. This is confirmed by the longer luminescence lifetime for the complexes in butanol-OD solutions compared to the KBr tablets (see Fig. 2.6). However,

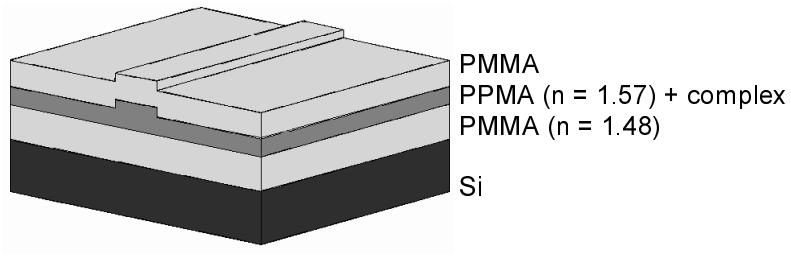

Figure 2.8 Polymer channel waveguide structure for optical gain calculations. A high refractive index polymer (n=1.57, PPMA), doped with organic Er^{3+} complexes, is embedded in a low index polymer (n=1.48, PMMA) on top of a silicon substrate.

even in solution the lifetimes are still much shorter than the expected 4 ms calculated from Eq. 2.1. There are three possible quenching mechanisms: 1) temperature quenching, 2) quenching by the nearest C-H neighbours, 3) quenching by O-H groups.

1) Temperature quenching: Figure 2.7 shows measurements of the integrated 1.54 μm PL intensity between 15 - 300 K for the KBr tablets. Cyc-H and cyc-D show the same trend as a function of temperature, with a quenching by a factor 3 between 15 K and room temperature. For acyc-H the temperature quenching is slightly smaller, a factor 2 in the same temperature range. The quenching is small and can be mainly attributed to a decrease in the absorption coefficient as the temperature is increased (resulting in less efficient excitation). This indicates that temperature quenching is not the major quenching mechanism.

2) Quenching by nearest C-H neighbours: the second order vibrational energy of C-H (E_0 = 2960 cm^{-1}) is resonant with the Er^{3+} first excited state (E = 6500 cm^{-1}). This band around 1.7 μm can also be seen in Fig. 2.5. Thus, a C-H bond positioned near the Er^{3+} ion can quench the Er^{3+} luminescence. Such coupling should be less for C-D (E_0= 2100-2200 cm^{-1}). Comparison of the PL intensity of cyc-H with that of cyc-D for the DMF solutions (see Table 2.1), shows that selective deuteration of the first co-ordination sphere has no influence on the PL intensity and thus it is concluded that quenching by these C-H bonds is not dominant.

3) Quenching by O-H groups: O-H groups are present in the liquids (mainly alcohols) used in the preparation of the Er^{3+} complexes, and they can also be present in the solvents used in the measurements: both DMF and butanol are highly hygroscopic. It is therefore very likely that O-H groups are coordinated to the Er^{3+} ion. Indeed, molecular dynamics simulations of rare-earth complexes in solution show that one O-H molecule can penetrate the first coordination shell of the ion.[20] In particular water may preferentially solvate the

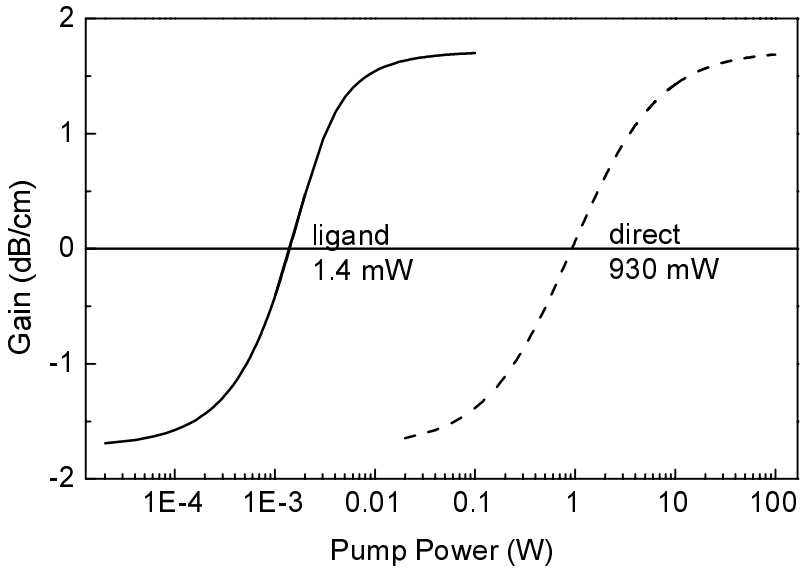

Figure 2.9 Calculated differential optical gain as a function of pump power for direct excitation (dashed line) and for excitation via the ligand (solid line) for a waveguide amplifier with a 2×1 μm^2 cross section. The threshold power is indicated for each calculation.

Er^{3+} ion.[24] It is the most potent quencher of rare-earth luminescence, and has a significantly stronger interaction to the rare-earth than, for instance, alcohols. An O-H group positioned near the Er^{3+} ion will result in efficient quenching of the luminescence, because its first vibrational overtone (E_0 = 3400 cm^{-1}) is strongly resonant with the $^4I_{13/2} \rightarrow {}^4I_{15/2}$ Er^{3+} transition (E = 6500 cm^{-1}). Work by Ermolaev *et al.*[25] shows that the rate constant for deactivation of the Er^{3+} excited state via O-H groups, located at a distance of 2.2-2.5 Å is in the order of (3-5)×10^8 s^{-1}, which is much larger than deactivation via C-D bonds at 2.2-2.5 Å (k = 5×10^6 s^{-1}). This would explain that, with O-H attached to the complex, substitution of C-H by C-D will have no significant effect on the PL intensities measured in solution (see Table 2.1).

2.4 Optical gain calculation

With the coefficients determined in the previous paragraphs, an estimate of the threshold pump power for a planar optical amplifier based on Er-doped organic complexes can be made. In such a polymer channel waveguide, a high refractive index polymer (e.g. poly(phenyl methacrylate) (PPMA), n = 1.57) doped with organic Er complexes, is embedded in a low index polymer (e.g. poly (methylmethacrylate) (PMMA), n =1.48) (see Fig. 2.8). A typical waveguide core dimension is 2×1 μm^2.

A calculation is done for direct excitation of Er^{3+} into the $^4F_{7/2}$ excited state (see Fig. 2.1). Assuming that the population of the $^4F_{7/2}$ state decays rapidly to the first excited state, the rate equations reduce to those for a quasi two-level system.[26] Solving these rate equations for steady-state conditions, the populations become:

$$N_g = \frac{W_e}{W_e + R} N, \tag{2.2}$$

$$N_e = \frac{R}{W_e + R} N \tag{2.3}$$

where $R=\sigma_a P\lambda/(hca)$ is the Er^{3+} excitation rate, N_e the population of the first excited state, N_g the population of the ground state, N the Er^{3+} concentration, $W_e = 1/\tau_e$ the erbium decay rate, P the pump power in the waveguide, σ_a the absorption cross section, λ = 488 nm the excitation wavelength and a the waveguide core cross section. As a first estimate we have taken the (unknown) absorption cross section at 488 nm equal to the measured value at 1.53 μm from Section 2.3. The differential optical gain (dB/cm) is given by $10\times^{10}\mathrm{Log}(I/I_0)$, where I_0 is the intensity at the beginning of the waveguide and $I=I_0e^{kx}$ along the waveguide, with k the gain factor given by:

$$k = \sigma_e \left(N_e - N_{ge}\right)\alpha \tag{2.4}$$

and α the estimated fraction of light which is confined in the core of the waveguide, and σ_e the emission cross section from Section 2.3. The optical gain as a function of pump power is calculated using the values given in Table 2.2. The result is shown in Fig. 2.9. The maximum gain is 1.7 dB/cm, indicating that for instance a loss free (1×2) splitter could be made with a few cm long waveguide. The threshold pump power is 930 mW. This is much higher than the minimum power needed in Er-doped glass or Al_2O_3 amplifiers[9] and is due to the much smaller luminescence quantum efficiency of the Er^{3+} ion in the organic complexes as compared to that in the inorganic materials.

The power of 930 mW needed for optical amplification is too high for any practical application. However, this problem can be solved by excitation of the complex via the aromatic part of the ligand, at 287 nm. At this wavelength the absorption cross section of the ligand is about 8.5×10^{-18} cm^2, much higher than the cross section for direct absorption of the Er^{3+} ion at 488 nm. This makes excitation via the ligand very efficient. Energy transfer from the ligand excited state to the Er^{3+} ion then results in population of the Er^{3+} $^4I_{13/2}$ luminescent excited state. Taking this process into account, a new gain calculation can be made. Assuming that the transition from the singlet (S_1) to the triplet (T) state of

Table 2.2 Typical values for the parameters used in the optical gain calculation of an Er-doped planar polymer optical amplifier for direct optical pumping of the amplifier.

Parameter	Symbol	value
Erbium decay rate	W_e	1.25×10^{6} s^{-1}
Erbium absorption cross section λ=488 nm	σ_a	1.1×10^{-20} cm^2
Erbium emission cross section λ=1.54 μm	σ_e	1.1×10^{-20} cm^2
Waveguide cross section	a	2×1 μm^2
Total erbium concentration	N	9×10^{19} cm^{-3}
Estimated fraction of light confined in the core	α	0.4
Ligand absorption cross section	σ_l	8.5×10^{-18} cm^2
Ligand radiative decay rate	W_{lr}	2×10^{8} s^{-1}
Ligand non-radiative decay rate	W_{lnr}	1×10^{9} s^{-1}

the ligand is fast (see Fig. 2.1), a quasi two-level system can be used for the ligand and the Er^{3+} ion. The rate equations then become:

$$\frac{dN_l}{dt} = R_l N_{gl} - W_{lr} N_l - W_{lnr} N_l N_{ge} \tag{2.5}$$

$$\frac{dN_e}{dt} = -W_e N_e + W_{lnr} N_l N_{ge} \tag{2.6}$$

in which $R_l = \sigma_l P\lambda/(hca)$ is the ligand excitation rate, N_e and N_l the population fraction of the first excited state of Er^{3+} ion and the ligand respectively, N_g and N_{gl} the population fraction in the ground state of Er^{3+} ion and the ligand respectively, W_{lr} the ligand radiative decay rate, W_{lnr} the ligand non-radiative decay rate (transfer rate), and σ_l the ligand absorption cross section.

Solving these equations for steady-state conditions, the gain can be calculated using Eq. 2.4 and typical values given in Table 2.2. The result is also plotted in Fig. 2.9. The threshold pump power reduces from 930 mW to 1.4 mW. These low pump powers are very interesting for practical applications. Note that in the final design pump loss has to be taken into account as will be discussed in Chapter 5. The next challenge is to engineer the ligand and to shift the excitation wavelength to the visible in order to be able to use standard semiconductor lasers as pump lasers. Alternatively, sensitisers with a high absorption coefficient and a high intersystem crossing efficiency, may be attached to the complex, to further optimise the pump efficiency. This work is described in Chapter 3. Finally we

note that the above calculations do not take into account upconversion effects, which may increase the pump power needed for amplification.[27] More measurements are required to determine the cooperative upconversion and excited state absorption cross sections for these Er-doped organic complexes.

2.5 Conclusions

Erbium-doped polydentate hemispherand organic cage complexes show a broad (70 nm FWHM) photoluminescence spectrum at room temperature centered around 1.54 μm. The Er^{3+} ion can be excited directly in the 4*f* manifold, or indirectly via the aromatic rings of the complex. The absorption cross section at λ=1.54 μm is 1.1×10^{20} cm^{-2}. When dissolved in butanol-OD the luminescence lifetime is 0.8 μs, much shorter than the estimated radiative lifetime of 4 ms. This is attributed to the presence of O-H groups in molecules located in the first co-ordination shell of the complex which serve as quenching sites for the excited Er^{3+} ion. The O-H most likely originates from the water, present during the chemical synthesis or in the solution in which the complexes are dissolved. Optical gain calculations show that these Er^{3+}-doped organic complexes, when dissolved in a polymer channel waveguide, may show net optical amplification for a pump power as low as 1.4 mW and a typical gain of 1.7 dB/cm.

References

1 E. Desurvire, Sci. Am. **266**, 96 (1992)

2 A. M. Glass, Phys. Today **46**, 34 (1993)

3 E. Desurvire, Phys. Today **47**, 20 (1994)

4 W. J. Miniscalco, J. Lightwave Techn. **9**, 234 (1991)

5 E. Snoeks, G. N. van den Hoven, and A. Polman, J. Appl. Phys. **73**, 8179 (1993)

6 G. N. van den Hoven, E. Snoeks, A. Polman, J. M. W. van Uffelen, Y. S. Oei, and M. K. Smit, Appl. Phys. Lett. **62**, 3065 (1993)

7 T. Feuchter, E. K. Mwarania, J. Wang, L. Reekie, and J. S. Williams, IEEE Phot. Techn. Lett. **4**, 542 (1991)

8 T. Kitagawa, K Kitagawa. Hattori, K. Shuto, M. Yasu, M. Kobayashi, and M. Horiguchi, Electron. Lett. **28**, 1818 (1992)

9 G. Nykolak, M. Haner, P. C. Becker, J. Schmulovich, and Y. H. Wong, IEEE Photon. Techn. Lett. **5** (1993)

10 K. Hattori, T. Kitagawa, M. Oguma, Y. Ohmori, and M. Horiguchi, Electron. Lett. **30**, 856 (1994)

11 D. Barbier, P. Gastaldo, B. Hyde, J. M. Jouanno, and A. Kevorkian, in Proc. 7th European Conference on Integrated Optics, page 241 (Delft University of Technology, Delft, 1995)

12 M. Hempstead, J. E. Román, C. C. Ye, J. S. Wilkinson, P. Camy, P. Laborde, and C. Lerminiaux, in Proc. 7th European Conference on Integrated Optics, page 233 (Delft University of Technology, Delft, 1995)

[13] G. N. van den Hoven, R. J. I. M. Koper, A. Polman, C. van Dam, J. W. M. van Uffelen, and M. K. Smit, Appl. Phys. Lett. **68**, 1886 (1996)
[14] P. Becker, R. Brinkmann, M. Dinand, W. Sohler, and H. Suche, Appl. Phys. Lett. **61**, 1257 (1992)
[15] R. Brinkmann, I. Baumann, M. Dinand, W. Sohler, and H. Suche, IEEE J. Quantum Electron. **30**, 2356 (1994)
[16] B. Booth, in Polymers for Lightwave and Integrated Optics, edited by L. A. Hornak (Dekker, New York 1992)
[17] V. P. Gapontsev, A. A. Izyneev, Yu. E. Sverchov, and M. R. Syrtlanov, Sov. J. Quantum Electron. **11**, 1101 (1981)
[18] A. J. Bruce, W. A. Reed, A. E. Neeves, L. R. Copeland, W. H. Grodkiewicz, and A. Lidgard, Mat. Res. Soc. Symp. Proc. **244**, 157 (1992)
[19] Yingchao Yan, A. J. Faber, and H. de Waal, J. Non-Chryst. Solids **181**, 283 (1995)
[20] M. P. Oude Wolbers, F. C. J. M. van Veggel, B. H. M. Snellink-Ruël, J. W. Hofstraat, F. A. J. Geurts, and D. N. Reinhoudt, J. Am. Chem. Soc. **119**, 138 (1997)
[21] A. Polman, D. C. Jacobson, D. J. Eaglesham, R. C. Kistler, and J. M. Poate, J. Appl. Phys. **70**, 3778 (1991)
[22] J. N. Sandoe, P. H. Sarkies, and S. Parke, J. Phys. D: Appl. Phys. **5**, 1788 (1972)
[23] G. N. van den Hoven, E. Snoeks, J. A. van der Elsken, C. van Dam, J. M. W. van Uffelen, and M. K. Smit, Appl. Opt. **36**, 3338 (1996)
[24] M. P. Oude Wolbers, Lanthanide Ion Complexes and Their Luminescence Properties, Ph.D. Thesis, University of Twente (1997)
[25] V. L. Ermolaev, E. B. Sveshnikova, Russ. Chem. Rev. **63**, 905 (1994)
[26] C. K. Jørgensen, in Lasers and Excited States of Rare Earths (Springer-Verlag, New York 1977)
[27] G. N. van den Hoven, E. Snoeks, A. Polman, C. van Dam, J. M. W. van Uffelen, and M. K. Smit, J. Appl. Phys. **79**, 1258 (1996)

3 Optical properties of lissamine functionalised Nd^{3+} complexes in polymer waveguides and solution

Lissamine functionalised terphenyl-based neodymium complexes are synthesised, and incorporated in deuterated dimethylsulfoxide solutions and in partially fluorinated planar polymer waveguides. Optical excitation of the lissamine sensitiser around 500 nm, followed by intramolecular energy transfer to the Nd^{3+} ion, results in near-infrared photoluminescence (890 nm, 1060 nm, 1340 nm) due to intra-4f transitions in the Nd^{3+} ion. The intramolecular energy transfer rate is larger than 10^{7} s^{-1}. Due to the large absorption cross section of the sensitiser (>10^{-17} cm^{2} around 500 nm), the Nd^{3+} is excited 10^{4} times more efficiently than in a pure complex without sensitiser. The Nd^{3+} luminescence lifetime is relatively short, both in solution (2.2 μs) and in a polymer host (0.8 μs), which is attributed to coupling to vibrational states of nearby C-H and O-H groups. Spin-coated fluorinated polymer planar waveguides, doped with these sensitised organic Nd^{3+} complexes show excellent waveguide properties. Upon continued illumination, photo-degradation is observed in the doped polymer films.

3.1 Sensitised Nd^{3+} complexes

Trivalent rare-earth ions are well known for their special optical properties.[1] The 4*f*-shell of these ions is not completely filled and shielded from the surroundings by filled 5*s* and 5*p* shells. This shielding minimises the effect of the crystal field of the host material on the energy levels of the 4*f*-shell and as a result the absorption and emission bands remain rather sharp. The small influence of the crystal field induces mixing of wave functions with opposite parity within the 4*f*-shell, making the parity forbidden transitions slightly allowed. Due to the forbidden nature, the lifetimes of these transitions are relatively long.

The neodymium (Nd) ion is often used, as it has an intra-4*f* transition from the $^4F_{3/2}$ to the $^4I_{11/2}$ level at 1.34 μm, which coincides with the low dispersion window of standard optical fibers. Neodymium doped lasers and amplifiers have been achieved in inorganic hosts like silica,[2] YAG,[3] YLF,[4] and $LiNbO_3$.[5,6] Recently, research has also focussed on rare-earth doped polymer-based materials.[7,8] These polymer waveguide amplifiers could then be integrated with existing polymer devices such as splitters, switches, and multiplexers.[9]

Rare-earth ions cannot be dissolved directly into a polymer film. Therefore, the ions have to be encapsulated by an organic ligand to form a complex, which can be dissolved in the polymer matrix. In Chapter 2, we have shown that optically active Er-doped polydentate cage complexes can be synthesised, and show room temperature photoluminescence at 1.535 μm when optically excited either directly into an Er intra-4*f* level, or indirectly via the cage which also acts as a chromophore.[10] We found that the luminescence lifetime of these complexes is rather short (0.8 μs), which was attributed to energy transfer of the excited state of the Er^{3+} ion to O-H vibrational states of the solvent molecules.[11,12]

Obviously these non-radiative quenching processes are a disadvantage of the use of organic cage complexes. On the other hand, an advantage is that highly absorbing antenna chromophores can be incorporated in the organic complex. Once this chromophore is excited it can transfer its excitation energy to the rare-earth ion by a Dexter mechanism. If the energy transfer from chromophore to rare-earth ion is efficient, this process strongly enhances the excitation efficiency of the rare-earth ion.

In this Chapter we will report the optical properties of terphenyl-based Nd^{3+} complexes with and without a highly absorbing lissamine antenna chromophore. Complexes were dissolved either in hexadeuterodimethylsulfoxide (DMSO-d6) solutions or in partially fluorinated polycarbonate planar waveguides. In complexes without lissamine, excitation of the Nd^{3+} ion at a wavelength of 515 nm leads to population of the $^4G_{7/2}$ level, from where it decays to the $^4F_{3/2}$ level (see Fig. 3.1). Decay from this level leads to the

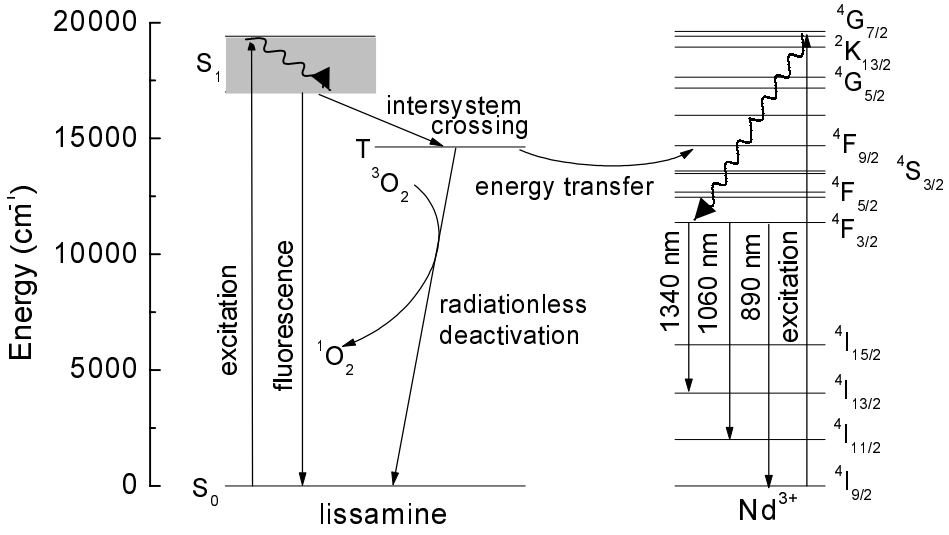

Figure 3.1 Schematic energy level diagram of the lissamine Nd^{3+} complex. The arrows indicate the excitation mechanisms of the Nd^{3+} ion: either directly into the $^4G_{7/2}$ level by pumping at 515 nm, or through the lissamine sensitiser ($S_0 \rightarrow S_1$ transition followed by intersystem crossing and energy transfer).

characteristic Nd^{3+} luminescence at 890, 1060 and 1340 nm due to transitions to the $^4I_{9/2}$, $^4I_{11/2}$ and $^4I_{13/2}$ levels, respectively. In complexes with the lissamine sensitiser, the 515 nm light is mainly absorbed by the high absorbing lissamine, which becomes excited into the singlet state (S_1). This is followed by intersystem crossing to the triplet state (T, E_T = 14600 cm^{-1}) (see Fig. 3.1). From the triplet state energy transfer to the Nd^{3+} ion can occur, which results in excitation of the Nd^{3+} ion into the $^4S_{3/2}$ and $^4F_{9/2}$ levels. After relaxation to the $^4F_{3/2}$ level the 890, 1060 and 1340 nm luminescence can be observed. The luminescence intensities, lifetimes, excitation mechanisms, waveguide properties, and photo-stability of these complexes will be discussed.

3.2 Experiment

Terphenyl-based Nd^{3+} complexes were synthesised using the procedure described in Ref. 13. Some complexes were functionalised with lissamine, a Rhodamine-B derivative.[14] Figure 3.2 shows a schematic picture of the structure of the terphenyl-based Nd^{3+} complexes (a) with two benzoyl side-groups (Bz.Nd) and (b) with one benzoyl side-group and a lissamine sensitiser (Ls.Nd). Both complexes have a cage-like configuration, encapsulating the Nd^{3+} ion. The complexes were dissolved in DMSO-d6 to a concentration of 10^{-2} M for Bz.Nd and 10^{-6} M for Ls.Nd, or dissolved in partially fluorinated polycarbonate[15]

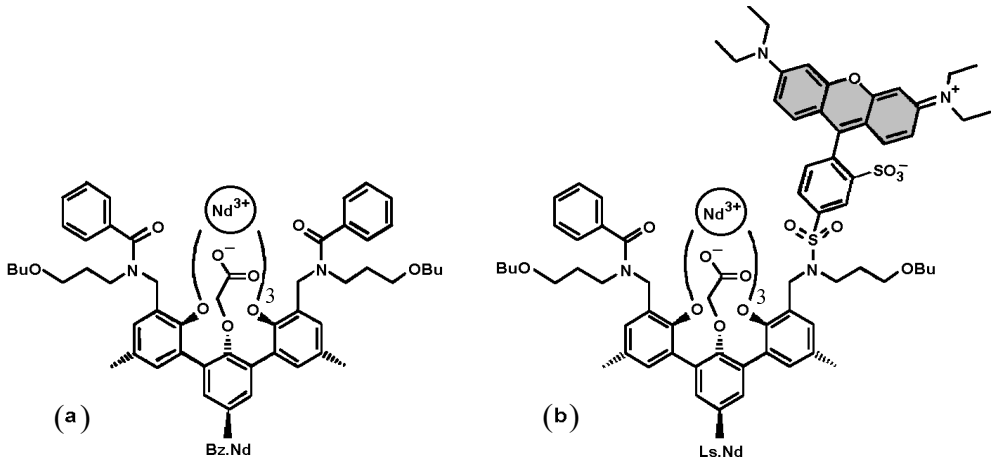

Figure 3.2 Schematic picture of (a) benzoyl-Nd^{3+} complex (Bz.Nd) and (b) lissamine functionalised Nd^{3+} complex (Ls.Nd).

waveguides at a concentration of 1 wt.% and 3 wt.% (complex). The polycarbonate waveguides were made by spin-coating a cyclohexylacetate solution of polycarbonate and complex onto a Si substrate covered with a 3 μm thick thermally grown SiO_2 layer. The spin-coating was performed for 30 seconds at a spin-rate of 3000 rpm and followed by thermal annealing at 190 ^oC (in vacuum) for one hour. The thickness of the polymer layer was 3.55 μm.

The real and imaginary parts of the refractive index of the polymer waveguide were measured using a variable angle spectroscopic ellipsometer. The optical losses were measured using the sliding prism method.[16] Diiodomethane was used as an index matching liquid for optimum output coupling. A white light source as well as lasers operating at 633, 838, 1305 and 1565 nm were used.

Photoluminescence (PL) measurements were performed using various lines of an Ar ion laser as an excitation source. The complexes in DMSO-d6 solution were analysed in square quartz cells. The power on the cell was 60 mW, at a spot diameter of 1 mm. The beam was modulated using an acousto-optic modulator, operating at different frequencies. The emitted luminescence was focused into a monochromator and detected with a photomultiplier tube or a liquid-nitrogen cooled Ge detector. All spectra were corrected for the detector response. Absorption measurements were performed using a spectrophotometer. Measurements on waveguide films were performed by pumping the waveguide (total length about 25 mm) with a rectangular spot (5×15 mm) from the top near the entrance facet of the waveguide. The luminescence was collected at the output facet, using a multi-mode optical fiber. The fiber was led to an objective in front of the monochromator. The spectral resolution ranged from 0.2-6 nm. Photoluminescence decay curves were measured using a photomultiplier tube and a photon counting system. The time resolution of the system was about 100 ns.

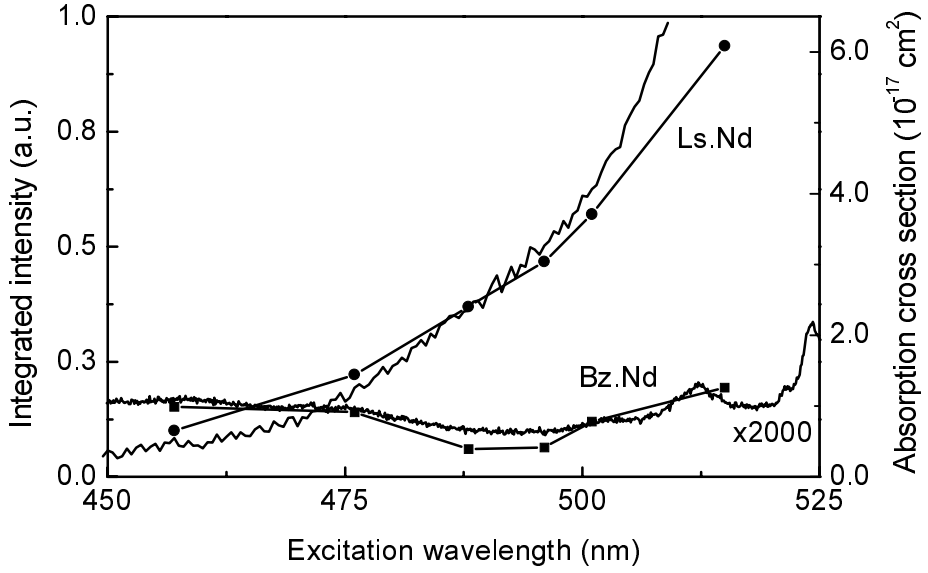

Figure 3.3 Photoluminescence at 1060 nm as a function of excitation wavelength for Bz.Nd (10^{-2} M, squares) and Ls.Nd (10^{-6} M, circles) in DMSO-d6 solutions. The absorption spectra of Bz.Nd and Ls.Nd are also shown (drawn lines). Note that the absorption data for the Bz.Nd solution are multiplied by a factor 2000.

3.3 Luminescence properties

Figure 3.3 shows the PL intensities at 1060 nm for a 10^{-2} M solution of Bz.Nd and a 10^{-6} M solution of Ls.Nd (lissamine sensitised), both in DMSO-d6, at different excitation wavelengths as available from the Ar ion laser. The pump power for excitation was 60 mW for all excitation wavelengths. The absorption spectrum measured for the same solutions is also included in the figure (drawn lines). The excitation spectrum for the complex without sensitiser (Bz.Nd) shows some structure, which is roughly similar to that found in the absorption measurement, and is consistent with the absorption bands of the Nd^{3+} ion around 475 nm and 513 nm. The excitation spectrum for the complex with sensitiser (Ls.Nd) shows a completely different behavior: the 1060 nm emission intensity increases strongly with excitation wavelength, again very similar to what is found for the absorption spectrum. Given the fact that the lissamine complex shows a broad absorption band around 580 nm, this clearly indicates that the excitation of Nd^{3+} around 500 nm takes place via the sensitiser. The absorption of the lissamine occurs at the xanthene unit (i.e. the gray part in the structure for Ls.Nd in Fig. 3.2(b)). Note that the measured absorption cross section is in the 10^{-17} cm^2 range, 4 orders of magnitude higher than the typical Nd^{3+} intra-4*f* transition cross section.

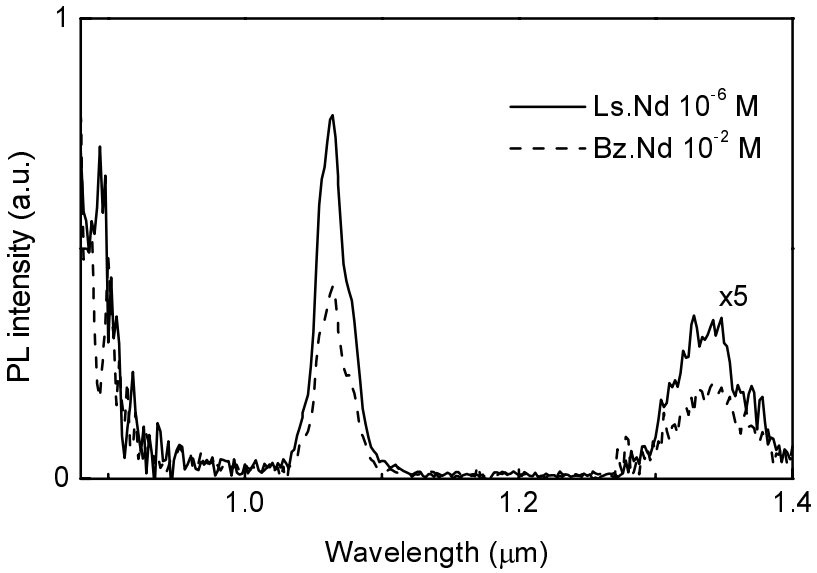

Figure 3.4 Photoluminescence spectra of Ls.Nd (10^{-6} M) and Bz. Nd (10^{-2} M) in DMSO-d6 solutions. The excitation wavelength is 515 nm, at a pump power of 60 mW. Note that around 1340 nm the spectra are multiplied by a factor 5.

Figure 3.4 shows room-temperature PL spectra for 10^{-2} M Bz.Nd and 10^{-6} M Ls.Nd in DMSO-d6, recorded using excitation at 515 nm at a pump power of 60 mW. The complexes show room-temperature photoluminescence of Nd^{3+} at 890, 1060, and 1340 nm. Although the concentration of Ls.Nd is 10^4 times lower than the concentration of Bz.Nd, the PL intensity is 2 times higher. Optical absorption measurements at 515 nm for both solutions show an almost equal absorption: 0.033 cm^{-1} for 10^{-2} M Bz.Nd and 0.031 cm^{-1} for 10^{-6} M Ls.Nd. The fact that the sensitised complex shows higher luminescence than the complex without a sensitiser, even though the measured absorption was the same, indicates that the internal energy transfer efficiency within the sensitised complex is quite high. The factor two difference can be due to the fact that upon direct excitation into the higher lying state of the Nd^{3+} ion, the Nd^{3+} ion can also decay radiatively to the ground level (indeed, 524 nm luminescence has been observed, resulting from the transition from the $^2K_{13/2} \rightarrow {}^4I_{9/2}$ transition), leading to a lower quantum yield for the near-infrared transitions in the case of direct optical excitation of the Nd^{3+} at 515 nm.

The measured luminescence lifetime (not shown) at 1060 nm for the Bz.Nd complex in DMSO-d6 is 2.5 μs, and for the sensitised Ls.Nd complex 2.2 μs. The luminescence lifetime of Nd^{3+} in inorganic materials can be as high as 250 μs.[17] The low quantum yield in the organic complexes is attributed to quenching of the Nd^{3+} excited state by coupling to overtones of nearby C-H and O-H vibrational states.

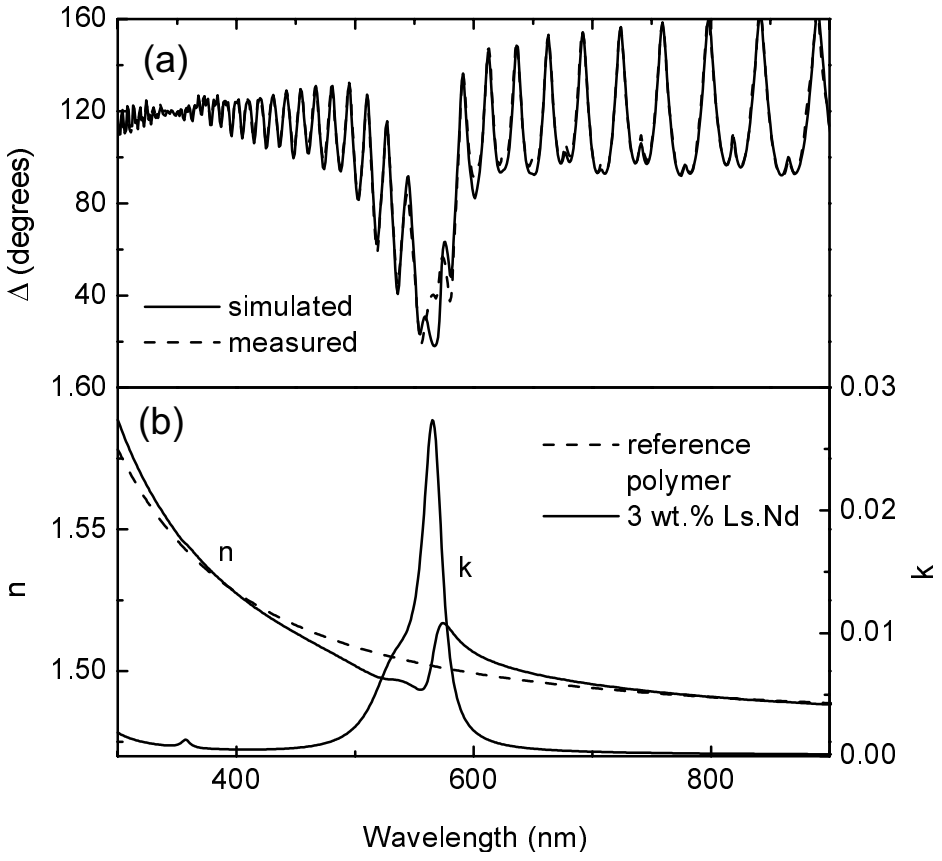

Figure 3.5 (a) Measured and calculated ellipsometric parameter Δ as a function of wavelength for a 3 wt.% Ls.Nd doped partially fluorinated polycarbonate waveguide. (b) Real (n) and imaginary (k) part of the refractive index derived from the simulation data indicated by the solid line in (a). The real index for an undoped reference waveguide is shown for reference (dashed line in (b)).

Figure 3.5(a) shows the measured (dashed line) and simulated (solid line) ellipsometry parameter Δ as a function of wavelength for a partially fluorinated polycarbonate planar polymer waveguide doped with 3 wt.%. Ls.Nd. The interference structure is caused by reflections at the air/polymer, polymer/SiO_2, and SiO_2/Si interfaces. A clear dip in Δ is observed around 580 nm, which is caused by the high absorption of the lissamine. The simulated data are based on a Lorentz oscillator model and correspond well with the measured data. From the simulation parameters, the real (n) and imaginary (k) part of the refractive index of the Nd-doped polymer waveguide layer can be calculated, as shown in Fig. 3.5(b). Also shown is the measured refractive index of an undoped reference polymer. Outside the resonance region, the refractive index of the Nd-doped waveguide layer is very similar to that of the undoped layer, indicating that the spincoating technique leads to Nd-doped waveguide layers with similar density as pure waveguide layers. The maximum value of k is 0.027 at 580 nm which

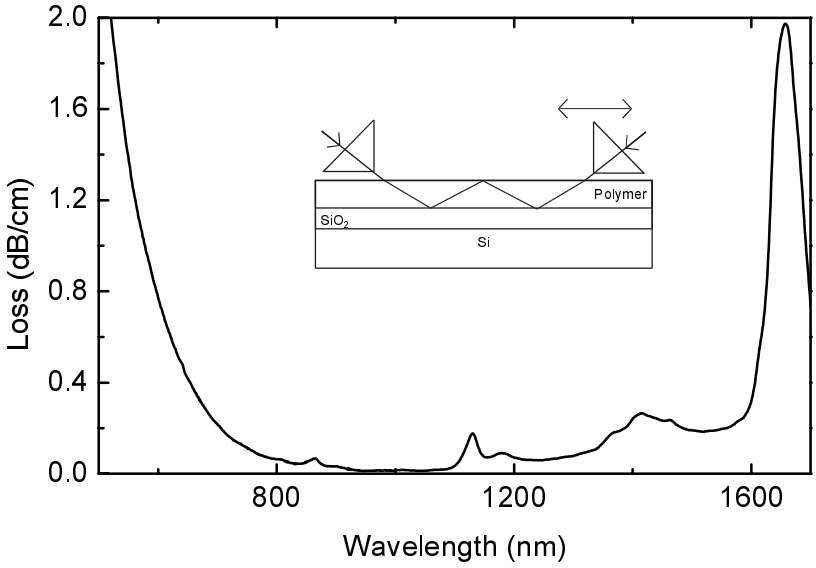

Figure 3.6 Optical loss spectrum of an undoped partially fluorinated polycarbonate waveguide measured using the sliding prism method (see inset).

corresponds to an absorption cross section of 4.5×10^{-16} cm^2, which is roughly 2-3 times higher than the literature value for Rhodamine-B.[14] It is clearly seen that the high absorption of the lissamine causes a change in the real part of the refractive index around 580 nm as described by Kramers-Kronig theory.

Optical loss measurements were performed on an undoped partially fluorinated polycarbonate waveguide using the prism coupling technique. The result is shown in Fig. 3.6. The peak around 1650 nm is due to overtone absorption by C-H bonds. The band around 1400 nm is attributed to absorption by C-H bonds and O-H bonds in the polymer. The two peaks around 1150 nm arise from second overtone absorption by aromatic and aliphatic C-H bonds. The background loss at the Nd^{3+} emission wavelengths is < 0.05 dB/cm at 1060 nm and 0.08 dB/cm at 1305 nm. This indicates that these polycarbonate waveguides are ideally suited for planar waveguide applications.

Figure 3.7 shows the PL spectra of a 3 wt.%. Ls.Nd doped fluorinated polycarbonate waveguide excited at a wavelength of 515 nm. The dashed line shows the luminescence measured using excitation and collection of the light from the top of the sample (P = 40 mW). The 890 nm and 1060 nm luminescence of the Nd^{3+} ion are clearly seen. Spectra taken in the near-infrared region (not shown) also show the 1340 nm luminescence. The emission observed in the lower wavelength region is due to luminescence of the lissamine, which has a peak emission wavelength ($S_1 \rightarrow S_0$ transition) at 580 nm. The small peaks at the shoulder of the lissamine luminescence are attributed to an interference effect in the waveguide layers. The solid line in Fig. 3.7 is the spectrum observed for excitation from the top and collecting from the output facet of the waveguide

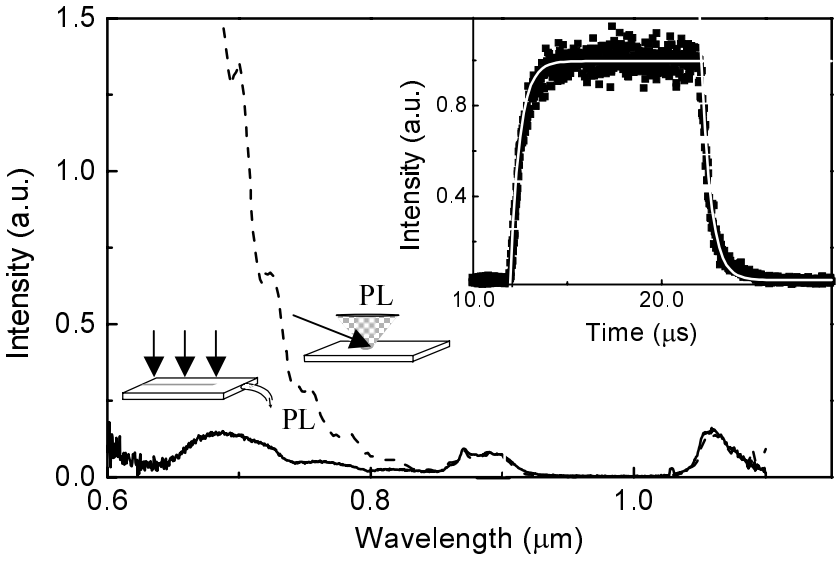

Figure 3.7 Photoluminescence spectra of a 3 wt.% Ls.Nd doped polymer waveguide. The dashed line indicates the spectrum collected from the top of the waveguide using excitation at 515 nm at a power of 40 mW. The solid line indicates the spectrum using excitation at 515 nm at a power of 140 mW and collected from the output face of the waveguide using a multimode optical fiber. Schematics of the two measurement configurations are shown in the figure. The inset shows the time dependence of the 1060 nm luminescence upon pulsed excitation.

(P = 140 mW, spot 5×15 mm^2). Again the 890 nm and 1060 nm luminescence are observed, but here the luminescence of the lissamine is strongly decreased, which is attributed to re-absorption by the lissamine itself. This indicates that self-absorption should be taken into account when designing waveguide devices.

The inset of Fig. 3.7 shows the time dependence of the 1060 nm PL signal after switching the 515 nm pump on and off. An exponential fit through the decay part results in a PL lifetime of 0.8 μs. This is significantly lower than the decay measured for complexes in DMSO-d6 solution (2.2 μs), which indicates that quenching by C-H and O-H groups in the polymer matrix also contributes to the radiation-less deactivation of the Nd^{3+}.

The energy transfer from the lissamine to the Nd^{3+} ion occurs via the triplet state of the lissamine. However, the triplet state can also be quenched by e.g. O_2 that is always present in solution or in a polymer film.[18,19] In order to investigate this, we measured the Nd^{3+} luminescence intensity of Ls.Nd in DMSO-d6 solutions before and after degassing (not shown). The Nd^{3+} PL intensities were similar, indicating that quenching by O_2 does not play a role in the DMSO-d6 solutions. As it is known that the quenching rate by O_2 in solution is about 10^7 s^{-1}, it can be estimated that the intramolecular energy transfer rate to the Nd^{3+} ion has to be $>10^7$ s^{-1}.[20] This transfer rate is of the same order of

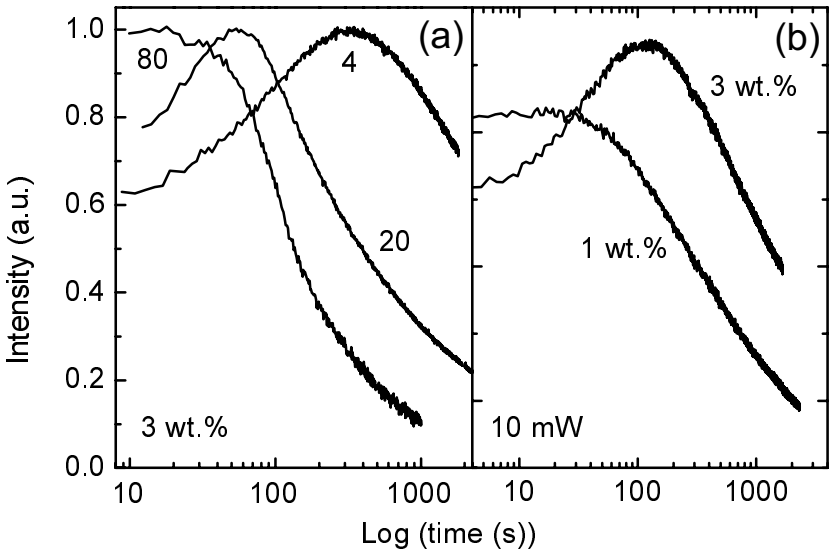

Figure 3.8 (a) 580 nm lissamine photoluminescence of a 3 wt.% Ls.Nd-doped waveguide at pump powers of 4, 20 and 80 mW. Each measurement was made at a fresh spot on the sample. (b) Similar measurements on a 3 wt.% and 1 wt.% Ls.Nd-doped waveguide at a pump power of 10 mW.

magnitude as for triphenylene sensitised Eu^{3+} in acetonitrile solutions.[21]

A space filling model of Ls.Nd, in which all atoms are represented by their van der Waals radius, shows that the distance between lissamine and the Nd^{3+} ion is 7-8 Å, whereas the effective average Bohr radius for the excited lissamine and the unexcited Nd^{3+} ion is about 2.5 Å. According to Dexter,[22] this means that 3 % of the maximum possible energy transfer rate is reached. This could be improved by reducing the distance between the lissamine and the Nd^{3+} ion by changing the configuration of attachment of the lissamine. Another possibility to increase the energy transfer rate is to improve the spectral overlap between the sensitiser and the Nd^{3+} ion.[23] In the present case, the energy of the triplet state of lissamine matches with the 14600 cm^{-1} band of Nd^{3+} which shows weak absorption. If a sensitiser could be used that matches the strong $^4I_{9/2} \rightarrow {}^4S_{3/2}$ absorption band (13600 cm^{-1}), the energy transfer rate could be increased.

Finally, time-dependent measurements of the 580 nm lissamine luminescence were performed on polymer waveguides doped with 3 wt.% (complex) and are shown in Fig. 3.8(a) for near-normal incidence irradiation at three different pump powers. Each measurement was made on a fresh spot at the sample. The luminescence signal was detected normal to the waveguide. For a pump power of 4 mW the luminescence intensity slowly rises to a maximum and then decreases again. At higher pump powers the same effect is observed, but both the increase and the decrease processes occur faster. This photo-degradation process may be the result of oxygen induced quenching. Another possibility is

that upon photo-excitation radicals are formed, which react with the sensitiser.[24] Figure 3.8(b) compares the luminescence intensity versus illumination time for 1 wt.% and 3 wt.% films. The 1 wt.% doped film does not show the initial increase in the luminescence intensity. This might indicate that concentration quenching plays a role in the time-dependent behavior as well. In Chapter 4 this effect will be studied in more detail.

3.4 Conclusions

Room-temperature photoluminescence of Nd^{3+} complexes in DMSO-d6 solution and partially fluorinated polycarbonate waveguides has been observed for both direct excitation of the Nd^{3+} ion into a higher excited state, and excitation via a highly absorbing sensitiser (lissamine). It is shown that the excitation efficiency upon excitation via the sensitiser is 10^4 times higher than for direct excitation. The intramolecular transfer rate from the sensitiser to the Nd^{3+} ion is $>10^7$ s^{-1}. The luminescence lifetime is relatively short, both in DMSO-d6 (2.2 μs) and in the polymer waveguide (0.8 μs), which is attributed to coupling to O-H and C-H vibrations of the complex and the host material. Good quality optical waveguides can be spin-coated with optical losses for the undoped polycarbonate waveguide of < 0.05 dB/cm at 1060 nm and 0.08 dB/cm at 1340 nm. Strong photo-degradation of the lissamine luminescence is observed that might be due to the presence of oxygen in the polymer film or due to radicals, which are formed upon photo-excitation.

References

1 S. Hüfner, Optical Spectra of Transparent Rare-Earth Compounds (Academic, New York, 1978)

2 T. Kitagawa, K. Hattori, and Y. Hibino, J. Lightw. Techn. **12**, 436 (1994)

3 D. P. Shepherd, C. T. A. Brown, T. J. Warburton, D. C. Hanna, A. C. Tropper, and B. Ferrand, Appl. Phys. Lett. **71**, 876 (1997)

4 J. Hulliger, P. Rogin, and R. Burkhalter, Laser Physics **8**, 764 (1998)

5 R. Brinkmann, W. Sohler, H. Suche, and C. Wersig, IEEE J. Quantum Electronics **28**, 466 (1992).

6 E. Lallier, J. P. Pocholle, M. Papuchon, M. De Micheli, M. J. Li, Q. He, D. B. Ostrowsky, C. Grezes-Besset, and E. Peletier, IEEE J. Quantum Electronics **27**, 618 (1991).

7 R. Gao, C. Koeppen, G. Zheng and A. F. Garito, SPIE Proc. **3280**, 14 (1998)

8 R. T. Chen, M. Li, S. Tang, and D. Gerald, SPIE Proc. **2149**, 77 (1994)

9 B. Booth, in Polymers for Lightwave and Integrated Optics, edited by L. A. Hornak (Dekker, New York 1992)

10 L. H. Slooff, A. Polman, M. P. Oude Wolbers, F. C. J. M. van Veggel, D. N. Reinhoudt, and J. W. Hofstraat, J. Appl. Phys. **83**, 497 (1998)

11 G. Stein, and E. Würzberg, J. Chem. Phys. **62**, 208 (1975)

[12] V. L. Ermolaev, and E. B. Sveshnikova, Russ. Chem. Rev. **63**, 905 (1994)
[13] S. I. Klink, Ph. D. Thesis University of Twente, Enschede, The Netherlands (2000), ISBN 90-3651436-3
[14] I. B. Berlman, Handbook of Fluorescence Spectra of Aromatic Molecules (Academic Press, New York, 1971)
[15] R. H. Woudenberg, and T. O. Boonstra, Polymers comprising a fluorinaed carbonate moiety, International patent, deposited September 3, 1998, # WO 9838237
[16] H. P. Weber, F. A. Dunn, and W. N. Leibolt, Appl. Opt. **12**, 755 (1973)
[17] M. J. Weber, Phys. Rev. **171**, 283 (1968)
[18] M.G. Kucherenko, and M. P. Mel'nik, J. Appl. Spec. **60**, 344 (1994)
[19] F. Wilkinson, W. P. Helman, and A. B. Ross, J. Phys. Chem. Ref. Data **22**, 113 (1993)
[20] it is assumed that the quenching by O_2 is a diffusion controlled mechanism at a rate $k_q=10^{10}\ M^{-1}s^{-1}$, for a typical O_2 concentration in solution the total quenching rate is $k_q[O_2]\approx10^7\ s^{-1}$
[21] E. van der Tol, Ph. D. Thesis, University of Amsterdam, Amsterdam, The Netherlands (1998), ISBN 90-9011458-0
[22] D. L. Dexter, J. Chem. Physics **21**, 836 (1953)
[23] M. H. V. Werts, J. W. Hofstraat, F. A. J. Geurts, and J. W. Verhoeven, Chem. Phys. Lett. **276**, 196 (1998)
[24] R. P. Wayne, in: Principles and Applications of Photochemistry (Oxford University Press, Oxford, 1988)

4 Concentration effects in the photo-degradation of lissamine-functionalised Nd complexes in a polymer waveguide

The photo-degradation of lissamine-functionalised neodymium complexes doped at a concentration of 10 wt.% in a fluorinated polycarbonate waveguide has been studied. Upon illumination at 458 nm and at 488 nm, the luminescence spectrum of the lissamine sensitiser shifts to shorter wavelength, while the luminescence intensity first increases and then decreases. The spectral shape of the Nd luminescence does not change upon illumination, and the luminescence intensity shows a gradual decrease as a function of time. The difference in response between the lissamine and the neodymium luminescence can be described by a model that assumes the existence of two different types of complexes. One type exhibits energy transfer from the lissamine to the neodymium ion, with a large lissamine intersystem crossing rate, and hence low sensitivity to concentration quenching. The other type does not show energy transfer to Nd, and does experience concentration quenching.

4.1 Introduction

Neodymium-doped polymer films may find applications in planar optical amplifiers operating at 1.3 μm. In Chapter 3 we have described how an organic complex can be incorporated in a polymer waveguide at concentrations as high as 3 wt.%. A strongly absorbing antenna group was attached to the organic complex. Very efficient energy transfer (at a rate > 10^7 s^{-1}) can take place from the lissamine sensitiser to the Nd^{3+} ion.[1] In Chapter 3 we found that upon optical excitation the emission from Nd strongly decreases in time, which was attributed to photo-degradation of the lissamine sensitiser. This is an important limiting effect for the use of such complexes in optical amplifiers. In this Chapter we will study this effect in more detail, using time-dependent measurements of the luminescence and absorption of both the lissamine sensitiser and the Nd^{3+} ion. The observations can be explained by a model that assumes that there are two types of complexes. One in which the lissamine sensitiser can transfer the excitation energy to the Nd^{3+} ion, and in which concentration quenching does not play an important role, and one in which the lissamine cannot transfer the energy to the Nd^{3+} ion and concentration quenching is present.

4.2 Experiment

Lissamine (sulfo-rhodamine-B) functionalised terphenyl-based Nd^{3+} complexes were synthesised using the procedure described in Ref. 2. A two-dimensional representation of the structure of the complex was reported in Fig. 3.2(b). The complexes were dissolved in partially fluorinated polycarbonate[3] waveguides at a concentration of 10 wt.% (complex). The waveguides were made by spin-coating a cyclohexylacetate solution containing both polycarbonate and complex onto a microscope glass slide. The spin-coating was performed for 30 seconds at a spin-rate of 3000 rpm and followed by thermal annealing at 190 ^oC (in vacuum) for one hour. The thickness of the polymer layer was 1 μm, as measured by ellipsometry.

Luminescence measurements were performed at an excitation wavelength of 488, or 515 nm using an Ar ion laser as an excitation source. The power on the sample was 1 W, with a Gaussian spatial intensity distribution and a full width at half-maximum between 1 and 5 mm. For each measurement a fresh spot was taken on the sample. The beam was modulated using an acousto-optic modulator, operating at 12.5 Hz. The emitted luminescence was focused into a monochromator and detected with a photomultiplier tube or a liquid-nitrogen cooled Ge detector. All spectra were corrected for the detector response. The light intensity transmitted through the sample was monitored using a silicon

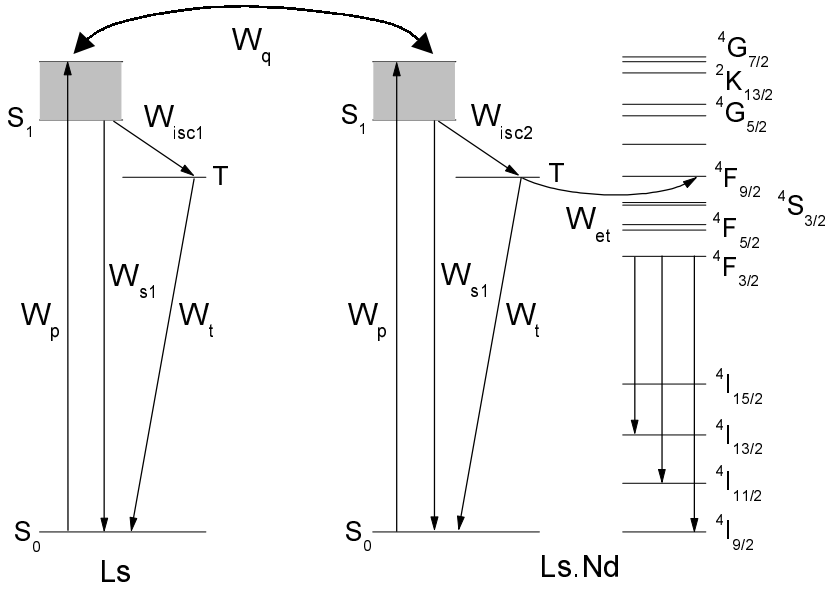

Figure 4.1 Schematic energy level diagram of the lissamine-Nd^{3+} complex. The arrows indicate the excitation and decay mechanisms. Complexes with and without energy transfer to Nd are shown, and the interaction between the two types is indicated by W_q.

photodiode positioned behind the sample, and changes in transmission were converted to absorption coefficients using the known film thickness and Lambert-Beer's law. Absorption spectra were measured before and after laser illumination using a variable-angle spectroscopic ellipsometer.

Luminescence lifetime measurements were performed under excitation at a wavelength of 337 nm using a 1.5 ns pulsed N_2 laser with a pulse energy of 20 μJ. The luminescence signal was detected using a Hamamatsu streak camera system. The time resolution of the system was ~300 ps.

4.3 Results and discussion

Figure 4.1 shows the schematic energy level diagram of the lissamine/Nd system. The lissamine is excited from the singlet ground state (S_0) into the excited singlet state (S_1) at a pump rate W_p. From there it can decay back to the ground state at a rate W_{s1}, or decay via intersystem crossing (W_{isc}) to the triplet state. From the triplet state it can decay to the ground state (W_t) or transfer its energy to the neodymium ion (W_{et}), in which case it also returns to the singlet ground state. After energy transfer from the lissamine sensitiser, the Nd will be excited into the $^4F_{9/2}$ and $^4S_{3/2}$ level, from which it will decay rapidly to the luminescent $^4F_{3/2}$ state. In our experiment direct absorption by the Nd^{3+} ion can be neglected, because its direct absorption cross section is four orders of magnitude smaller

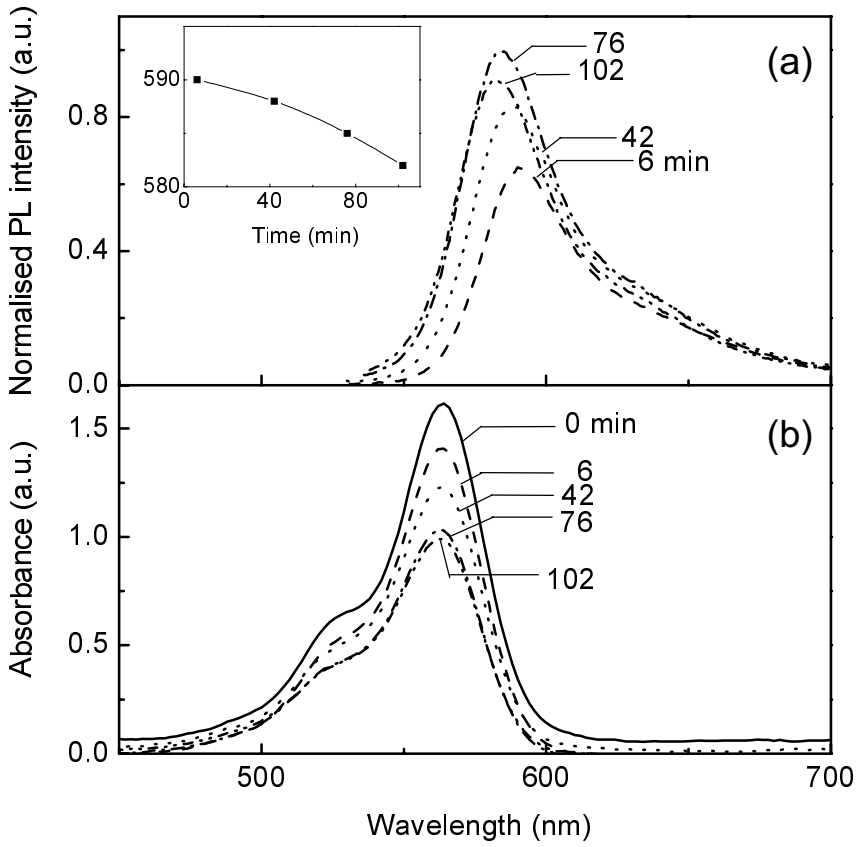

Figure 4.2 Luminescence (a) and absorption (b) spectra of the lissamine sensitiser for different illumination times. The excitation wavelength was 488 nm at a pump power of 1 W in a 5 mm spot. The inset shows the peak position in nm as a function of the illumination time.

than that of the lissamine. Figure 4.1 also shows the energy diagram of a lissamine complex not coupled to Nd, which will be discussed later on.

Figure 4.2(a) shows the luminescence spectra of a lissamine/Nd complex-doped polymer film excited at an excitation wavelength of 488 nm at a pump power of 1 W and a spot diameter of 5 mm. The emission is attributed to the lissamine sensitiser (W_{s1} in Fig. 4.1). The time to take each spectrum was 6 min., and the time given in the figure is the total elapsed time at the end of the measurement. As can be seen from the spectra, continued illumination results in a small blue shift of the peak luminescence from the lissamine sensitiser, as is also shown in the inset of Fig. 4.2. The integrated luminescence intensity increases for the first three measurements, and then decreases. The absorption spectra of the lissamine/Nd complex-doped polymer film for different illumination times are shown in Fig. 4.2(b). As can be seen, the spectral shape of the absorption spectrum remains the same, but the absorption decreases upon illumination. The blue shift and the increase in the intensity of the luminescence

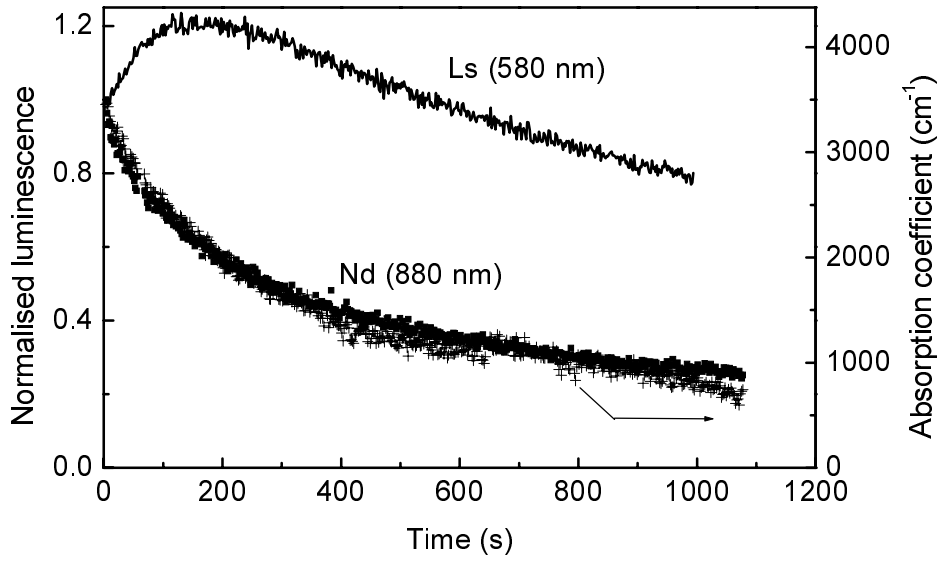

Figure 4.3 Lissamine luminescence intensity (580 nm, solid line) and Nd^{3+} luminescence intensity (880 nm, solid squares) as a function of illumination time. Also shown is the absorption coefficient of the film measured at 515 nm during illumination (crosses). A pump excitation wavelength of 515 nm at a power of 1 W and a 1 mm diameter spot was used.

spectra could in principle be explained by the bleaching of dimers or aggregates of complexes, that may be present at the high concentrations applied,[4-6] because these species have a different emission spectrum than monomers due to the electronic interaction between the molecules. However, this should also result in a change of the shape of the absorption spectrum upon bleaching, which is not observed in Fig. 4.2(b), so that this dimer bleaching model may be excluded. Alternatively, the blue shift can be explained by a change in self-absorption as the density of optically active lissamine decreases upon illumination (as seen in Fig. 4.2(b)). Figure 4.2 shows that the absorption and emission spectra of lissamine strongly overlap. The absorption cross section of lissamine, determined in Chapter 4, is 4.5×10^{-16} cm^2 at 580 nm and the concentration in the 1 μm thick film is 5×10^{19} cm^{-3}, which results in an absorption depth of roughly 0.5 μm. This means that a rather large fraction of the lissamine luminescence is reabsorbed by the surrounding lissamine molecules. As the concentration of optically active lissamine is reduced due to the illumination, the self-absorption reduces, and as a result, the collected luminescence intensity can increase in the region where the absorption and emission spectra overlap. This results in an apparent blue shift of the luminescence spectrum, as is observed in Fig. 4.2(a).[7] Note that the pump absorption depth at 488 nm is 6.6 μm, so that absorption by the lissamine causes no significant depletion of the pump intensity through the film.

Figure 4.3 shows measurements of the lissamine luminescence at 580 nm as well as the Nd^{3+} luminescence at 880 nm as a function of illumination time. The pump power was 1 W at an excitation wavelength of 515 nm, and at a spot diameter of 1 mm. The Nd^{3+} emission spectrum does not show a spectral change upon illumination (not shown). The lissamine luminescence first increases and then decreases as was also seen in Fig. 4.2(a). Also shown is the absorption coefficient measured at 515 nm during illumination (crosses), which shows that the concentration of optically active lissamine is gradually decreasing. Without self-absorption, the lissamine luminescence intensity would scale with the absorption coefficient, but at high lissamine concentration (short illumination time), the self-absorption reduces the detected luminescence intensity. This would result in a more constant intensity for short times, but it cannot explain the initial increase in the luminescence intensity as observed in Fig. 4.3. The increase may be explained by a concentration quenching model: at the high lissamine concentration used (10 wt.%), the lissamine molecules are spaced by only a few nm, so that excitations can easily transfer from one lissamine to another by a Förster energy transfer mechanism. In this way the excitation can migrate through the film, until it reaches a quenching center and is lost. In such a quenching model, the luminescence quantum efficiency increases with decreasing lissamine concentration. So, if the active lissamine concentration reduces as a result of illumination, the quantum efficiency increases. This additional reduction of the luminescence intensity for high concentration can describe the initial increase in the luminescence intensity with time. For a lower intrinsic lissamine concentration in the film, one would expect the initial increase to be smaller or even absent. Indeed, this is seen in Fig. 3.8(b) for a 1 wt.% doped polymer film. Using the combined effect of self-absorption and concentration quenching, the data of Fig. 4.3 can be described qualitatively. A quantitative description could not be made, which is ascribed to several unknown effects such as changes in the refractive index as a result of the photo-bleaching, changes in the active lissamine depth profile within the layer due to the gradient of the pump power in the film, and the effect of the standing wave pattern in the pump intensity throughout the film, which results from multiple reflections at the interfaces of the layers.

As can be seen in Fig. 4.3, the Nd^{3+} luminescence intensity shows a completely different time dependence than the lissamine luminescence: it precisely follows the decrease in absorption coefficient due to the decreasing active lissamine concentration. As the excitation of the Nd^{3+} ion occurs via the triplet state of the lissamine, one would also expect an initial increase in the Nd^{3+} luminescence. However, this is not observed. One way to explain the different behaviour of the lissamine and Nd intensities is by assuming that two types of complexes exist in the polymer film (see Fig. 4.1). One which shows the behaviour as observed in Fig. 4.3, explained by concentration quenching, and that does not couple to the Nd^{3+} ion (denoted as Ls), and one that couples to the

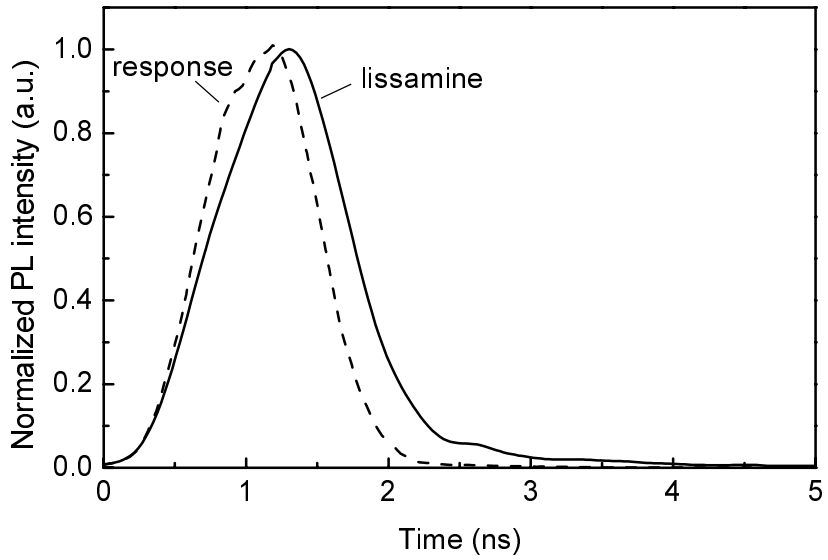

Figure 4.4 Time-dependent luminescence trace at λ=580 nm for a lissamine/neodymium doped polymer film (solid line) after excitation with a 1.5 ns (FWHM) pulse at 337 nm and a pulse energy of 20 μJ. The dashed line shows the system response after excitation.

Nd^{3+} ion, but does not show concentration quenching (denoted as Ls.Nd). The fact that no concentration quenching would be observed for complexes that couple to Nd^{3+} could be explained by the 'heavy-atom' effect.[8,9] The presence of a heavy atom like Nd increases the intersystem crossing rate within the lissamine.[2,10] If the intersystem crossing rate would be larger than the effective quenching rate due to concentration quenching (~10^8 s^{-1}, in the order of the luminescence decay rate) the latter would not be observed.

To study the heavy atom effect, we have performed measurements of the luminescence lifetime of the lissamine singlet state at 580 nm on Ls and Ls.Nd complexes in dimethylsulfoxide (not shown), and found a luminescence lifetime of 2.6 ns for the free lissamine and 1.2 ns for the complex. Assuming that this reduction in luminescence lifetime is the result of an increase in the intersystem crossing rate due to the presence of Nd^{3+}, the intersystem crossing rate in the presence of the Nd^{3+} ion can be calculated to be 4×10^8 s^{-1}. Indeed, this is much higher than the intrinsic intersystem crossing rate of pure lissamine, which is known to be 8×10^6 s^{-1}. Note that these measurements were done in solution, in which the equilibrium position of the sensitiser with respect to the Nd^{3+} ion can be substantially different compared to that in a polymer film, and hence the found intersystem crossing rate may not be representative for the polymer film. However, these data clearly indicate the possible effect of Nd on the intersystem crossing rate and hence, as argued above, on the concentration quenching. Figure 4.4 shows time-dependent measurements of the 580 nm emission of a lissamine-doped film, together with the system response. Deconvolution of the system

response and the measured trace results in a luminescence lifetime of the lissamine singlet state with a component shorter than the system resolution (< 300 ps), and a small component with a lifetime of ~0.6 ns, which is consistent with the above assumption of the existence of two different types of complexes. In that case, the lissamine complexes exhibiting energy transfer to the Nd^{3+} ion would have a lifetime of less than 300 ps, corresponding to an intersystem crossing rate of $> 1.6\times10^{9}$ s^{-1}, which would indeed explain the absence of a concentration quenching effect for these complexes. The lissamine complexes without energy transfer to the Nd would then have a luminescence lifetime of 0.6 ns. The fact that this lifetime is shorter than that measured for the same complexes in the solution (2.6 ns) is probably due to the concentration quenching which reduces the luminescence lifetime.

4.4 Conclusions

Lissamine-functionalised terphenyl-based neodymium complexes were dissolved into a polycarbonate film at a concentration of 10 wt.%. Upon continuous laser illumination at 488 nm (~ 1 W), the lissamine sensitiser shows photo-bleaching, which results in a blue shift of the lissamine emission spectrum due to reduced self-absorption within the film. At a fixed wavelength the lissamine luminescence intensity first increases and then decreases during illumination, which is attributed to self-absorption and a concentration quenching effect that reduces the emission quantum efficiency at high concentrations. The Nd^{3+} luminescence intensity shows no initial increase, although it would be expected based on the fact that the neodymium is excited via the lissamine. This suggests that concentration quenching has no effect on the Nd^{3+} luminescence. The difference in behaviour of the emission intensity with illumination time is explained by a model that assumes the presence of two different types of complexes. One type exhibits energy transfer to the Nd^{3+} ion, which increases the intersystem crossing rate within the lissamine, thereby reducing the influence of concentration quenching. The other type does not have energy transfer to the neodymium, and shows concentration quenching. The lack of energy transfer in some of the complexes might be explained by a larger distance between the sensitiser and the Nd^{3+} ion, which reduces the energy transfer rate.

References

1 L. H. Slooff, A. Polman, S. I. Klink, G. A. Hebbink, L. Grave, F. C. J. M. van Veggel, D. N. Reinhoudt, and J. W. Hofstraat, Opt. Mat. **14**, 101 (2000)

2 S. I. Klink, Ph. D. Thesis, University of Twente, Enschede, The Netherlands (2000), ISBN 90-3651436-3

[3] R. H. Woudenberg, and T. O. Boonstra, Polymers comprising a fluorinated carbonate moiety, International patent, deposited September 3, 1998, # WO 9838237
[4] T. Förster, and E. Koning, Z. Elektrochem. **61**, 344 (1957)
[5] E. G. McRae, and M. Kasha, J. Chem. Phys. **28**, 721 (1958)
[6] R. W. Chambers, T. Kijiwara, and D. R. Kearns, J. Phys. Chem. **78**, 380 (1974)
[7] S. A. Ahmed, Z-W. Zang, K. M. Yoo, M. A. Ali, and R. R. Alfano, Appl. Opt. **33**, 2746 (1994)
[8] S. Tobita, M. Arakawa, and I. Tanaka, J. Chem. Phys. **88**, 2697 (1984)
[9] S. Tobita, M. Arakawa,and I. Tanaka, J. Chem. Phys. **89**, 5649 (1985)
[10] M. H. V. Werts, J. W. Hofstraat, F. A. J. Geurts, J. W. Verhoeven, Chem. Phys. Lett. **276**, 196 (1997)

5 Pumping planar waveguide amplifiers using a coupled waveguide system

A novel scheme is presented that can be used to efficiently pump optical waveguide amplifiers. It is based on the coupling between two adjacent waveguides, where pump light is gradually coupled from a non-absorbing pump waveguide into the amplifier waveguide. The coupling between the waveguides in such a configuration is calculated using an improved coupled mode theory. The proposed distributed coupling scheme can enhance the optical gain in systems that exhibit a reduced pumping efficiency at high pump power. A numerical example is given for a sensitised neodymium-doped polymer waveguide amplifier, in which the optical gain increases from 0.005 dB to 3.0 dB by changing from conventional butt-coupling to distributed coupling.

5.1 Introduction

The rapid expansion of optical telecommunication technology increases the need for planar optical amplifiers that can be used to compensate losses in splitters, switches multiplexers, and other devices. Planar optical amplifiers are widely studied and they often use the rare-earth ions erbium or neodymium as the active element as these ions exhibit intra-4*f* transitions around 1550 nm and 1340 nm respectively, two of the standard telecommunication wavelengths.[1] Amplification is obtained by optical pumping of the rare-earth ions in order to create population inversion. Stimulated emission induced by the signal light then results in optical amplification.

The pumping of optical waveguide amplifiers is usually done by coupling the pump beam into the waveguide at the input facet of the waveguide (butt-coupling). The pump light is absorbed by the rare-earth ions as it travels through the waveguide, resulting in a decrease in pump power along the waveguide. In order to maintain sufficient pump power over the entire length of the waveguide, relatively high pump powers are coupled into the input section of the waveguide. This pumping scheme can be successfully used for materials in which high pump powers do not affect the pumping efficiency. However, in several materials systems an optimum pump power for amplification exist. Such systems include highly Er-doped waveguides in which co-operative upconversion and excited state absorption take place,[1] or systems in which the rare earth ions are excited via energy transfer from a sensitiser,[2,3] such as described in Chapter 3 and 4. In these systems, butt-end coupling is not efficient. The excess pump power at the beginning of the waveguide will result in pump absorption that does not contribute to the optical gain.

In this Chapter we introduce a coupling configuration that can distribute the pump power evenly over the full length of the (signal) waveguide. It is based on the coupling between two waveguides in close proximity. In this scheme, the pump light is gradually coupled from a non-absorbing pump guide into the adjacent amplifier guide. By gradually increasing the coupling (i.e. reducing the distance between the guides), it is possible to maintain a constant pump power along the signal guide. We will study the coupling between two parallel waveguides using coupled mode theory. A numerical example is given that shows that the optical gain of a sensitised Nd-doped polymer waveguide amplifier can be enhanced using this novel pump scheme.

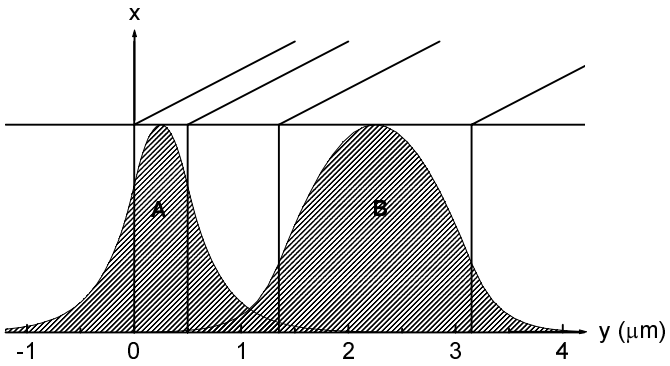

Figure 5.1 Schematic presentation of a two-dimensional coupled waveguide system consisting of parallel optical waveguides A and B. The calculated waveguide mode intensity along the x-axis is shown for the waveguide geometry described in the text (515 nm pump A, 1.353 μm signal B).

5.2 Coupled mode theory for dissimilar waveguides

The waveguide structure under consideration is shown in Fig. 5.1. It consists of a pump waveguide A and a signal waveguide B. In order to evaluate the performance of this system, we first need to calculate the coupling of pump power into the signal waveguide. This can be done using coupled mode theory.

The conventional coupled mode theory[4,5] deals with the coupling between two weakly interacting, nearly identical optical waveguides. The total field of the waveguide system can be written as a linear superposition of the individual waveguide modes $\mathbf{E}^a(x,y)$ and $\mathbf{E}^b(x,y)$:

$$\begin{aligned}\mathbf{E} &= a(z)\mathbf{E}^a(x,y) + b(z)\mathbf{E}^b(x,y)\\ \mathbf{H} &= a(z)\mathbf{H}^a(x,y) + b(z)\mathbf{H}^b(x,y)\end{aligned} \tag{5.1}$$

with z the propagation direction. The coupled mode equations, defining the mode amplitudes a(z) and b(z) along the waveguide are given by:

$$\begin{aligned}\frac{d}{dz}a(z) &= i\gamma_a a(z) + ik_{ab}b(z)\\ \frac{d}{dz}b(z) &= ik_{ba}a(z) + i\gamma_b b(z)\end{aligned} \tag{5.2}$$

in which $\gamma_{a,b}$ are propagation constants and $k_{ab,ba}$ mutual coupling constants which in this case are identical. If the waveguides are not identical, or in the case

of strong coupling, the mutual coupling coefficients are different for the two waveguides, and as a result power is not conserved in the conventional theory. This problem can be dealt with using modified propagation and coupling parameters γ_a, γ_b, k_{ab} and k_{ba}, as given in appendix 5.A.[6] These parameters are known non-linear functions of the fields of the unperturbed individual waveguide modes. Consequently, when the unperturbed modal solutions for the individual waveguides are known, the fields of the coupled waveguide system can be calculated.

The optical modes of the individual waveguides are a solution to the (Helmholtz) wave equation that is associated with Maxwell's equations. In principle one should take into account the complete two-dimensional field pattern over the cross section of the waveguide. However, in good approximation the field $\mathbf{E}(x,y)$ can be written as $\mathbf{E}(x)\mathbf{E}(y)$. In this approximation, it can be easily shown that if the waveguides have the same thickness (defined in the x-direction, see Fig. 5.1), the coupling only depends on $\mathbf{E}(y)$. Using the correct boundary conditions, the TE field pattern for the first even mode of the pump waveguide A is given by:

$$E^a(y) = C_a \begin{cases} \cos\left(k_y \frac{d}{2}\right) e^{-\alpha(y-d/2)} & y \geq +\frac{d}{2} \\ \cos\left(k_y y\right) & |y| \leq \frac{d}{2} \\ \cos\left(k_y \frac{d}{2}\right) e^{+\alpha(y+d/2)} & y \leq -\frac{d}{2} \end{cases} \tag{5.3}$$

in which k_y and α are determined from the eigenvalue equation, which is obtained by substituting Eq. 5.3 into the wave equation, C_a is a normalization constant, and d the waveguide width. The above calculation can also be done to obtain the TE field of the signal guide B.

With the modal fields of Eq. 5.3 as input for the coupled mode equations of Eq. 5.2, the modal amplitudes a(z) and b(z) can be calculated. If all pump power is launched into waveguide A at z = 0 (a(0) = 1, b(0) = 0), the solution can be written as:[7]

$$\begin{aligned} a(z) &= \left(\cos(\psi z) - i \frac{\Delta}{\psi} \sin(\psi z) \right) e^{i \varphi z} \\ b(z) &= i \frac{k_{ba}}{\psi} \sin(\psi z) e^{i \varphi z} \end{aligned} \tag{5.4}$$

where:

Table 5.1 Waveguide parameters of the coupled optical waveguide system as used in the calculation.

guide	λ(nm)	n_{guide}	k_{guide}	$n_{cladding}$	$k_{cladding}$
pump	515	1.5067	0	1.4616	0
	1340	1.4845	0	1.4465	0
signal	515	1.4973	0.0125	1.4616	0
	1340	1.4831	0	1.4465	0

$$\varphi = \frac{\gamma_a + \gamma_b}{2}$$
$$\psi = \sqrt{\Delta^2 + k_{ab}k_{ba}} \qquad (5.5)$$
$$\Delta = \frac{\gamma_b - \gamma_b}{2}$$

We can now calculate the pump coupled into the signal guide B:

$$P(z) = \frac{1}{2}\mathrm{Re}\int\int \mathbf{E}\times\mathbf{H}^* \cdot \hat{\mathbf{z}}\,dxdy = \qquad (5.6)$$
$$|a(z)|^2 + |b(z)|^2 + \mathrm{Re}\left[a(z)b^*(z)C_{ba} + b(z)a^*(z)C_{ab}\right]$$

where the cross overlap integrals C_{ab} and C_{ba} are given by:

$$C_{ab} = \frac{1}{2}\iint \mathbf{E}^b \times \mathbf{H}^a \cdot \hat{\mathbf{z}}dxdy, \qquad C_{ba} = \frac{1}{2}\iint \mathbf{E}^a \times \mathbf{H}^b \cdot \hat{\mathbf{z}}dxdy \qquad (5.7)$$

and the integration is done over the cross section of the signal waveguide.

Using the same set of equations, it is also possible to calculate the coupling of the signal mode into the pump guide. In the present waveguide geometry (a broad single-mode signal guide and a narrow single-mode pump guide) this loss can be neglected.

5.3 Numerical example

Using the equations derived above, we can now calculate the effect of distributed coupling. As an example we will consider the sensitised Nd^{3+}-doped polymer waveguide described in Chapter 3. The Nd ions are incorporated in an organic complex that also contains an organic sensitiser group. In these complexes,

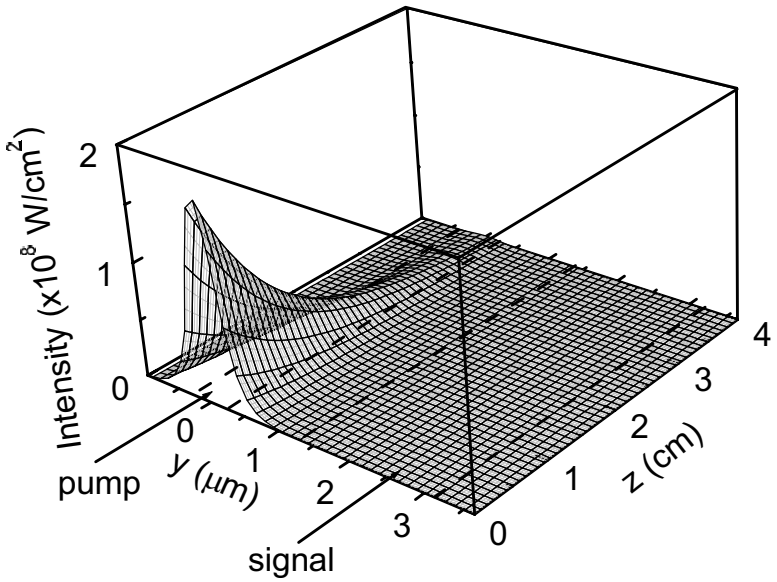

Figure 5.2 Pump intensity in the waveguide structure as a function of distance z along the waveguide.

1340 nm emission of Nd is observed after excitation via the lissamine sensitiser. In this way the Nd^{3+} ion can be excited efficiently, as a result of the high absorption of the lissamine at the pump wavelength (515 nm). However, if the pump power is higher than the value needed for complete population inversion of the Nd, the excess pump light is absorbed by the lissamine, leading to a reduced pumping efficiency. Therefore, the pump power should be kept below a certain limit over the length of the waveguide.

In this example, the pump power (λ = 515 nm) is coupled through a 0.5 μm wide waveguide parallel to a 1.8 μm wide signal (λ = 1340 nm) waveguide at a spacing between the centers of the waveguide of 2 μm. Both waveguides support only the fundamental mode (see Fig. 5.1). The real (n) and imaginary (k) part of the refractive index are listed in Table 5.1 for the two waveguides. In the present geometry coupling from the signal waveguide into the pump waveguide is negligible, as the narrow pump guide does not support the 1340 nm mode.

Figure 5.2 shows the calculated intensity distribution of the pump over the length of the waveguide, using an input pump power of 1 W. The intensity decrease in the non-absorbing pump guide is entirely due to absorption of pump light coupled into the highly absorbing signal waveguide. In the present configuration the pump power is almost completely absorbed after a distance of about 4 cm. The pump power in the signal guide as a function of the distance follows the same decreasing trend, as the coupling constant is constant over the length of the waveguides. It is not visible on the scale of Fig. 5.2, as the coupling

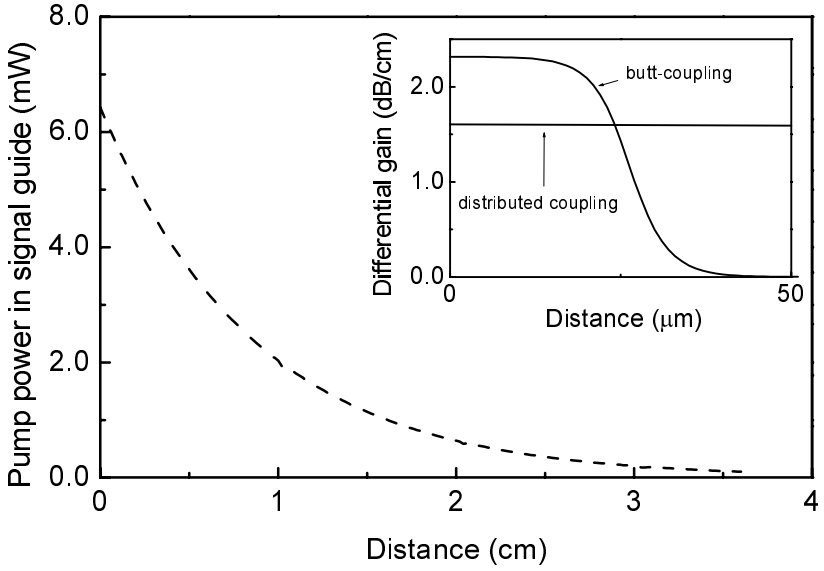

Figure 5.3 Pump power in the signal guide as function of distance z in a sensitised Nd-doped polymer waveguide. The inset shows the calculated differential gain as a function of distance along the waveguide for a coupled waveguide system, and a butt-coupled waveguide. The input power in the pump waveguide is 1 W in both cases.

constant is very small. It can be determined by integrating the data in Fig. 5.2 across the signal waveguide. The result is shown in Fig. 5.3. As can be seen, the power in the signal guide decreases from about 6 mW to almost zero over a distance of 4 cm.

The Nd^{3+} system can be described by a four level system, in which there is no minimum pump power required for optical gain. The differential gain along the amplifier is calculated using the known rate equations for the Nd^{3+} level system, which are given in appendix 5.B, and the pump power as a function of distance along the guide calculated above. The result is shown in the inset of Fig. 5.3. Note that even with a pump power as low as 6 mW at the beginning of the signal guide, the differential gain is still reasonably high (~1.6 dB/cm). The total optical gain for this waveguide amplifier is given by :

$$\text{gain(dB)} = 4.34 \times \eta \times \left(\int_0^L \sigma_{se} N\, f(z)\, dz \right) \qquad (5.8)$$

in which $\sigma_{se} = 1\times10^{-20}$ cm^2 the cross section for stimulated emission at 1340 nm,[8-10] $N = 5\times10^{19}$ cm^{-3} the Nd^{3+} concentration, f(z) the fraction of excited Nd (see appendix 5.B), L the length of the waveguide, and η = 78% the relative overlap between pump and signal mode in the signal waveguide. For the example given above, the total gain is calculated to be 3.0 dB for a 4 cm long waveguide amplifier. To show the effect of distributed coupling, the inset of Fig. 5.3 also

includes the differential gain obtained by using conventional butt-coupling at the same input pump power of 1W. Note that all pump power is completely absorbed within the first 50 μm. The maximum gain for this case is only 0.005 dB.

5.4 Conclusions

We have introduced an optical waveguide system, consisting of two closely spaced parallel waveguides, that can be used to optimise the pumping of planar waveguide amplifiers. The interaction between the two waveguides is calculated using coupled mode theory for non-identical waveguides. It is shown that light coupled into the pump guide will gradually couple to the signal guide, resulting in a more efficient power distribution along the signal guide. Calculations on a sensitised Nd^{3+}-doped polymer waveguide system show that using a butt-coupled waveguide the total optical gain is 0.005 dB, whereas an optical gain of 3.0 dB is possible using a coupled waveguide system (1 W input pump power). This clearly shows the advantage of the coupled waveguide system over the conventional butt-coupling.

Appendix 5.A

From the reciprocity theorem[6] it follows that:

$$\left.\begin{aligned}\gamma_a &= \beta_a + \frac{K_{aa} - CK_{ba}}{1-C^2}\\ \gamma_b &= \beta_b + \frac{K_{bb} - CK_{ab}}{1-C^2}\end{aligned}\right\} \quad \text{(modified propagation constants)}$$

$$\left.\begin{aligned}k_{ab} &= \frac{K_{ab} - CK_{bb}}{1-C^2}\\ k_{ba} &= \frac{K_{ba} - CK_{aa}}{1-C^2}\end{aligned}\right\} \quad \text{(modified coupling constants)} \qquad (5.9)$$

$$C=(C_{ab}+C_{ba})/2$$

with the conventional propagation constant β and coupling constant K_{ab}, and K_{ba} given by:

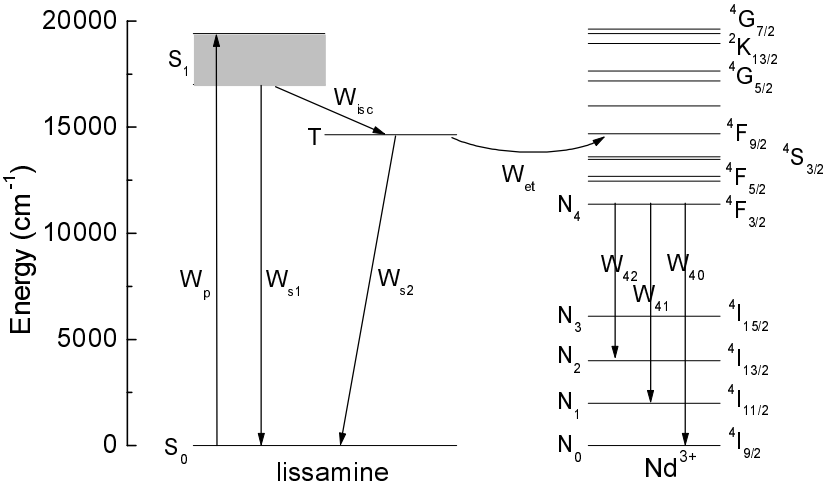

Figure 5.4 Schematic energy level diagram of the Ls.Nd system. The different rate constants W_i used in the calculations are indicated.

$$\beta_{a,b} = \frac{2\pi\left(n_{a,b} + k_{a,b}\right)}{\lambda}$$

$$K_{ab} = \frac{\omega}{4}\iint \varepsilon^{b}(x,y)\left[E_t^a \cdot E_t^b - E_z^a \cdot E_z^b\right]dxdy \qquad (5.10)$$

$$K_{ba} = \frac{\omega}{4}\iint \varepsilon^{a}(x,y)\left[E_t^b \cdot E_t^a - E_z^b \cdot E_z^a\right]dxdy$$

where $\varepsilon^{a,b}(x,y) = \varepsilon(x,y) - \varepsilon^{a,b}(x,y)$

Here $n_{a,b}$ is the real part of the refractive index, $k_{a,b}$ is the imaginary part of the refractive index, $\varepsilon(x,y)$ is the permittivity function for the complete waveguide system and $\varepsilon^{a,b}(x,y)$ the permittivity function for the isolated waveguides A and B.

Appendix 5.B

Figure 5.4 shows the schematic energy level diagram for the lissamine-neodymium system. The lissamine is excited from the singlet ground state (S_0) into the excited singlet state (S_1) at a pump rate W_p, after which it can decay to the ground state at a rate W_{s1}, or to the triplet state (T) via intersystem crossing at a rate W_{isc}. From the triplet state it can then decay to the ground state radiatively at a rate W_{s2}, or non-radiatively by transferring its energy to the neodymium ion via Dexter energy transfer at a rate W_{et}. After the energy transfer process, the neodymium will be in the $^4F_{9/2}$ and $^4S_{3/2}$ level, from which it decays

Table 5.2 Values for the different rates used in the optical gain calculation. P(W) is the pump power in the signal guide.

rate	W_p (s^{-1})	W_{s1} (s^{-1})	W_{s2} (s^{-1})	W_{isc} (s^{-1})	W_{et} (s^{-1})	W_{40} (s^{-1})
value	5×10^{9} P(W)	4×10^{8}	10^{4}	4.3×10^{8}	10^{8}	10^{6}

rapidly to the luminescent $^4F_{3/2}$ state. We assume that the decay between adjacent levels is very fast, so that effectively the neodymium is excited directly into the $^4F_{3/2}$ level (N_4). We also assume rapid decay from the N_1, and N_2 levels to the ground state. The rate equations can then be written as:

$$\begin{aligned}
\frac{dS_0}{dt} &= -W_p S_0 + W_{s1} S_1 + W_{s2} T + W_{et} T N_0 \\
\frac{dS_1}{dt} &= +W_p S_0 - W_{s1} S_1 - W_{isc} S_1 \\
\frac{dT}{dt} &= +W_{isc1} S_1 - W_{s2} T - W_{et} T N_0 \\
\frac{dN_0}{dt} &= -W_{et} T N_0 + W_{40} N_4 \\
\frac{dN_4}{dt} &= +W_{et} T N_0 - W_{40} N_4
\end{aligned} \qquad (5.11)$$

The Nd population in N_4 is derived by solving these rate equations for steady state. The total concentration of lissamine is equal to the Nd concentration, i.e. $S_0+S_1+T = N_0+N_4 = N$. The fraction of excited Nd is given by: $f = N_4/N$. The values of the different rate constants are given in Table 5.2 and have been derived from spectroscopic measurements described in Chapter 3 except from W_{et}, which is estimated from oxygen quenching experiments,[11] and W_{s2} which is an estimate based on typical triplet state lifetimes.

References

1 P. G. Kik, and A. Polman, MRS Bulletin **23**, 48 (1998)

2 P. G. Kik, and A. Polman, Appl. Phys. Lett. **76**, 2325 (2000)

3 L. H. Slooff, A. Polman, S. I. Klink, G. A. Hebbink, L. Grave, F. C. J. M. van Veggel, D. N. Reinhoudt, and J. W. Hofstraat, Opt. Mat. **14**, 101 (2000)

4 H. Kogelnik, "Theory of dielectric waveguides" in Integrated Optics, Chapter 2, T. Tamir, 2nd ed. (New York, Springer-Verlag, 1979)

5 H. F. Taylor and A. Yariv, "Guided Wave Optics", Proc. IEEE **62**, 1044 (1974)

[6] S.-L. Chuang, J. Lightwave Techn. **5**, 5 (1987)
[7] S.-L. Chuang, in Physics of optoelectronic devices (Wiley-Interscience Publication, New York, 1995)
[8] S. Hongyuan, L. Tianguan, Z. Ruirong, Z. Yuping, Y. Guijang, H. Chenghui, L. Hong, and Z. Ahengdong, IEEE J. Quant. Elec. **25**, 144 (1989)
[9] H. Dai, O. M. Stafsudd, and B. Dunn, Appl. Opt. **30**, 4330 (1991)
[10] A. Sennaronglu, Opt. Comm. **164**, 191 (1999)
[11] S. I. Klink, Ph. D. Thesis, University of Twente, Enschede, The Netherlands (2000), ISBN 90-3651436-3

6 Luminescence properties of erbium-doped silica sol-gel films

Erbium-doped sol-gel films with Er concentrations between 0.05 and 1.0 at.% were formed by spin-coating a solution of erbium nitrate, tetra-ethoxy-silane, ethanol, water and HCl on a Si substrate. Refractive index, film thickness and composition were measured as a function of Er concentration. The Er concentration in the film is roughly proportional to the Er/Si ratio in solution, while the Si/O ratio varies with Er concentration. The film thickness increases for increasing Er concentration, which is attributed to the increased viscosity of the spin-coat solution compared to pure SiO_2. All films show a lower refractive index and atomic density than pure SiO_2,, which is ascribed to a slightly porous structure. After annealing at 900 °C the films show clear room-temperature luminescence at 1.53 μm from Er^{3+}. The luminescence lifetime is rather constant (10-12 ms) up to Er-concentrations of 1.0 at.%. The observation of a long luminescence lifetime implies that after annealing the films contain only a small amount of OH impurities. Annealing the films in air rather than in vacuum, leads to shorter lifetimes.

6.1 Er-doped sol-gel films

Er-doped silica glass materials are finding more and more applications in photonic technology. For example, Er-doped fibers are used as the gain medium in long-distance optical fiber links, operating at 1.53 μm. Er-doped silica channel waveguides find applications in planar optical amplifiers that are used in photonic integrated circuits,[1] and Er-doped colloidal silica particles might be integrated with polymer technology to fabricate nano-composite waveguide materials.[2] As the quantum efficiency of the luminescent Er^{3+} transition at 1.53 μm can be quite high, Er-doped silica could also find applications in photonic crystals, as a probe of the local optical density of states.[3]

Several methods have been developed to fabricate Er-doped silica films, including plasma-enhanced chemical-vapour-deposition,[4] ion implantation,[5] flame hydrolysis,[6] and ion exchange.[7] An alternative technique to deposit thin Er-doped silica films is by using a wet chemical process, in which a solution containing a silica precursor and erbium-nitrate is spin-coated on a substrate, followed by a drying step (the sol-gel process). The advantage of this technique is that many different constituents can be added to the solution in order to tailor the film composition, refractive index, and Er solubility. Besides that, the spin-coat technique makes it possible to use virtually any substrate.

Quite some research has been done on Er-doped sol-gel films.[8-14] In most cases, composite silica-based materials were studied, or bulk glasses were made rather than thin films, but only a few focus on pure silica sol-gel films. In this Chapter we make a systematic study of the effect of Er concentration on the film stochiometry, thickness, atomic density and refractive index for pure silica films with Er concentrations in the range 0.05-1.0 at.%. Luminescence spectra and lifetimes are studied versus Er concentration. We find that the luminescence lifetime depends critically on the annealing ambient. Films annealed in vacuum show lifetimes as high as 11 ms, the highest reported for Er-doped sol-gel films so far.

6.2 Experiment

Er-doped sol-gel films (set I) were prepared in the following way. First a tetra-ethoxy-silane (TEOS) reaction mixture was made: 23.0 g TEOS (Fluka 99%), 5.0 g ethanol (pro analysi, Merck), 5.9 g H_2O and 2.2 g 0.1 M HCl (Aldrich) were mixed, and then stirred while heated to a temperature of 70 °C, at which it was kept for 5 minutes. After stirring for three minutes, the solution changed from opaque to transparent. An Er solution was prepared by dissolving 3.1 g of $Er(NO_3)_3 \cdot 5H_2O$ (Aldrich 99.9%) into 10.0 ml ethanol. Solutions with different Er

concentrations were made by adding 0.05, 0.1, 0.3, 0.6, and 1.0 ml of the Er solution to 7.0 ml of the TEOS reaction mixture. In order to have a similar ethanol concentration in the different reaction mixtures, the volume of all solutions was made equal to 8.0 ml by adding ethanol. This solution was aged for 4.5 hours and then spin-coated onto pre-cleaned Si substrates, covered by a ~2 nm thick native oxide. Spin-coating was performed at 3500 rpm for 60 seconds.

After spin-coating the samples were dried at 60 °C for 10 minutes in air. For the annealing experiments two additional sets of samples (set II and III) were prepared using a mixture of 4.8 g TEOS, 1.1 g ethanol, 0.4 g H_2O and 0.5 g 0.1 M HCl, together with a solution of 0.29 g $Er(NO_3)_3 \cdot 5H_2O$ dissolved into 1 ml ethanol. After the same ageing period as mentioned above, the solution was spin-coated at 2000-4000 rpm, followed by a heat treatment of 60 ^oC for 10 minutes in air.

Sets I and II were annealed for one hour in vacuum (10^{-6} mbar) at 100 °C, followed by one hour at 900 ^oC (set I) or 750 ^oC (set II). Set III was annealed in air rather than vacuum at the same temperatures as set II.

Erbium depth profiles and film stoichiometry were measured by Rutherford Backscattering Spectrometry (RBS) using 2 MeV He^+ ions at a backscattering angle of 165°. Layer thickness and refractive index were measured using spectroscopic ellipsometry at incoming angles of 55, 60, 65, 70 and 75° relative to the surface normal. The wavelength was scanned from 300 to 1700 nm in 5 nm steps.

Photoluminescence (PL) measurements were performed using the 488 and 515 nm lines of an Ar ion laser as an excitation source operating at a power of 30 or 100 mW. The emitted luminescence was projected onto the entrance slits of a 48-cm monochromator and detected with a liquid-nitrogen cooled Ge detector. Standard lock-in techniques were employed, using a mechanical chopper to modulate the laser beam. The spectral resolution was 2-6 nm. Photoluminescence lifetime measurements were performed by monitoring the decay of the luminescence after switching off the light source. A digitising oscilloscope was used to average the decay curves. The time response of the system was 30 μs. An optical microscope was used to study the surface morphology of the sol-gel layers.

6.3 Film optical properties

RBS spectra of the Er-doped sol-gel layers of set I (before annealing) are shown in Fig. 6.1 for different Er concentrations. Surface channels for the elements O, Si and Er are indicated by dashed lines. The Si surface channel is observed around channel 260, corresponding to the Si in the SiO_2 film. The edge at channel 210 shows the interface between the Si substrate and the SiO_2 film. The

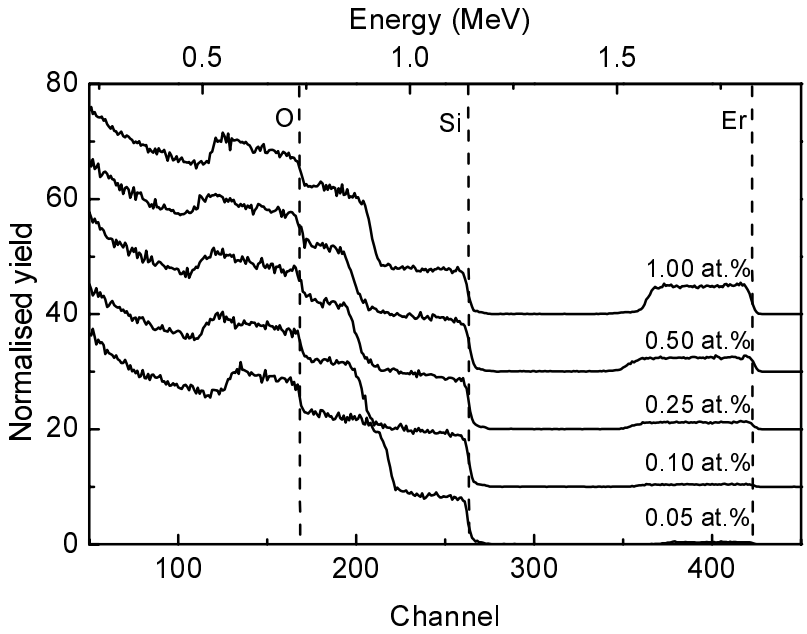

Figure 6.1 RBS spectra for Er-doped sol-gel films before annealing (set I). Data are shown for concentrations ranging from 0.05 to 1.0 at.%. Spectra are offset for clarity. Surface channels for O, Si, and Er are indicated.

Table 6.1 Er concentration estimated from the Er/Si ratio in the solution together with the areal density and layer composition of Er-doped sol-gel films derived from RBS measurements. The atomic density is derived from the areal density data together with the thickness measurements from ellipsometry in Fig. 6.2.

Er concentration from Er/Si ratio in solution (at.%)	Film composition (at.%)			Film areal density (10^{15} atoms/cm^2)	Atomic density (cm^{-3})
	Si	O	Er		
1.05	35	64	1.00	3000	4.1×10^{22}
0.63	45	55	0.50	3400	5.0×10^{22}
0.32	45	55	0.25	3400	5.1×10^{22}
0.11	45	55	0.10	3400	5.4×10^{22}
0.05	40	60	0.05	2500	4.6×10^{22}

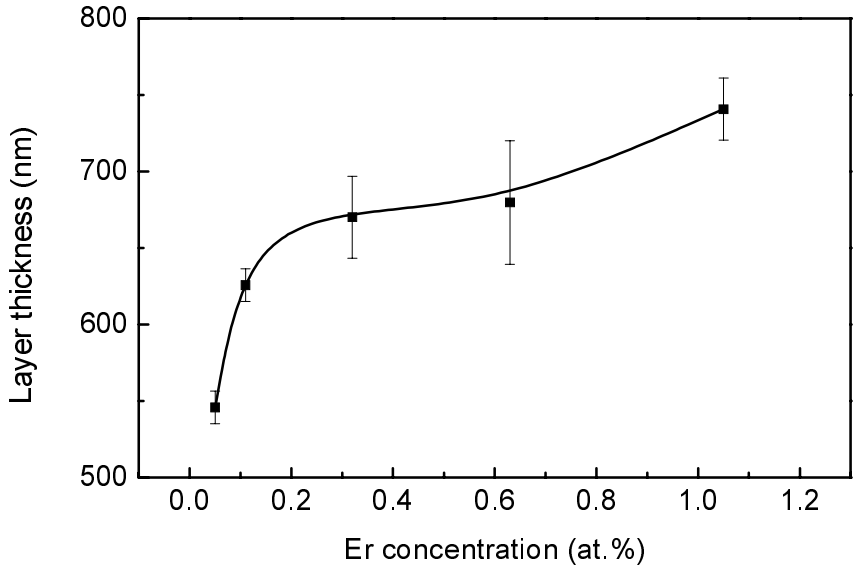

Figure 6.2 Layer thickness of the spin-coated Er-doped layers before annealing (set I) versus Er concentration, as derived from spectroscopic ellipsometry measurements.

plateau below channel 165 relates to the oxygen in the SiO_2 layer. The width of this plateau varies for the different Er concentrations, indicating differences in the layer thickness. The SiO_2 coverage derived from the width of these plateaus agrees with that derived from the width of the plateaus around channel 400, which show the erbium distribution in the film. From the ratio of erbium-nitrate to TEOS in the reaction solution, an estimate of the Er atomic concentration in each film can be made, assuming a stochiometric SiO_2 film composition. These estimates are shown in Table 6.1 together with the film compositions as derived from fits to the RBS spectra (fits not shown). As can be seen, the Er concentrations in the film are quite similar to the estimated values. This makes it possible to tailor the Er concentration rather accurately. Table 6.1 also shows the film areal density for all five layers as derived from RBS. As can be seen, the areal density and film composition are slightly different for the five Er concentrations. The layer with the highest Er concentration has an almost pure SiO_2 stoichiometry, while the other layers are somewhat Si-rich.

The thickness of the spin-coated layers of set I (before annealing), as measured by ellipsometry, is plotted in Fig. 6.2 versus the nominal Er concentration derived from the Er/Si ratio in solution. All measurements were performed in the center of the sample. As can be seen, the layer thickness increases with increasing Er concentration. This was also observed by Bruynooghe *et al.*[14] and was attributed to an increase in the initial solution viscosity for increasing Er concentration. Using the measured film thickness, the areal density from Table 6.1 can be converted into an atomic density, which is

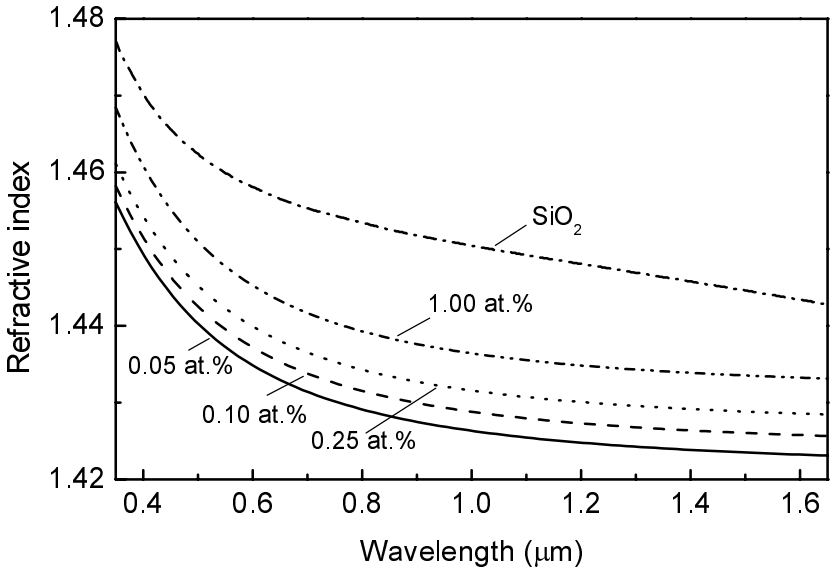

Figure 6.3 Refractive index as a function of wavelength for spin-coated films doped with different Er concentrations (before annealing). Data for thermally grown SiO_2 are also shown.[15]

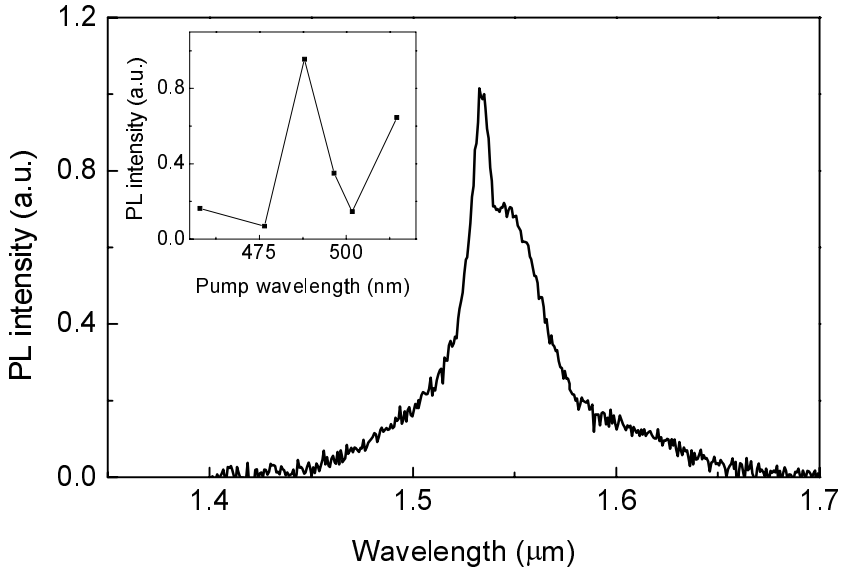

Figure 6.4 Photoluminescence spectrum of a 1.0 at.% Er-doped film (set I) annealed at 900 °C in vacuum. The excitation wavelength was 488 nm at a pump power of 30 mW. The inset shows a photoluminescence excitation spectrum of the 1.53 μm emission intensity.

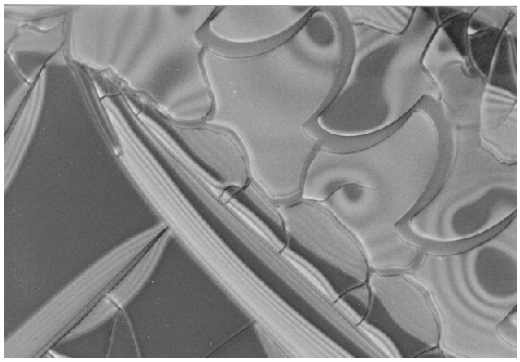

Figure 6.5 Optical microscope image of a vacuum annealed (900 °C, 1 hr) pure sol-gel film without Er. Cracks due to shrinkage of the film are clearly seen.

also shown in Table 6.1. The resulting atomic density is in the range $(4.1\text{-}5.5)\times10^{22}$ cm^{-3}, which is lower than that for pure SiO_2 (6.6×10^{22} cm^{-3}). Figure 6.3 shows the refractive index for these samples before annealing as a function of wavelength (set I) as obtained from ellipsometry measurements. The refractive index increases with increasing Er concentration, but stays well below that for thermally grown SiO_2 that is shown for reference. This, together with the fact that all films are relatively Si-rich (which would increase their refractive index compared to that of stochiometric SiO_2), and the lower atomic density compared to pure SiO_2 leads to the conclusion that the spin-coated materials have a porous structure before annealing.

Figure 6.4 shows a normalized PL spectrum of a 1.0 at.% Er-doped sol-gel film of set I, after annealing at 900 °C in vacuum for 1 hour. The spectrum was taken using an excitation wavelength of 488 nm at a pump power of 30 mW. The Er^{3+} luminescence around 1.53 μm is clearly visible and results from the intra-4*f* transition from the first excited state ($^4I_{13/2}$) to the ground state ($^4I_{15/2}$). The inset of Fig. 6.4 shows the 1.53 μm luminescence intensity as a function of excitation wavelength for the same sample. This spectrum reflects the structure of the optical absorption bands from the ground state ($^4I_{15/2}$) to the $^4F_{7/2}$ state (490 nm) and the $^2H_{11/2}$ state (514 nm), showing that the Er^{3+} ions in these SiO_2 layers are excited through direct optical excitation. This is well known for Er^{3+} in insulating materials,[16] in contrast to the case of Er in Si-rich oxide materials like e.g. amorphous Si/SiO_2[17] or Si nanocrystal-doped SiO_2[18,19] in which the Er^{3+} excitation is photocarrier-mediated.

We have tried to measure the PL intensity as a function of the Er concentration. Cracking of the films after annealing resulted in strong scattering of the laser light, making comparison of the absolute intensities difficult. However, in general the intensity increases for increasing concentration. An

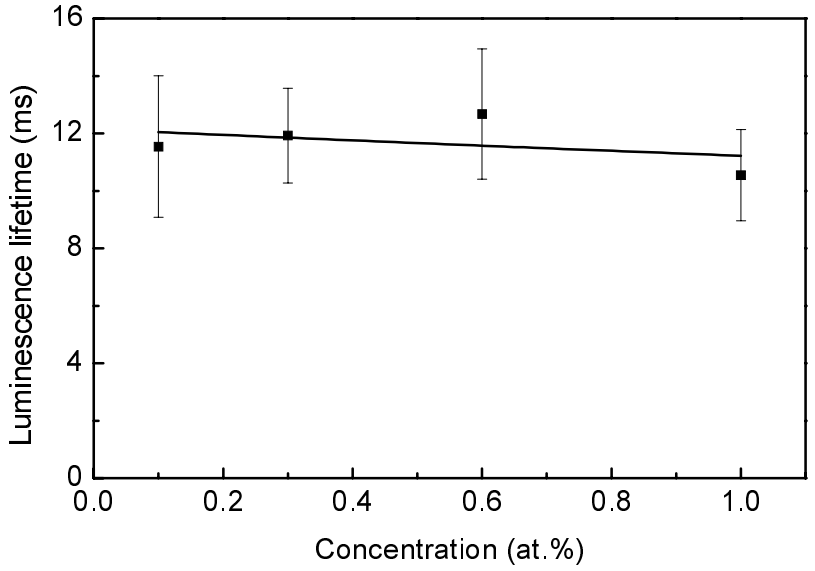

Figure 6.6 Luminescence lifetime for spin-coated sol-gel films annealed in vacuum (set I) as a function of Er concentration. The excitation wavelength was 515 nm at a pump power of 30 mW. The drawn line is a guide to the eye.

optical microscope image of a pure sol-gel film without Er annealed in vacuum at 900 ^{o}C for 1 hour is shown in Fig. 6.5. One can observe 'jig-saw-puzzle'-like pieces that clearly fit together, indicating that the cracks are the result of shrinkage.[20] It is well known that sol-gel films of several hundred nanometer thickness crack during annealing when water and organic residues evaporate from the film. It is also known that growing thinner layers and repeating the spin-coat-drying step several times can overcome this problem.[21]

The luminescence lifetimes for different Er concentrations are shown in Fig. 6.6 for the films of set I (samples annealed in vacuum at 900 ^{o}C). For Er concentrations up to 1.0 at.%, the luminescence lifetime remains more or less constant at 10-12 ms. Often, in highly Er doped materials, the luminescence lifetime is seen to decrease with concentration due to quenching by O-H impurities (the second overtone of the O-H stretch vibration is resonant with the Er transition at 1.53 μm).[22-26] This effect becomes apparent at high Er concentrations, when Er-Er energy migration takes place. The fact that we measure long luminescence lifetimes at high Er concentration thus indicates that most of the water is removed from the film during the anneal treatment. By taking a simple linear concentration quenching model, and assuming a typical Er-Er coupling constant of 10^{-51} m^3/s, we can estimate from the data in Fig. 6.6 the O-H concentration to be < 1 ppm. Note that this analysis is based on the assumption that Er does not precipitate after annealing, an effect that would reduce the amount of optically active Er. This assumption is supported by the observed increase in the luminescence intensity with Er concentration. Electron

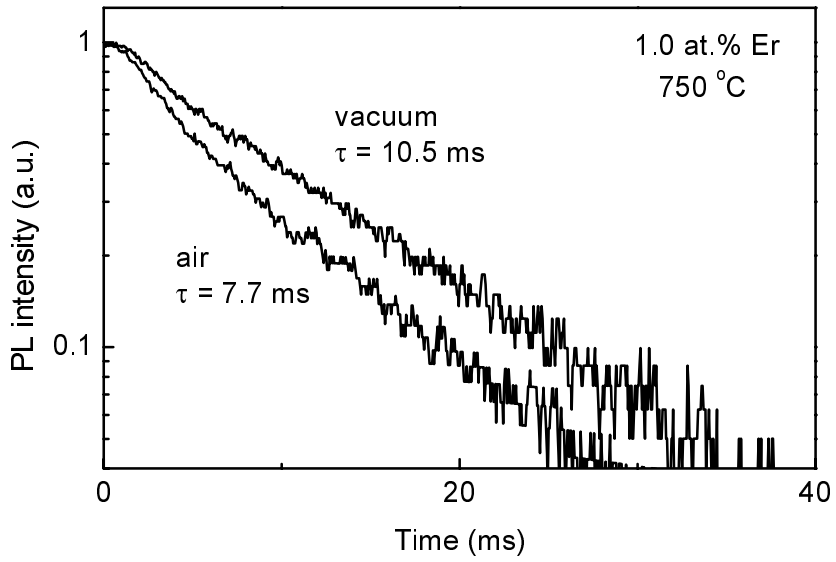

Figure 6.7 Luminescence decay traces (λ = 1.53 μm) for 1.0 at.% Er^{3+}-doped sol-gel films, annealed at 750 °C in vacuum (set II) or air (set III). The excitation wavelength was 515 nm at a pump power of 100 mW.

microscopy was performed to verify this, and although some dark spots with a size of several nm were visible, these could not be identified as being Er-rich. More work is necessary to confirm this.

The luminescence lifetimes in Fig. 6.6 are much longer than the lifetime of 1.78 ms reported by Orignac *et al.*[13] for similar Er-doped sol-gel films. The main difference between that work and the samples described here, is the fact that our films were annealed in vacuum, whereas the films by Orignac *et al.* were annealed in air. To study the effect of the annealing ambient, we prepared two new sets of 1.0 at.% Er-doped silica films. One set was annealed at 750 °C in vacuum (set II) and the other set in air (set III). Figure 6.7 shows PL decay traces for the two films. Clearly the air-annealed sample has a shorter lifetime (7.7 ms) than the vacuum-annealed sample (10.5 ms). A possible explanation is that in the case of an anneal in air more O-H remains in the film compared to the case of an anneal in vacuum, which might be due to a slower release of physically and chemically absorbed water. More research is needed to verify this.

6.4 Conclusions

Er-doped silica films were prepared by spin-coating a solution of erbium-nitrate, tetra-ethoxy-silane, ethanol, water and HCl on a Si substrate. Film thickness (550-750 nm) and composition vary slightly with Er concentration in the range 0.05-1.0 at.%. The refractive index and atomic density of the films is lower than

that of pure SiO_2, indicating that the films are porous. After annealing at 900 ^oC, room temperature photoluminescence at 1.53 μm is observed with a luminescence lifetime as long as 10-12 ms, for Er concentrations up to 1.0 at.%. Using a concentration quenching model we conclude that most of the water is removed from the film by the anneal treatment; the O-H content is estimated to be below 1 ppm. Anneals were also performed in air and lead to shorter luminescence lifetimes, possibly caused by a higher O-H content. Our measurements show that the sol-gel process in combination with vacuum annealing is ideally suited to obtain Er-doped silica exhibiting long Er luminescence lifetimes.

References

1 see for a review: P. G. Kik, and A. Polman, MRS Bulletin **23**, 48 (1998)

2 L. H. Slooff, M. J. A. de Dood, A. van Blaaderen, and A. Polman, Appl. Phys. Lett. **76**, 3682 (2000)

3 E. Snoeks, A. Lagendijk, and A. Polman, Phys. Rev. Lett. **74**, 2459 (1995)

4 K. Shuto, K. Hattori, T. Kitagawa, Y. Ohmori, and M. Horiguchi, Electr. Lett. **29**, 139 (1993)

5 A. Polman, J. Appl. Phys. **82**, 1 (1997)

6 T. Kitagawa, K. Hattori, K. Shuto, M. Yasu, M. Kobayashi, and M. Horiguchi, Electr. Lett. **28**, 1818 (1992)

7 T. Feuchter, E. K. Mwarania, J. Wang, L. Reekie, and J. S. Wilkinson, IEEE Phot. Techn. Lett. **4**, 542 (1992)

8 C. K. Ryu, H. Choi, and K. Kim, Appl. Phys. Lett. **66**, 2496 (1995)

9 X. Fan, M. Wang, and G. Xiong, Mat. Lett. **27**, 177 (1996)

10 B. T. Stone, and K. L. Bray, J. Non-Cryst. Solids **197**, 136 (1996)

11 Y. Kurokawa, T. Ishizaka, T. Ikoma, and S. Tero-Kubota, Chem. Phys. Lett. **287**, 737 (1998)

12 M. Benatsou, B. Capoen, M. Bouazaouni, W. Tchana, and J. P. Vilcot, Appl. Phys. Lett. **71**, 428 (1997)

13 X. Orignac, A. Barbier, X. M. Xu, and R. M. Almeida, Appl. Phys. Lett. **69**, 895 (1996)

14 S. Bruynooghe, A. Chabli, F. Bertin, and F. Pierre, J. Mater. Res. **12**, 2779 (1997)

15 E. D. Palik, in: Handbook of Optical Constants in Solids I (Academic Press, 1985)

16 V. Dierolf, and M. Koerdt, Phys. Rev. B. **61**, 8043 (2000)

17 S. Lombardo, S. U. Campisano, G. N. van den Hoven, A. Cacciato, and A. Polman, Appl. Phys. Lett. **63**, 1942 (1993)

18 P. G. Kik, M.L. Brongersma, and A. Polman, Appl. Phys. Lett. **76**, 2325 (2000)

19 M. Fujii, M. Yoshida, Y. Kanzawa, S. Hayashi, and K. Yamamoto, Appl. Phys. Lett. **71**, 1198 (1997)

20 L. C. Klein, Ann. Rev. Mater. Sci. **15**, 227 (1985)

21 A. S. Holmes, R. R. A. Syms, M. Li, and M. Green, Appl. Opt. **32**, 4916 (1993)

22 V. P. Gapontsev, A. A. Izyneev, Yu. E. Sverchov, and M. R. Syrtlanov, Sov. J. Quantum Electron. **11**, 1101 (1981)

23 E. Snoeks, P. G. Kik and A. Polman, Optical Materials **5**, 159 (1996)

[24] A. J. Bruce, W. A. Reed, A. E. Neeves, L. R. Copeland, W. H. Grodkiewicz, and A. Lidgard, Mat. Res. Soc. Symp. Proc. **244**, 157 (1992)
[25] Y. Yan, A. J. Faber, and H. de Waal, J. Non-Cryst. Sol. **181**, 283 (1995)
[26] F. Auzel, in: Radiationless Processes, B. DiBartolo, ed. (Plenum Press, New York, 1980)

7 Erbium-implanted silica colloids with high luminescence quantum efficiency

Silica colloids with a diameter of 244 or 360 nm, grown by wet chemical synthesis using ethanol, ammonia, water, and tetra-ethoxysilane, were implanted with 350 keV Er ion, to peak concentrations of 0.2-1.1 at.% and deposited onto a silicon or glass substrate. After annealing at 700-900 °C the colloids show clear room-temperature photoluminescence at 1.53 μm, with lifetimes as long as 17 ms. By comparing data for different Er concentrations the purely radiative lifetime is estimated to be 20-22 ms, indicating a high quantum efficiency of about 80 %. This high quantum efficiency indicates that after annealing the silica colloids are almost free of O-H impurities. Spinning a layer of polymethylmethacrylate over the silica spheres results in an optically transparent nanocomposite layer, that can be used as a planar optical waveguide amplifier at 1.5 μm that is fully compatible with polymer technology.

7.1 Introduction

Because of the increasing importance of polymer optical technology it is interesting to fabricate Er-doped planar polymer waveguides, for application in optical amplifiers operating at 1.5 μm. In Chapter 2-4, we have investigated organic rare earth complexes which can be dissolved in a polymer matrix.[1-3] Most of these complexes contain C-H bonds of which the second vibrational overtone can quench the rare-earth luminescence,[4,5] and an alternative approach is desired to incorporate Er in a polymer. As shown in Chapter 6, SiO_2 is an excellent host for rare-earth ions, yielding long luminescence lifetimes.[6,7] It would therefore be interesting to study if the easy processing of polymers could be combined with the long luminescence lifetime of Er in silica. In this Chapter we study the optical doping of colloidal silica particles using Er ion implantation. The influence of Er concentration and anneal temperature on the luminescence intensity and lifetime is determined. It is found that the silica colloids are an excellent host for Er, yielding a high quantum efficiency. As a first demonstration of the possible application in polymer waveguides, optical transmission measurements are shown for a polymer film doped with these Er-doped silica colloids.

7.2 Experiment

Silica colloids with a diameter of 244 or 360 nm were synthesised as described by van Blaaderen *et al*.[8] Solutions of 10 ml ethanol, 0.7 ml NH_3 (28 wt.% in water), 0.8 ml H_2O and 0.4 ml tetraethoxysilane (TEOS, 99%) were mixed and stirred for 1 hour at room temperature, resulting in nucleation and growth of silica colloids with a diameter of 244±10 nm, as measured using scanning electron microscopy (SEM). In one set of samples, the diameter of the spheres was increased to 360 nm by subsequent addition of TEOS to the reaction vessel.[9] After the reaction, the suspension was centrifuged and the remaining colloids were dissolved in pure ethanol. Droplets of the solution were put onto a silicon substrate or a microscope cover glass (cleaned with a 1 M KOH/ethanol solution). After evaporation of the ethanol, a thin layer of colloids remained. Next, the samples were irradiated with 350 keV Er^+ ions at various fluences ranging from 0.9×10^{15} to 5.5×10^{15} ions/cm^2. The projected range of 350 keV Er^+ in silica is 160 nm. Implantation of these ion fluences into a planar film results in a Gaussian Er distribution with a full width at half maximum (FWHM) of 34 nm. It is obvious that in these non-uniform, colloidal layers a less well-defined concentration profile builds up. After implantation the samples were annealed in vacuum at 100 °C for one hour and then for another hour at different temperatures in the range 700-1000 °C.

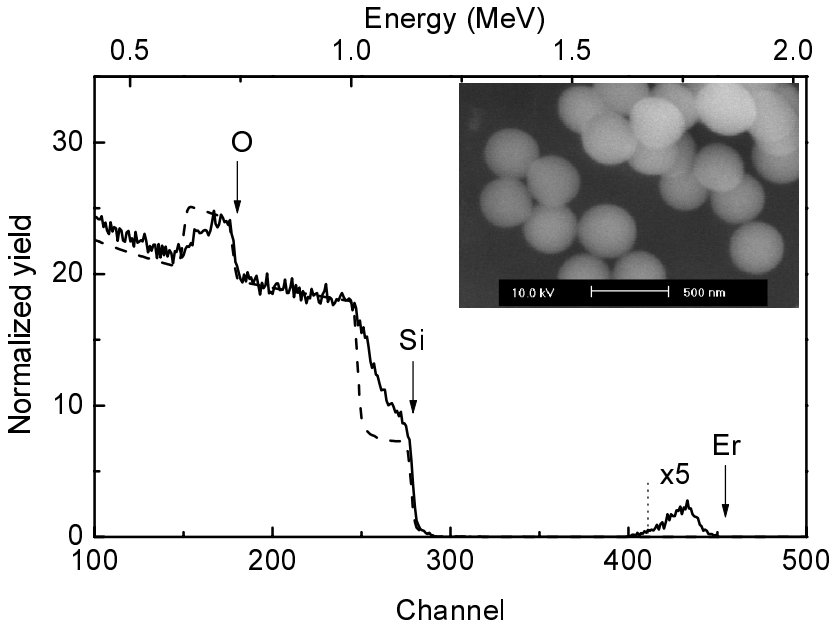

Figure 7.1 RBS spectrum of a single layer of Er-implanted (350 keV, 9×10^{15} Er/cm^2) silica colloids on a Si substrate (solid line). 2 MeV He^+ ions were used at a scattering angle of 165°. A simulation of a 360 nm SiO_2 film on a silicon substrate (dashed line) is also shown. The dashed line at channel 410 indicates the position of the SiO_2/Si interface for Er. The inset shows a SEM image of the same sample.

In order to study the Er incorporation in the colloids, Rutherford backscattering spectroscopy (RBS) measurements were performed, using a 2 MeV He^+ beam at a scattering angle of 165°. Scanning electron microscopy (SEM) was performed at an electron energy of 10 keV. Photoluminescence (PL) measurements were performed using the 488 nm and 515 nm lines of an Ar ion pump laser at a power density of 50-60 mW/mm^2. The laser beam was modulated with an acousto-optic modulator. The PL signal was focused into a 48-cm monochromator and detected with a liquid-nitrogen cooled Ge detector, using standard lock-in techniques, yielding a spectral resolution of 6 nm. Lifetime measurements were performed by monitoring the decay of the luminescence after switching off the light source. A digitising oscilloscope was used to average the decay curves. Optical transmission measurements were performed at normal incidence using a spectrometer at wavelengths ranging from 300-1700 nm.

7.3 Results and discussion

Figure 7.1 shows an RBS spectrum of a Si sample covered with a single layer of 360 nm diameter colloids, implanted with 9×10^{14} Er/cm^2. For reference, a simulation of a 360 nm pure SiO_2 layer on a Si substrate is shown (dashed line).

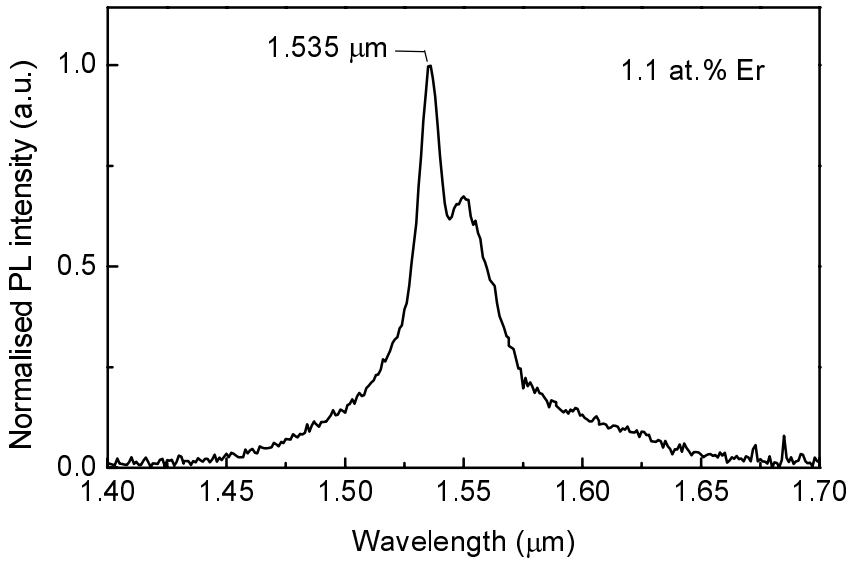

Figure 7.2 Photoluminescence spectrum for a thick layer of silica colloids, implanted with Er (1.1 at.%), taken using 515 nm pump light at a power density of 60 mW/mm^2.

The surface channels of Er, Si and O are indicated by the arrows. The Si content at the surface is almost similar to the Si content in pure SiO_2, indicating that the substrate is almost completely covered with colloids. The Si yield then increases with decreasing energy, as a result of the spherical shape of the colloids. The Si yield coincides with that of the simulation at channel 245, consistent with the colloid diameter of 360 nm. The signal between channel 400 and 500 is due to the implanted Er. The Er peak concentration is 0.18 at.%. Note that a small fraction of the implanted Er has entered the Si substrate, as is evident from the Er tail near channel 400. The inset in Fig. 7.1 shows a SEM image of deposited colloids (360 nm diameter), showing a rather disordered array of particles extending over several layers.

The samples used for PL measurements consisted of about 3-4 layers of silica colloids, as determined from RBS and SEM. Figure 7.2 shows the PL spectrum of colloidal silica particles implanted to a peak concentration of 1.1 at.% and annealed at 950 °C for 1 hour. SEM showed that the implantation and annealing caused no deformation of the silica spheres. The spectrum shows typical Er^{3+} luminescence around 1.53 μm due to transitions from the $^4I_{13/2}$ to the $^4I_{15/2}$ level. The two peaks result from Stark splitting of the Er^{3+} levels and are characteristic for Er^{3+} in SiO_2.[1] The width (32 nm FWHM) is due to the thermal distribution over the Stark levels as well as inhomogeneous broadening. It is difficult to compare PL intensities for different implanted samples as the colloid coverage varies from sample to sample, and because of the fact that the pump beam is strongly scattered by the silica spheres, which results in non-uniform pumping. However, on average the intensity increases for increasing doping

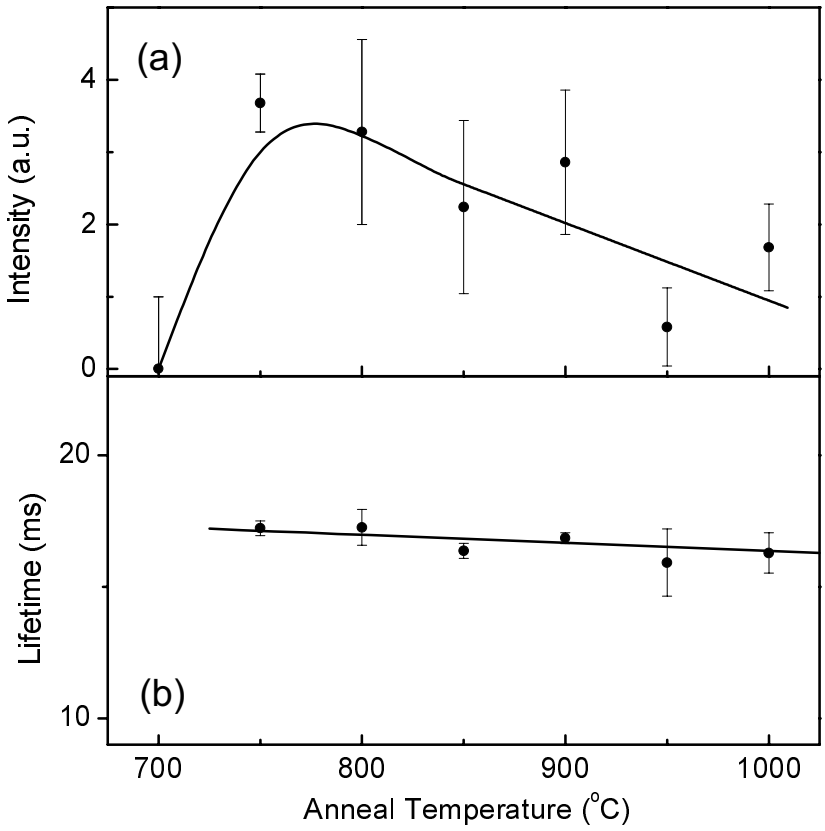

Figure 7.3 (a) Average peak photoluminescence intensity at 1.53 μm as a function of anneal temperature for Er-implanted silica spheres (0.2 at.%). Pump wavelength 488 nm, pump power 50 mW. The large error bars are due to the large variation in colloid coverage over the surface. (b) Luminescence lifetime of Er-implanted silica spheres (0.2 at.%) as a function of anneal temperature.

concentration up to at least 1.1 at.%.

Figure 7.3(a) shows the peak PL intensity of samples implanted with 0.2 at.% Er, annealed at various temperatures for 1 hour. Below 700 °C, no measurable PL was observed. This might be due to water that is physisorbed on the surface or trapped in the pores of the silica matrix. Water is known to quench the Er^{3+} luminescence, as the first overtone of the O-H vibration ($E_0 = 3400$ cm^{-1}) is strongly resonant with the Er^{3+} transition ($E = 6500$ cm^{-1}). Indeed, work by Fan *et al.*[10] and Tien *et al.*[11] on bulk silica samples, grown in a similar way as the colloids, shows that between room temperature and 200 °C, weakly bound water and residual organic molecules vaporise, followed by the removal of chemically bound molecular water between 300 and 800 °C. Figure 7.3(a) shows large scatter in the data above 700 °C, but the general trend is a decrease in PL intensity, certainly for temperatures above 900 °C. This may be due to the precipitation of Er, as has been observed before in Er implanted SiO_2.[8]

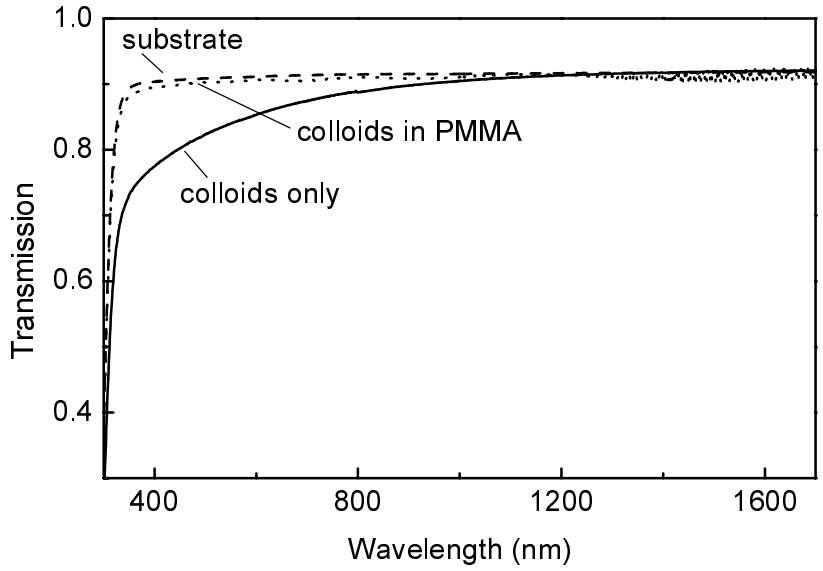

Figure 7.4 Optical transmission measurements of a 1 μm silica/polymer nanocomposite film on a microscope cover glass (dotted line) and of a cover glass with colloids only (solid line). Measurements are also shown for a bare cover glass (dashed line).

Figure 7.3(b) shows luminescence lifetime measurements as a function of anneal temperature for an Er concentration of 0.2 at.%. For anneal temperatures below 700 °C the PL intensity was too low to perform lifetime measurements. The lifetime for anneal temperatures between 750 and 1000 °C is about 17 ms and is almost independent of anneal temperature.

We have also performed lifetime measurements for samples implanted at higher doses, and found that increasing the Er concentration from 0.2 to 1.1 at.% results in a decrease in the luminescence lifetime from 17 to 10 ms. These lifetimes are among the highest observed in silica glass. Assuming that the decrease in lifetime is due to concentration quenching, we can estimate the radiative lifetime by linearly extrapolating to zero Er concentration[12] and find τ_{rad} = 20-22 ms. The long lifetimes observed in this work show that silica glass made by wet chemical synthesis is an excellent host for Er. It indicates that the water impurity content in this glass after annealing is very small (< 1 ppm). [13] We note that the long radiative lifetime can be partly attributed to the fact that the Er-implanted colloids are surrounded by air and are relatively far away from the high-index Si substrate, causing the local optical density of states in the colloids to be lower than that of bulk SiO_2.[13,14] This will be further discussed in Chapter 8.

Two months after the first PL measurements on the Er-implanted colloidal particles, we performed the same measurements again and found that the luminescence intensity and lifetime were strongly reduced. After annealing at 475 °C, both the luminescence intensity and lifetime returned to the level

observed after the initial anneal. This suggests that some time after the anneal, a thin film of water covers the colloids. This makes it necessary to coat the silica spheres with a protective layer, e.g. a polymer.

In order to investigate the application of these colloids in polymer waveguides, undoped silica colloids with a diameter of 244 nm were deposited onto a microscope cover glass. Next, the samples were annealed for one hour at 100 °C, and subsequently a solution of 1.5 g polymethylmethacrylate (PMMA) in 10 ml chloroform was spun onto the substrate at a spin-rate of 2000 rpm for 30 s, resulting in a 1 μm thick film. An optical transmission measurement on this colloid/polymer nanocomposite film is shown in Fig. 7.4 as the dotted line. For reference, a spectrum of the glass substrate is shown (dashed line), together with the transmission spectrum of the substrate covered with silica spheres (without polymer, solid line). As can be seen, without the polymer coating, the transmission at short wavelengths is strongly reduced due to scattering by the silica spheres. Covering the spheres (n = 1.43) with a PMMA (n = 1.48) layer reduces the scattering by reducing the refractive index difference between the SiO_2 colloids and its surroundings. Note that in this measurement the interaction length is only ~1 μm. In a homogeneously doped polymer waveguide with a length of a few cm the effect of scattering will be stronger. This will be discussed in the next section.

7.4 Performance estimate of a polymer/colloid nano-composite waveguide amplifier

Calculation of scattering losses

Er-doped silica spheres can be coated with alkoxy-groups, which make them soluble into a polymer layer. These polymer-colloid nanocomposite layers can then be used in a polymer based optical amplifier operating at 1.5 μm. For this kind of application, it is important that the Er-doped layers have very low intrinsic losses. One loss component may be caused by the refractive index mismatch between colloid and polymer. In the Rayleigh limit, where the colloid radius r is smaller than the wavelength, the scattering cross section of a colloid with refractive index n_c embedded in a medium with refractive index n_m is given by:

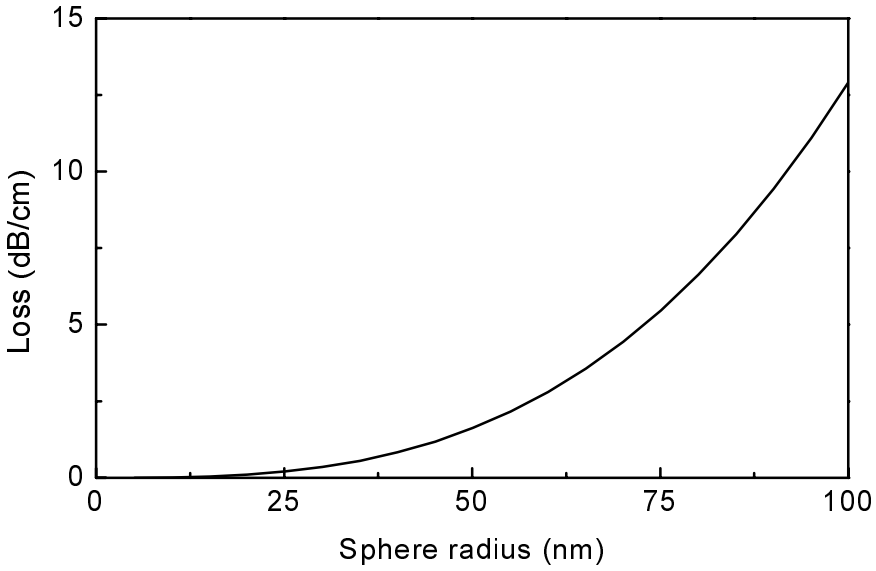

Figure 7.5 Scattering loss per unit length as a function of sphere radius for SiO_2 spheres (n = 1.45) embedded in a PMMA film (n = 1.48).

$$C_{sca} = \frac{8}{3}\left(\frac{2\pi n_c r}{\lambda}\right)^4 \cdot \left(\frac{\left(\frac{n_c}{n_m}\right)^2 - 1}{\left(\frac{n_c}{n_m}\right)^2 + 2}\right)^2 \pi r^2 \qquad (7.1)$$

The total scattering coefficient is then given by:

$$\alpha_{sca} = \frac{3\eta C_{sca}}{4\pi r^3} \qquad (7.2)$$

where η is the fill fraction of the spheres in the polymer host.

Figure 7.5 shows the scattering loss per unit length as a function of sphere radius for a typical case, i.e. a refractive index of the polymer n_m = 1.48 (typical for PMMA at 1.5 μm), and n_c = 1.45 for the silica spheres, and a fill fraction of 0.6. As can be seen, the scatter loss rapidly increases for increasing particle size, and (for this particular index mismatch) the sphere radius should be kept below ~ 40 nm in order to keep the scattering losses below 1 dB/cm.

Figure 7.6 shows the maximum particle radius as a function of index mismatch, that is calculated to yield a waveguide loss of 0.1 dB/cm. As can be seen, for a particle with a radius of 50 nm, the refractive index difference has to be kept below ~0.008. One should also keep in mind that the dependence of

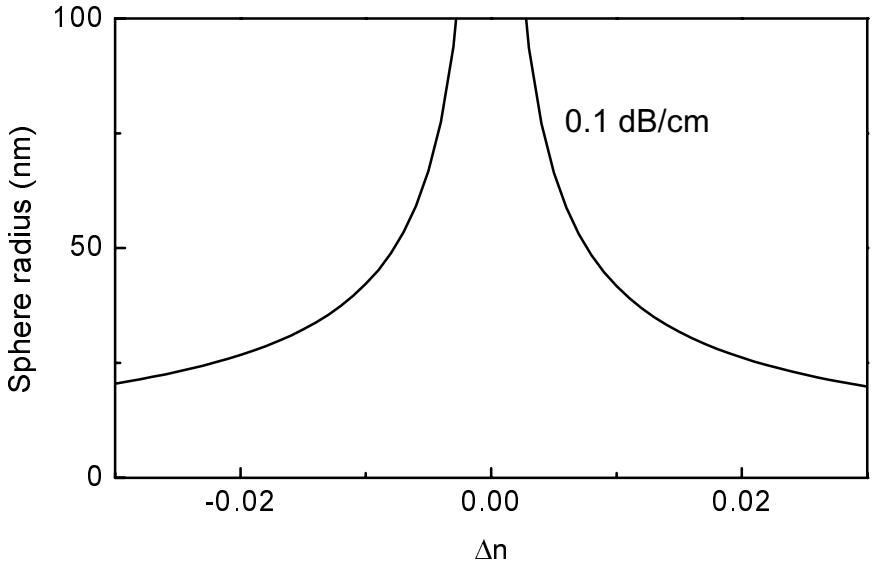

Figure 7.6 Maximum sphere radius as a function of refractive index mismatch Δn between the polymer layer and SiO_2 spheres, yielding a scattering loss of 0.1 dB/cm.

refractive index on temperature is different for the SiO_2 and the polymer. An increase of 100 ^oC in temperature results in a relative index difference of 0.02 as calculated using the Clausius-Mossotti relation and the known thermal expansion coefficients of the polymer and SiO_2. As can be seen in Fig. 7.6, this means that the maximum particle radius has to be about 25 nm, in order to keep the scattering losses below 0.1 dB/cm over a temperature range of 100 ^oC. The data in Figs. 7.5 and 7.6 illustrate that the refractive index of the polymer must be tuned very precisely.

Optical gain

Assuming that the waveguide loss due to scattering can be eliminated, an estimate of the optical gain for an Er-doped silica sphere/polymer nano-composite optical waveguide can be made. The optical gain as function of the waveguide length L is calculated using the following equation:

$$\text{gain (dB)} = 4.34 \times \int_0^L \left(\sigma_{21s} N_2 - \sigma_{12s} N_1 - \sigma_{24} N_2\right) dz \qquad (7.3)$$

in which σ_{21s} and σ_{12s} are the cross sections for stimulated emission and absorption at the signal wavelength (λ = 1535 nm), σ_{24} the signal excited state absorption cross section, and N_1 and N_2 the populations of the ground and first

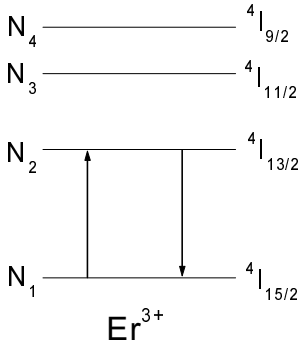

Figure 7.7 Schematic energy diagram of Er^{3+}. The notation on the right shows the Russel-Saunders notation of the different levels, whereas the notation on the left shows the symbols as used in the rate equations of Eq. 7.4.

excited state of the Er^{3+} ion, respectively (see Fig. 7.7). These populations are obtained by solving the following rate equations for steady state conditions, and include the effect of cooperative upconversion,[15-18] in which two neighbouring excited Er^{3+} ions interact and exchange energy, as well as excited state absorption,[19,20] in which an Er^{3+} ion in the N_2 level absorbs a pump photon, exciting it into the N_4 level:

$$\begin{aligned}
\frac{dN_1}{dt} &= -R_{12}N_1 + R_{21}N_2 + \frac{N_2}{\tau_2} + C_{24}N_2^2 = 0 \\
\frac{dN_2}{dt} &= R_{12}N_1 - R_{21}N_2 - \frac{N_2}{\tau_2} + \frac{N_3}{\tau_3} - 2C_{24}N_2^2 - R_{24}N_2 = 0 \\
\frac{dN_3}{dt} &= -\frac{N_3}{\tau_3} + \frac{N_4}{\tau_4} = 0 \\
\frac{dN_4}{dt} &= -\frac{N_4}{\tau_4} + C_{24}N_2^2 + R_{24}N_2 = 0 \\
N_1 + N_2 + N_3 + N_4 &= N
\end{aligned} \qquad (7.4)$$

where N_i are the Er^{3+} populations in the first 4 energy levels (see Fig. 7.7), N the total Er^{3+} concentration, τ_i is the luminescence lifetime of state N_i, R_{12} the pump rate, R_{21} the rate of stimulated emission by the pump, R_{24} the excited state absorption rate and C_{24} the coefficient for cooperative upconversion. The rates R_{ij} are equal to $(\sigma_{ij}P\lambda)/(hca)$, with σ_{12} and σ_{21} the absorption and stimulated emission cross sections at the pump wavelength (λ = 1480 nm), σ_{24} the excited state absorption cross section, h Planck's constant, c the speed of light, a the waveguide cross section, η the mode overlap with the waveguide core, and P the pump power along the length of the waveguide.

Calculating P over the length of the waveguide, the populations of the ground state and first excited state can be calculated over the entire waveguide. These populations are then put into Eq. 7.4 in order to calculate the optical gain. The parameters used in the calculation are given in Table 7.1. Cross sections and lifetimes were taken from earlier work on Er-implanted silica glass. The

Table 7.1 Parameters and their symbols as used in the optical gain calculation for the Er-doped silica sphere/polymer nano-composite optical waveguide amplifier

Parameter	Symbol	Value
refractive index of sphere	n_c	1.45
refractive index of medium	n_m	1.45
pump wavelength	λ	1.480 μm
pump absorption cross section[21]	σ_{12}	1.0×10^{-21} cm^2
pump emission cross section[21]	σ_{21}	0.5×10^{-21} cm^2
signal absorption cross section[21]	σ_{12s}	4.1×10^{-21} cm^2
signal emission cross section[21]	σ_{21s}	5.0×10^{-21} cm^2
upconversion coefficient[18]	C_{24}	3.2×10^{-18} cm^3/s
excited state absorption cross section[22]	σ_{24}	0.5×10^{-21} cm^2
luminescence lifetime level 2 [23]	τ_2	$0.8\times(48+46\times N_{at})^{-1}$ s
luminescence lifetime level 3 [24]	τ_3	10^{-6} s
luminescence lifetime level 4 [21]	τ_4	10^{-9} s
erbium concentration in spheres	N_{at}	0.4 at.%
fill fraction of spheres/medium	η	0.6
atomic density of SiO_2	ρ	6.60×10^{22} at/cm^3
total erbium concentration	N	$\eta\times N_{at}\times\rho$ at/cm^3
input pump power	P_0	5 mW
waveguide cross section	a	2.56×10^{-8} cm^2
mode overlap	η	40%
waveguide loss		0 dB/cm

expression for τ_2 includes the effect of concentration quenching as measured in Fig. 8.4, and a factor 0.8 for the change in decay rate relative to the decay rate measured on Er-implanted colloids because of the enhanced local density of states due to the presence of the polymer (see paragraph 8.3). The waveguide cross section was chosen such that it supports the first-order mode in a waveguide based on a SiO_2 sphere doped polymethylmethacrylate (PMMA) guiding layer (n = 1.45) and a fluorinated PMMA cladding layer (n = 1.37). Note that due to the high index contrast that can be achieved using polymers, very well confined optical modes can be achieved, leading to a low pump threshold for optical gain. Figure 7.8 shows the calculated optical gain as a function of the length of the waveguide for two different Er concentrations at a pump power of 20 mW. As can be seen, for a given Er concentration, the gain first increases,

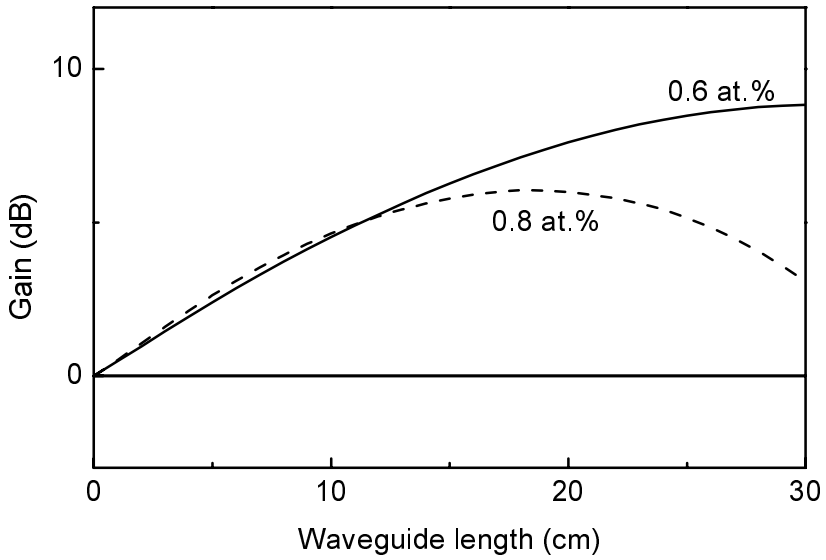

Figure 7.8 Total gain as a function of waveguide length for an Er-doped colloid/polymer composite waveguide amplifier pumped at 1.48 μm. Data are shown for Er concentrations in the colloid of 0.6 at.% (solid line) and 0.8 at.% (dashed line), at an input power of 20 mW.

reaches a maximum, and then decreases again. This is due to the fact, that at the entrance of the waveguide, the pump power is high enough to create population inversion between the first excited state and the ground state, but as the pump power decreases along the length of the waveguide, due to absorbing Er^{3+} ions, at some point the pump power is no longer sufficient to create population inversion, resulting in net absorption. The higher the Er^{3+} concentration, the shorter the waveguide length at which maximum gain is achieved. The fact that a lower maximum gain is achieved for the higher concentration is due to the effect of cooperative upconversion at high concentration.

Next the optical gain was calculated as a function of pump power for an Er^{3+} concentration of 0.8 at.% and an amplifier length of 15 cm. The result is shown in Fig. 7.9. At zero pump power the Er^{3+} ions only absorb and no population inversion is established, resulting in negative gain. At a pump power of about 10 mW, population inversion is reached and optical gain is achieved. Further increasing the pump power to 50 mW results in a maximum optical gain of 12 dB. Note that at a given pump power the optical gain in these silica colloid/polymer amplifiers is much higher than that in a pure silica waveguide amplifier. This is due to the fact that in this new design a large index contrast between polymer cladding and core can be chosen, leading to high mode confinement. This high index contrast also enables waveguide bends with relatively small bending radii so that by using the proper spiral geometry[24] a 15 cm long waveguide amplifier can be rolled up to a size of only 16 mm^2.

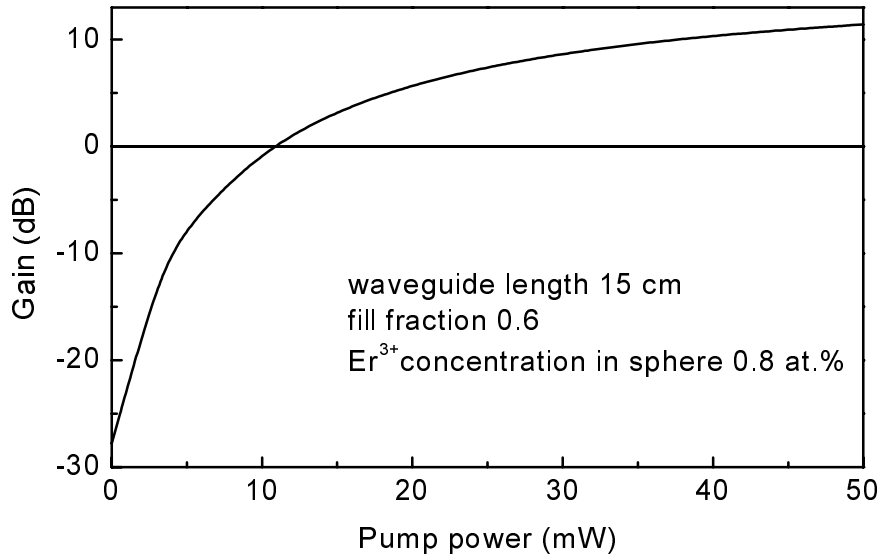

Figure 7.9 Total gain at 1.535 μm as a function of input pump power for a 15 cm long waveguide amplifier at an Er concentration of 0.8 at.%.

7.5 Conclusions

In conclusion, we have observed room-temperature luminescence at 1.5 μm from Er-implanted silica colloidal spheres. The luminescence lifetime of Er is about 17 ms, and the quantum efficiency is estimated to be 80 %. Thermal annealing at 750 °C is required to optimise the luminescence intensity. The colloids can be embedded in a polymer to achieve an optically active nanocomposite waveguide layer. It is shown that the refractive index of the polymer and colloids must be nearly matched, and that the size of the spheres has to be relatively small in order to have tolerable scattering losses. Calculations of the optical gain that can be achieved with these Er-doped silica sphere/polymer nano-composite optical waveguide amplifiers show a maximum gain of 12 dB for a 15 cm long amplifier and an Er concentration of 0.8 at.%.

References

1 S. Lin, J. Feuerstein, and A. R. Mickelson, J. Appl. Phys. **79**, 2868 (1996)

2 L. H. Slooff, A. Polman, M. P. Oude Wolbers, F. C. J. M. van Veggel, D. N. Reinhoudt, and J. W. Hofstraat, J. Appl. Phys. **83**, 497 (1998)

3 L. H. Slooff, A. Polman, S. I. Klink, G. A. Hebbink, L. Grave, F. C. J. M. van Veggel, D. N. Reinhoudt, and J. W. Hofstraat, Opt. Mat. **14**, 101 (2000)

[4] G. Stein, and E. Würzberg, J. Chem. Phys. **62**, 208 (1975)
[5] V. L. Ermolaev and E. B. Sveshnikova, Russ. Chem. Rev. **63**, 905 (1994)
[6] A. Polman, D. C. Jacobson, D. J. Eaglesham, R. C. Kistler, and J. M. Poate, J. Appl. Phys. **70**, 3778 (1991)
[7] W. J. Miniscalco, J. Lightwave Techn. **9**, 234 (1991)
[8] A. van Blaaderen and A. Vrij, Langmuir **8**, 2921 (1993)
[9] D. L. J. Vossen, M. J. A. de Dood, T. van Dillen, L. H. Slooff, C. M. van Kats, T. Zijlstra, E. van der Drift, A. Polman, and A. van Blaaderen, Adv. Mat. **12**, in press (October 1, 2000)
[10] X. Fan, M. Wang, and G. Xiong, Mat. Sc. Eng. B**21**, 55 (1993)
[11] P. Tien, and L-K Chau, Chem. Mater. **11**, 2141 (1999)
[12] E. Snoeks, P.G. Kik and A. Polman, Opt. Mat. **5**, 159 (1996)
[13] W. Barnes, J. Modern Optics **45**, 661 (1998)
[14] E. Snoeks, A. Lagendijk, and A. Polman, Phys. Rev. Lett. **74**, 2459 (1995)
[15] F. Auzel, J. Lumin. **45**, 341 (1990)
[16] P. Blixt, J. Nilsson, T. Carlnäs, and B. Jaskorzynska, IEEE Photon. Techn. Lett. **3**, 996 (1991)
[17] C. C. Ye, P. R. Morkel, E. R. Taylor, and D. N. Payne, in *Proc. 19th European Conference on Optical Communication*, **2**, 73, (Montreux, 1993)
[18] E. Snoeks, G. N. van den Hoven, A. Polman, B. Hendriksen, M. B. J. Diemeer, and F. Priolo, J. Opt. Soc. Am. B **12**, 1468 (1995)
[19] C. G. Atkins, J. R. Armitage, R. Wyatt, B. J. Ainslie, and S. P. Craig-Ryan, Opt. Com. **73**, 217 (1989)
[20] R. S. Quimby, W. J. Miniscalco, and B. Thompson, in Proc. SPIE, **1789**, 50 (1993)
[21] L. Cognolato, C. De Bernardi, M. Ferraris, A. Gnazzo, S. Morasca, and D. Scarano, CSELT Tech. Rep. **XIX**, 277 (1991)
[22] E. Desurvire, in: Erbium-Doped Fiber Amplifiers (Wiley, New York, 1994)
[23] see Chapter 8
[24] typical order of magnitude, see e.g. G. N. van den Hoven, A. Polman, C. van Dam, J. W. M. van Uffelen, and M. K. Smit, Appl. Phys. Lett. **68**, 1886 (1996)

8 Local optical density of states in SiO_2 colloidal spheres

The local optical density of states (DOS) in SiO_2 colloidal spheres was calculated using a Green's function method, and probed experimentally by measuring the 1.54 μm luminescence decay rate of Er ions implanted into the colloids. The radiative decay rate of Er in bulk SiO_2 was first determined in a planar SiO_2 film using a technique in which the DOS was varied by bringing the film in close contact with liquids with different refractive index. The obtained radiative decay rate ($W_r = 54 \pm 10\ s^{-1}$) was then used to analyse the changes in the Er decay rate in the SiO_2 colloids as they were embedded in a polymer film. Good agreement was found between the calculated and experimentally probed DOS in the colloids.

8.1 Introduction

The spontaneous emission rate of an atom in a given host is not exclusively an intrinsic property, but can be altered by changing the local optical environment of the atom. The presence of dielectric boundaries changes the local electric field fluctuations and modifies the spontaneous emission rate. Such effects have been demonstrated for atoms placed in microcavities,[1-3] photonic bandgap materials,[4-6] thin films,[7] or close to a dielectric interface.[8-11]

The changes in decay rate can be calculated by calculating the local density of states (DOS) and then applying Fermi's Golden Rule to obtain the radiative decay rate. It has been shown that the radiative decay rate is proportional to this local DOS, both in a scalar approximation[12] and for the full Maxwell equations.[13-15] For relatively simple geometries such a local DOS can be calculated using either a full set of eigenfunctions of the Helmholtz wave equation[16-18] or by using Green's functions.[19] For more complicated systems, such as photonic crystals[12,13] or absorbing materials[14,20-22] it is more difficult to calculate changes in decay rate, and optical probe atoms can be used to experimentally probe the DOS. In general, the measured changes in decay rate cannot be compared directly to theoretical results because non-radiative processes that occur parallel to the radiative decay have to be taken into account. Therefore, in experimental studies of the DOS, the ions must be incorporated in a reproducible way, and non-radiative and radiative decay rates must be known first.

Erbium-implanted silica colloids have been studied for use in polymer-based planar optical amplifiers and the results were discussed in Chapter 7. The Er showed very long luminescence lifetimes up to 17 ms, which are among the highest reported for Er-doped SiO_2. However, as these silica spheres were surrounded by air, the local DOS could be significantly different from that of Er-doped SiO_2 films, and as a result, the radiative lifetime could be different.

In this Chapter, a comparison is made between measured decay rates of optically active Er^{3+} ions incorporated in SiO_2 colloidal spheres and the calculated local DOS in the colloids. To separate radiative and non-radiative components in the decay, a reference sample was made composed of a planar erbium implanted SiO_2 layer on a silicon substrate. The local DOS in the film was changed by bringing it in contact with liquids with different refractive index. The resulting changes in the decay rate were used to determine the radiative decay rate of Er ions in bulk SiO_2. These data were then used to analyse the changes in decay rate of Er-doped SiO_2 spheres that were observed upon changing the DOS by embedding them in a polymer matrix.

8.2 Experiment

SiO_2 colloidal spheres with a diameter of 175 or 340 nm (± 5%) were made following the same procedure as described in Chapter 7. The spheres were deposited on Si(100) substrates that were cleaned for 15 min in a 1.0 M KOH solution. A droplet of the spheres dissolved in ethanol was put on the substrate and the ethanol was let to evaporate.

SiO_2 layers of 100 nm thickness were grown on a Si substrate in two consecutive steps using a reaction mixture of tetra-ethoxy-silane (TEOS), ethanol, water, and ammonia.[23] The substrates were put into the reaction mixture and the layer was grown under continuous stirring for 2 hours. Note that the both the colloids and the film are grown using the same (base catalised) wet chemical reaction.

The 100 nm thick SiO_2 layers and 175 nm diameter spheres were implanted at room-temperature with 70 keV Er^+ ions to fluences of 3.4×10^{14} ions/cm^2 and 9.1×10^{14} ions/cm^2. The 340-nm diameter spheres were implanted with 350 keV Er^+ ions at fluences from 0.9×10^{15}, 2.5×10^{15}, and 4.0×10^{15} ions/cm^2. The 350 keV implantation puts the Er ions at a depth of 160 nm with a standard deviation in the Gaussian depth profile of σ = 45 nm. The peak concentrations are 0.2 and 0.5 at.% for the films and 175 nm colloids, and 0.2, 0.5, and 0.8 at.% for the 340 nm colloids. After implantation the samples were annealed in a vacuum furnace (pressure < 5×10^{-7} mbar) at 100 ^{o}C for 1 hour and at 900 ^{o}C for another hour. Some of the samples with 175 nm spheres were coated with a ~ 1 μm thick polymethylmethacrylate (PMMA) layer at a spin-rate of 2000 rpm for 30 s.

Photoluminescence (PL) decay measurements were performed after excitation using the 488 nm line of an Ar ion laser. The pump beam was modulated at 13 Hz using an acousto-optic modulator. The PL signal was focused onto the entrance slit of a 48-cm grating monochromator and detected with a liquid-nitrogen cooled Ge detector employing standard lock-in techniques. The spectral resolution of the system was 6 nm. PL decay traces of the luminescence were recorded at the peak of the Er luminescence at 1.53 μm and averaged using a digitising oscilloscope. The overall time response of the system was measured to be 30 μs. Transparent liquids of different refractive index (water: n = 1.33, a mixture of ethylene-glycol and water: n = 1.45, a microscope immersion oil: n = 1.51, and iso-eugenol: n = 1.57) were brought into contact with the sample surface, while the luminescence signal was collected from the (unpolished) back-side of the Si substrate. The pump laser beam was directed along the surface normal. Since silicon is transparent in the wavelength region above 1.1 μm, the Er luminescence around 1.54 μm can be collected through the wafer without difficulties.

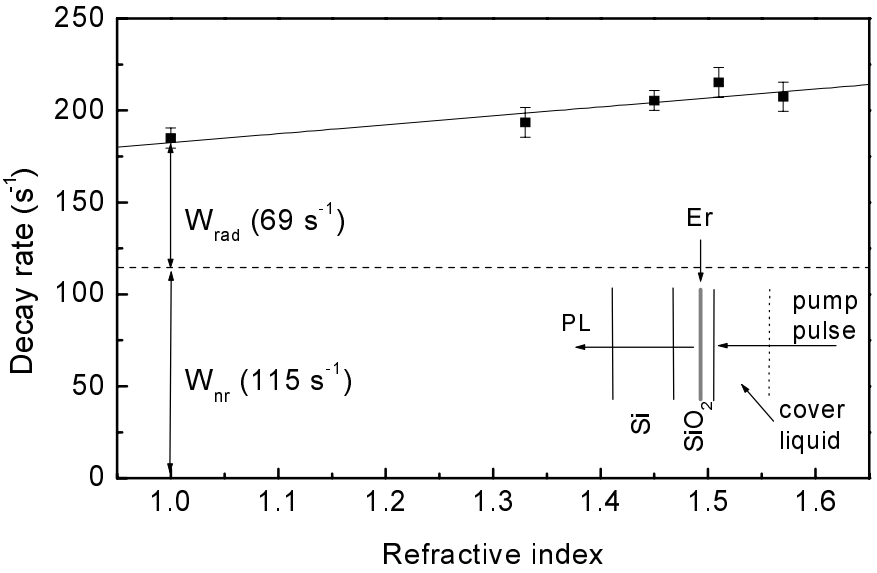

Figure 8.1 Measured decay rate at 1.54 μm of Er ions in a 100 nm thick SiO_2 layer (0.2 at.% Er) as function of the refractive index of a covering transparent liquid. The Er ions were excited through the liquid using the 488 nm line of an Ar ion laser. The inset shows a schematic picture of the experimental setup.

8.3 Results and discussion

Local density of states in a planar SiO_2 film

To study the DOS in colloidal particles, first the radiative decay rate of Er in planar SiO_2 films was determined. Luminescence decay rates of Er at $\lambda = 1.536$ μm were measured for Er-implanted SiO_2 layers brought into contact with a range of transparent liquids. Figure 8.1 shows the measured decay rate for a layer implanted to a peak concentration of 0.2 at.% Er, as function of the refractive index of the liquid. The decay rate was measured for the sample in air and in contact with liquids with refractive indices n of 1.33, 1.45 (index matching case), 1.51 and 1.57. An increase in decay rate from 184 s^{-1} to 205 s^{-1} is observed as the refractive index of the liquid is increased. A similar increase of the decay rate was observed for the sample with a peak concentration of 0.5 at.% (not shown).

As we have shown before,[10,11] the increase in decay rate with refractive index can be understood by considering the local DOS for the SiO_2 film in contact with the different liquids. According to Fermi's Golden rule the radiative decay rate can be written in terms of a local DOS ρ as:[10,18]

$$W_{rad}(\mathbf{r}) = \frac{\pi\omega}{\hbar\varepsilon(\mathbf{r})}|D|^2 \rho(\omega,\mathbf{r}) \qquad (8.1)$$

where $\varepsilon(\mathbf{r})$ is the position-dependent dielectric constant, ω is the transition frequency and $|D|^2$ is the dipole matrix element of the transition involved. This matrix element is determined by the interaction of the Er ion with its neighbouring atoms and is therefore not influenced by the optical properties of the interface. Thus the macroscopic ρ and $\varepsilon(\mathbf{r})$ are the only parameters in Eq. 8.1 that are varied in our experiments.

The local DOS ρ can be calculated as a function of position $\mathbf{r}$, via quantisation of the electromagnetic field. For a dielectric slab this calculation is done using a complete set of plane waves and the known Fresnel coefficients for the layer. Since the polarization of the emitted radiation is random, an integration over all angles and both polarizations is done. For an absolute determination of the radiative rate the local field should be used in the calculation. This local field seen by the atom is due to the microscopic environment of the atom and differs from the macroscopic field. We have assumed that we do not influence this microscopic environment with the liquid films in our experiment, since the Er ions are relatively far away from the interface.[24]

Figure 8.2 shows a calculation of the local DOS $f_{1.45}$ (normalised to the local DOS in a bulk material with n = 1.45) for a 100 nm thick SiO_2 slab (n = 1.45) on a Si substrate (n = 3.45). The calculation was done for a wavelength of 1.54 μm, corresponding to the peak of the Er^{3+} emission. The factor $\varepsilon(\mathbf{r})$ is included in the definition of $f_{1.45}$ making the DOS directly proportional to the radiative decay rate. The position z = 0 corresponds to the position of the Si/SiO_2 interface. The dashed line shows the calculated DOS for a sample in air (n =1.00) and the solid line shows the DOS for the same film in contact with a medium with the same index of refraction as the film (n = 1.45). The oscillations in the local DOS on both sides of the interface are caused by interference between incoming and reflected waves and have a periodicity of $\sim\lambda/(2n)$. Such oscillations are invisible in the SiO_2 film because the film thickness is much smaller than the emission wavelength. For the sample in air, the local DOS in the film is greatly increased relative to that in bulk SiO_2 ($f_{1.45}$ = 1) due to the presence of the Si substrate. A clear increase in the local DOS is observed over the entire film thickness if the air is replaced by a medium of higher refractive index. According to Eq. 8.1 this explains the increase in the decay rate with refractive index as observed in Fig. 8.1.

The change in decay rate with refractive index can be calculated quantitatively by considering the calculated DOS, the measured Er profile, and the distribution of the 488 nm pump light over the film. We found that the observed increase in decay rate with index is much smaller than that found in the

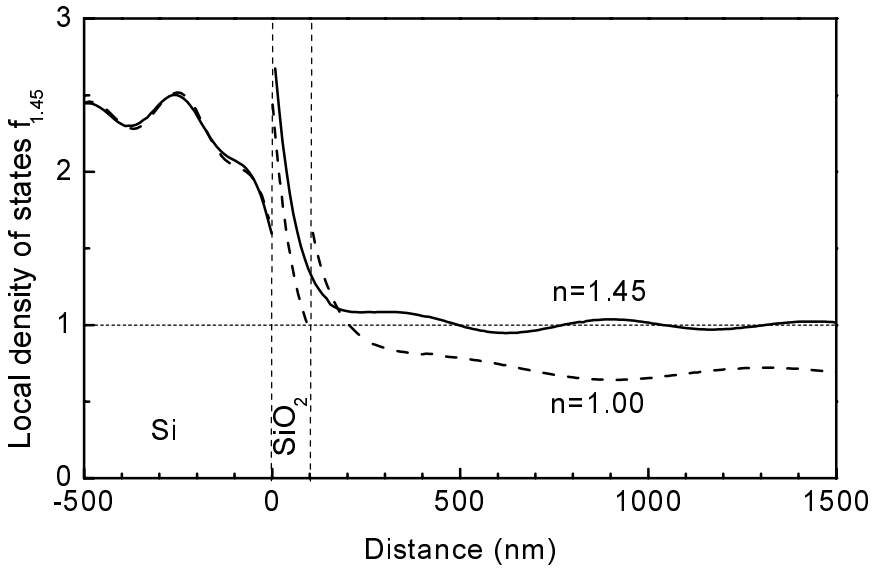

Figure 8.2 Polarization- and angle-averaged optical local DOS, for a 100 nm thick SiO_2 layer (n = 1.45). The layer is sandwiched between a Si substrate (n = 3.45) and an ambient with n = 1.00 (dashed line) or n = 1.45 (solid line). All calculations were done for a wavelength of 1.54 μm.

calculation that assumes the full decay to be due to radiative processes. Therefore non-radiative processes that are independent of the optical properties of the interface must be included. The total decay rate is a sum of the radiative and non-radiative decay rates:

$$W = W_{rad} + W_{non-rad} \tag{8.2}$$

Using Eq. 8.1 the total decay rate can be rewritten in terms of the local DOS $f_{1.45}$:

$$W(n,z) = f_{1.45}(n,z)W_{rad}^{1.45} + W_{non-rad} \tag{8.3}$$

where $W_{rad}^{1.45}$ is the radiative decay rate of Er ions in bulk SiO_2. The solid line in Fig. 8.1 is a fit of Eq. 8.3 to the measured data, resulting in $W_{rad}^{1.45} = 54\pm10\ s^{-1}$ and $W_{non\text{-}rad} = 115\pm10\ s^{-1}$. The contribution due to the non-radiative process is indicated by the dashed line. Note that the radiative rate of 69 s^{-1} indicated in the figure is higher than the radiative rate of 54 s^{-1} in bulk SiO_2. As mentioned before, this is due to the Er ions being close to the high-refractive index Si substrate.

The radiative decay rate of 54 s^{-1} for Er^{3+} ions in bulk SiO_2 is in agreement with measured lifetimes (W = 59 s^{-1}) for 10 μm thick SiO_2 layers grown by wet thermal oxidation of Si, implanted with 3.5 MeV Er ions.[25] In that

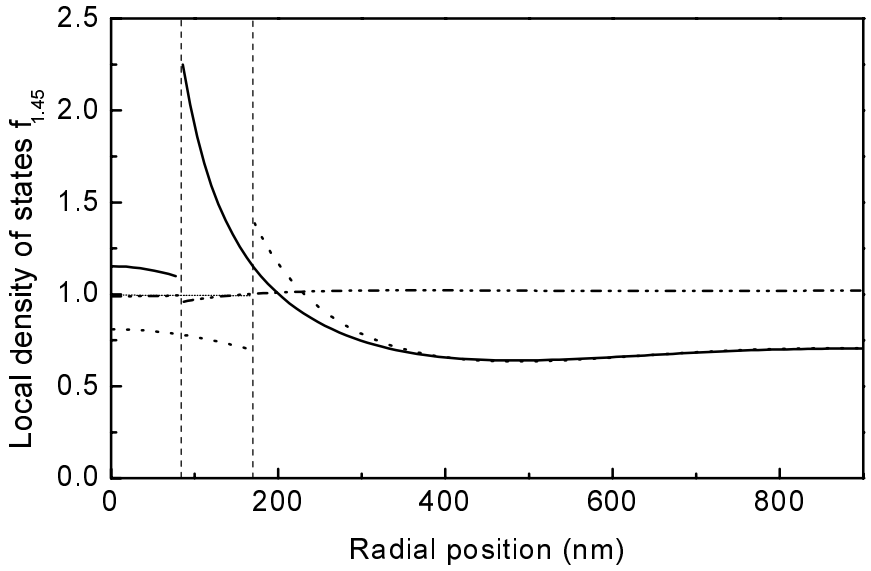

Figure 8.3 Polarization- and angle-averaged local DOS as function of radial position for a SiO_2 sphere (n = 1.45) in air, calculated at a vacuum wavelength of 1.54 μm. Data are shown for spheres with a diameter of 175 nm (solid line), and 340 nm (dashed line). Also shown is a calculation for 175 nm diameter spheres surrounded by PMMA (n = 1.49, dash-dotted line).

case the distance between the interfaces and the Er ions is so large that, within a few percent, the local DOS is equal to that of bulk SiO_2.

Local density of states in silica colloids

Now that the radiative decay rate of Er in bulk SiO_2 is determined, the radiative decay rate for Er-implanted SiO_2 spheres can be estimated. First, a calculation of the local DOS is done for a colloid sphere at a vacuum wavelength of 1.536 μm, as a function of radial distance. The result is shown in Fig. 8.3 for spheres with diameters of 175 nm, and 340 nm. The local DOS was obtained using the known Green's functions for a dielectric sphere and was normalised to the DOS in a bulk medium with n = 1.45. As can be seen the value of the local DOS inside the colloid differs strongly between spheres of different size. Depending on the size, the DOS is smaller or larger than the DOS for bulk SiO_2. Also, for a given size, very little variation in the local DOS is observed inside a sphere. This can be explained by the fact that for both colloid sizes the emission wavelength of 1.536 μm is larger than the wavelength of the first Mie resonance ($2\pi r = \lambda_0/n$). Assuming that the Er ions are distributed homogeneously over the SiO_2 sphere, the effect of the sphere on the radiative rate can be calculated by integrating the local DOS of Fig. 8.3 over the sphere. For a 340 nm diameter sphere the

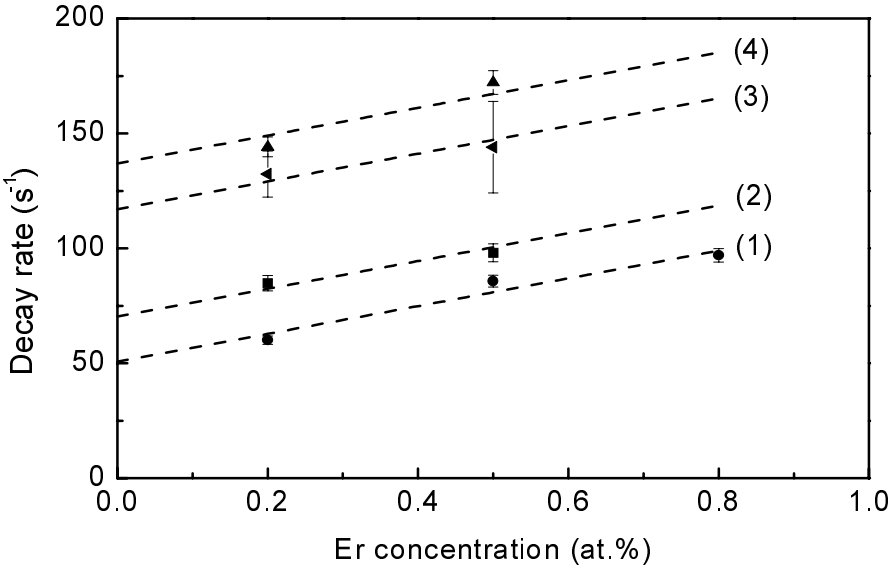

Figure 8.4 Measured decay rates for Er implanted samples as function of Er concentration. Data set (1) is taken on a 3-4 layers of 340 nm spheres on a Si substrate, set (2) on a monolayer of 175 nm spheres on a Si substrate, set (3) on a monolayer of 175 nm spheres coated with ~1 μm PMMA, and set (4) on a 100 nm thick film on Si. The dashed lines are a fit to all data points with a constant slope, but different offsets.

calculation yields $f_{1.45} = 0.74$, while for a 175 nm diameter sphere a value of 1.13 is found.

Figure 8.4 shows the luminescence decay rate for a variety of samples implanted to different Er concentrations. Data are shown for a sample consisting of 3-4 layers of 340 nm spheres (1), a mono-layer of 175 nm spheres (2), a layer of 175 nm spheres embedded in a ~1 μm thick PMMA-layer (3), and a 100 nm thick SiO_2 film (4). The dashed lines are a fit to all four data sets, assuming the same linear increase of the decay with concentration, but a different offset for each type of sample. The increase of the decay rate with concentration is generally known as concentration quenching,[26] and is due to an increased coupling to quenching sites as a result of excitation migration at high Er concentration.

It should be noted that the decay rates of the 100 nm SiO_2 layer (data set 4) in Fig. 8.4 are lower than the values found in Fig. 8.1, although the same samples were used. The experiments with the liquids in Fig. 8.1 were performed at least a month after the measurements presented in Fig. 8.4. The increase in decay rate over time is attributed to the diffusion of water into the SiO_2 network. It is well known that O-H groups quench the Er transition as the second overtone of the O-H stretch vibration is resonant with the Er transition. Indeed, the decay rate could be almost completely recovered to the values in Fig. 8.4 by drying the samples at 475 ^{o}C for 1 h in a vacuum furnace.

Table 8.1 Measured (W_{tot}) and calculated radiative decay rates for Er-doped colloids and SiO_2 films. Results are given for the same samples as in Fig. 8.4. The average local DOS in each material ($f_{1.45}$) is listed. Calculated values are obtained using a radiative rate in bulk SiO_2 of $W_{rad} = 54\ s^{-1}$. The quantum efficiency (QE) is also indicated.

set	sample	$f_{1.45}$ (s^{-1})	W_{tot} (s^{-1})	W_{rad} (s^{-1})	$W_{non\text{-}rad}$ (s^{-1})	QE (%)
1	340 nm spheres	0.74	51	40	11	78
2	175 nm spheres	1.13	69	61	8	87
3	175 nm + PMMA	1.30	117	70	47	60
4	100 nm layer	1.28	137	69	68	50

The offsets in Fig. 8.4 represent the pure Er decay rate in the absence of concentration quenching and are listed in Table 8.1 under W_{tot}. Using the calculated local DOS for spheres of 175 and 340 nm diameter as given in Fig. 8.3, the radiative decay rate is expected to be 40 s^{-1} for the 340 nm spheres and 61 s^{-1} for the 175 nm diameter spheres, given the determined bulk radiative decay rate of 54 s^{-1}. The difference between these rates and the measured offsets gives almost identical non-radiative decay rates (in absence of concentrtion quenching) for the 175 nm and 340 nm diameter spheres of 8 s^{-1} and 11 s^{-1} respectively (see also Table 8.1). This is to be expected, as the spheres consist of the same material, and shows that the data can be consistently described by the DOS model.

A calculation of the local DOS for 175 nm SiO_2 spheres embedded in PMMA (n = 1.49) is also shown in Fig. 8.3. As can be seen, the local DOS inside and outside the sphere is almost identical, showing that the embedded spheres can be treated as a uniform layer. Taking the local DOS for a SiO_2 layer on Si in a medium with refractive index n = 1.45 (see Fig. 8.2), and the average distance of the Er from the Si/SiO_2 interface (110 nm), the radiative rate in this sample can be calculated and is given in Table 8.1 (70 s^{-1}). The difference in the measured offset (117 s^{-1}) and calculated radiative lifetime results in a non-radiative lifetime of 47 s^{-1} for the PMMA-embedded spheres. This is higher than the non-radiative decay rate calculated for the spheres in air. To test if quenching centers in the surrounding medium (such as C-H in PMMA) could affect the decay rate of Er inside the colloids, we measured the decay rate for spheres immersed in hydrogenated dimethylsulfoxide (DMSO) and deuterated DMSO, but did not observe a difference in decay rate. As these liquids contain different concentrations of C-H quenchers, this disapproves the suggestion that PMMA would quench the Er transition inside the colloids. Alternatively, it might be that the spin-coated PMMA layer does not completely fill the airgaps between the spheres, resulting in a non-homogeneous layer, for which the above DOS

calculation does not hold. Note that in the calculations of the local DOS we have neglected the effect of the inhomogeneous Er-distribution over the sphere, and changes in the local field of a small fraction of the Er ions that is located close to the interface.

Finally, Table 8.1 shows the calculated value of W_{rad} = 69 s^{-1} for the Er implanted SiO_2 film, derived from Fig. 8.4 and the DOS calculation in Fig. 8.2. The non-radiative decay rate (68 s^{-1}) that can now be determined for this sample is much higher than that in the 175 and 340 nm diameter spheres. This might be the result of a difference in annealing behaviour between the spheres and the layer, which would result in a higher concentration of quenching centers (e.g. water) in the layer, compared to the spheres.

8.4 Conclusions

The decay rate at 1.5 μm of Er ions implanted into a 100 nm thick SiO_2 film on Si, made using a wet chemical process, was measured with and without liquids with different refractive index in contact with the film. For refractive indices in the range of 1.00-1.57, an increase in decay rate from 184 to 200 s^{-1} was observed. The increase in decay rate with refractive index is explained by a change in the local optical density of states at the position of the Er. By comparing a calculation of the local DOS with the measured decay rates, the radiative (69 s^{-1}) and non-radiative (115 s^{-1}) components were distinguished. Using a calculation of the DOS for a sphere in air and the radiative decay rate determined for a SiO_2 film, the decay rates of Er-implanted SiO_2 spheres with a diameter of 340 nm, and 175 nm were calculated, resulting in a radiative decay rate of 40 s^{-1} for the 340 nm spheres, and 61 s^{-1} for the 175 nm spheres, and a non-radiative decay rate in absence of concentration quenching of ~10 s^{-1}. Embedding the 175 nm diameter spheres in a ~1 μm thick PMMA layer, increased the decay rate to 117 s^{-1}. Good agreement was found between the calculated DOS and the experimentally probed DOS in the colloids. This paper shows that by careful consideration of (changes in) the local DOS in a variety of sample geometries (thin films, colloids) it becomes possible to achieve an accurate quantitative determination of radiative and non-radiative decay processes for Er in glass.

References

1 A. M. Vredenberg, N. E. J. Hunt, E. F. Schubert, D. C. Jacobson, J. M. Poate, and G. J. Zydzik, Phys. Rev. Lett. **71**, 517 (1993)

2 P. Goy, J. M. Raimond, M. Gross, and S. Haroche, Phys. Rev. Lett. **50**, 1903 (1983)

3 R. G. Hulet, E. S. Hilfer, and D. Kleppner, Phys. Rev. Lett. **55**, 2137 (1985)

[4] J. Martorell and N. M. Lawandy, Phys. Rev. Lett. **65**, 1877 (1990)
[5] E. P. Petrov, V. N. Bogomolov, I. I. Kalosha, and S. V. Gaponenko, Phys. Rev. Lett. 81, **77** (1998)
[6] M. Megens, J. E. G. J. Wijnhoven, A. Lagendijk, and W. L. Vos, Phys. Rev. A **59**, 4727 (1999)
[7] G. L. J. A. Rikken, Phys. Rev. A **51**, 4906 (1995)
[8] R. M. Amos, and W. L. Barnes, Phys. Rev. B **55**,7249 (1997)
[9] K. H. Drexhage, J. Lumin. **1,2**, 693 (1970)
[10] E. Snoeks, A. Lagendijk, and A. Polman, Phys. Rev. Lett. **74**, 2459 (1995)
[11] T. M. Hensen, M. J. A. de Dood, and A. Polman, J. Appl. Phys. **88** (Nov, 1, 2000, in press)
[12] R. Sprik and B. A. van Tiggelen and A. Lagendijk, Europhys. Lett. **35**, 265 (1996)
[13] A. Tip, Phys. Rev. A **56**, 5022 (1997)
[14] A. Tip, Phys. Rev. A **57**, 4818 (1998)
[15] R. J. Glauber, and M. Lewenstein, Phys. Rev. A **43**, 467 (1991)
[16] H. Khosravi and R. Loudon, Proc. R. Soc. Lond. A **436**, 373 (1992)
[17] H. Khosravi and R. Loudon, Proc. R. Soc. Lond. A **433**, 337 (1991)
[18] H. P. Urbach, and G. L. J. A. Rikken, Phys. Rev. A **57**, 3913 (1998)
[19] A. Moroz, Europhys. Lett. **46**, 419 (1999)
[20] S. M. Barnett, B. Huttner, and R. Loudon, Phys. Rev. Lett. **68**. 3698 (1992)
[21] S. M. Barnett, B. Huttner, R. Loudon, and R. Matloob, J. Phys. B **29**, 3763 (1996)
[22] G. Juzeliunas, Phys. Rev. A **55**, R4015 (1997)
[23] D. L. J. Vossen, M. J. A. de Dood, T. van Dillen, T. Zijlstra, E. van der Drift, A. Polman, and A. van Blaaderen, Adv. Mat. **12** (October 1, 2000), in press
[24] This assumption can be justified by considering the measured changes in the radiative decay rate of Er^{3+} ions in sodalime silicate glass, incorporated at two different depths, comparable to the depth scales in our experiments. In these experiments, changes in lifetimes were fully described by changes in the DOS, indicating that there was no variation in local field with depth. See Ref. 10.
[25] A. Polman, D. C. Jacobson, D. J. Eaglesham, R. C. Kistler, and J. M. Poate, J. Appl. Phys. **70**, 3778 (1994)
[26] H. C. Chow, and R. C. Powell, Phys. Rev. B **21**, 3785 (1980)

9 Infrared electroluminescence from lissamine-sensitised Nd-doped polymer LEDs

We report 890 nm electroluminescence from a neodymium-doped polymer light-emitting diode. The active layer was a blend of fluorene benzothiadiazole (F8BT) and a lissamine-functionalised terphenyl-based neodymium complex. It was embedded between a Ca-Al electrode, and a hole injection layer composed of poly(3,4-ethylene dioxythiophene) doped with poly(styrene sulfonate), that was deposited onto an indium tin oxide transparent anode. Electroluminescence from lissamine at 580 nm was observed as well. It is shown that the lissamine plays a crucial role in mediating the energy transfer from the F8BT host to the neodymium ion. The neodymium/lissamine luminescence intensity ratio is higher under electrical excitation than under optical excitation, which shows that a higher relative population of triplet states on the lissamine is generated under electrical excitation. A high turn-on voltage of ~15 V was measured, indicating that the lissamine-functionalised Nd^{3+} complex acts as a carrier trap.

9.1 Neodymium-doped polymer LEDs

Polymer light-emitting diodes (LEDs) are the focus of much commercial and academic interest owing to the potential for inexpensive fabrication of full-colour displays over large areas, and because a number of unresolved issues exist regarding the basic properties of neutral and charged excitations in these amorphous, carbon-based, molecular semiconductors.[1] Although most investigations have focused on electroluminescent devices emitting in the visible spectrum, there is considerable potential to be exploited for emission in the near-infrared and infrared spectral ranges, in particular in connection with optical telecommunication applications.

For example, planar optical amplifiers operating at wavelengths of 1.3 or 1.5 μm are essential ingredients in photonic integrated circuits, in which they can compensate for splitting and waveguide losses. Trivalent rare-earth ions like neodymium (Nd^{3+}) or erbium (Er^{3+}) are used as the active element in these planar amplifiers, due to their intra-4*f* transition at 1340 nm (Nd^{3+}, $^4F_{3/2} \rightarrow {}^4I_{11/2}$) or 1530 nm ($Er^{3+}$, $^4I_{13/2} \rightarrow {}^4I_{15/2}$). These amplifiers are typically made using inorganic hosts,[2] and are pumped using an external laser source. Recently, we (see Chapter 3) and others have reported the synthesis of rare-earth doped polymer waveguides.[3,4] By combining this work with the knowledge on electrical excitation processes in polymer LEDs, it may become possible to fabricate electrically pumped optical amplifiers based on rare-earth doped polymers.

As a first step towards this goal, we report electroluminescence at 890 nm from a lissamine-functionalised, terphenyl-based neodymium complex (Ls.Nd),[5] doped into poly(dioctylfluorene-alt-benzothiadiazole), F8BT. Although infrared luminescence from organic LEDs with small molecular weight emitters has already been reported,[6] we are particularly interested in the development of conjugated polymer-based active layers, as these tend to suffer less from recrystallisation problems, and are therefore more promising candidates for achieving a better diode durability. The organic Nd^{3+} complex used in this work was designed to shield the Nd^{3+} ion from its environment (see Chapter 3). It also offers the possibility to covalently bind a highly absorbing antenna group such as lissamine to the complex, such that it is positioned close to the Nd^{3+} ion. It was shown in Chapter 3 that after optical excitation of the lissamine sensitiser, energy is transferred very efficiently from the triplet state of the sensitiser to the Nd^{3+} ion by a Dexter mechanism, resulting in typical Nd^{3+} luminescence at 890, 1060, and 1340 nm.[4] Although we have chosen lissamine as the sensitiser, any absorbing group can be used, as long as the triplet state energy of the sensitiser is resonant with one of the Nd^{3+} energy levels.

In the case of electrical excitation, electrons and holes are first injected into the conjugated polymer host, which in our case is F8BT. Due to the overlap

between the emission spectrum of the polymer and the absorption spectrum of the sensitiser, Förster energy transfer from the polymer to the sensitiser can take place, and in this way the Nd^{3+} ion can be excited. Our results show that the luminescence from the polymer host is efficiently quenched by the Ls.Nd complex and that emission takes place both from the sensitiser and the Nd^{3+} ion. Comparison of Nd^{3+} photoluminescence (PL) and electroluminescence (EL) intensities indicates that upon electrical excitation a higher triplet population is reached in the lissamine compared to the case of optical excitation, presumably due to direct triplet transfer from F8BT to the lissamine.

9.2 Device fabrication

Lissamine-functionalised organic neodymium complexes (Ls.Nd) were synthesised using the procedure described in Ref. 5. Ls.Nd doped LEDs were fabricated in the following way. First an indium tin oxide (ITO) coated glass substrate was treated with an oxygen plasma. Then a ~40 nm thick hole injection layer of poly(3,4-ethylene dioxythiophene) (PEDOT), doped with poly(styrene sulfonate) (PSS) was spin-coated. After spin-coating, the film was heated for one hour at 100 ^{o}C under N_2 flow. Both the oxygen plasma treatment and the PEDOT/PSS layer serve to increase the work function of the anode,[7-9] and therefore reduce the energy barrier for injection of holes into the emissive layer. The emissive layer was prepared using a solution of 3.3 mg Ls.Nd and 35.3 mg fluorene benzothiadiazole (F8BT) dissolved in 5 ml of chloroform (chemical structures of the materials are shown in Fig. 9.1). This solution of 10 wt.% Ls.Nd/F8BT blend was spin-coated onto the PEDOT/PSS layer at a spin-rate of 1400 rpm, resulting in a ~80 nm thick film. Finally Ca/Al counter electrodes (area ~2 mm^2) were thermally evaporated at a background pressure of $\sim 5\times10^{-6}$ mbar.

9.3 Experiment

Devices were transported under nitrogen and characterisation was performed at $\sim 10^{-2}$ mbar in order to prevent oxidation of the Ca cathodes. The device current and light output as a function of applied voltage were measured at room temperature. The voltage was supplied by a Keithley 230 voltage source, and the current was measured by a Keithley 195A digital multimeter. A calibrated silicon photodiode was used to measure the luminance. Luminescence spectra were detected using a CCD spectrograph with a spectral resolution better than 5 nm.

Photoluminescence reference measurements were performed on Ls.Nd doped polycarbonate waveguides as described in Chapter 3, using the 458 nm line of an Ar ion laser at a power density of 2 W/cm^2 for excitation. Optical

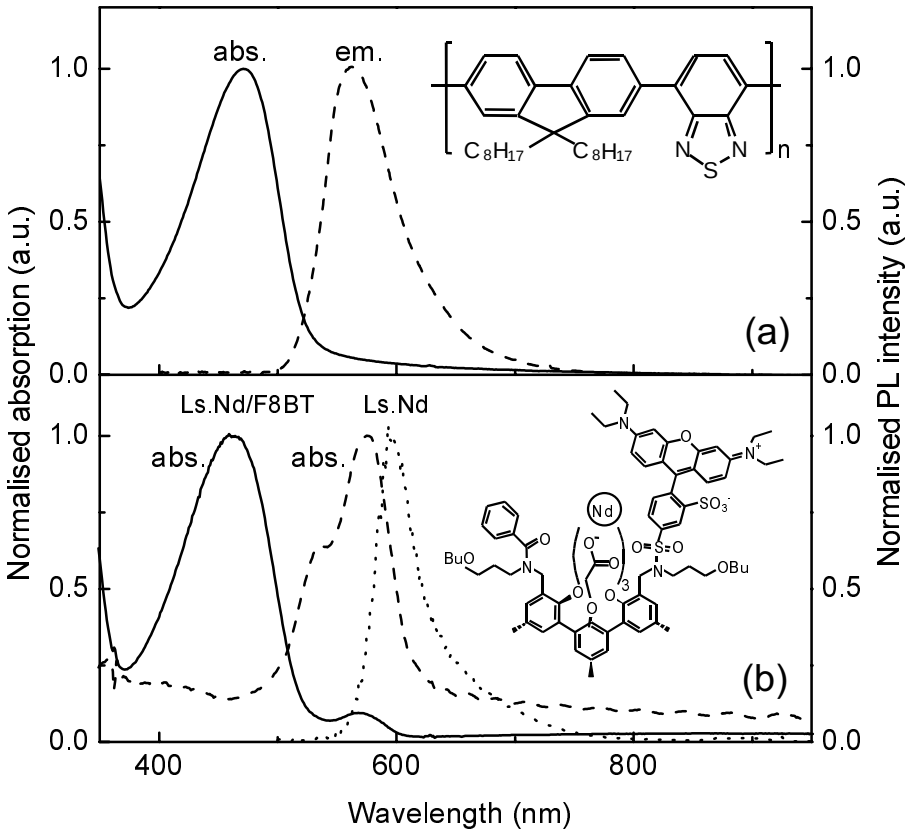

Figure 9.1 Absorption and photoluminescence emission spectra together with the chemical structures of F8BT (a), and of Ls.Nd (b). An absorption spectrum from the Ls.Nd/F8BT blend is also shown.

absorption measurements were performed at normal incidence using a spectrophotometer.

9.4 LED characterization

F8BT was chosen as the host material because it has a very high PL efficiency in the solid state (~0.6) along with good solubility in common organic solvents, and a high electron affinity (~2.9 eV), which facilitates electron injection from common cathodes, such as Ca. A very important additional property is that its emission spectrum overlaps the absorption spectrum of the lissamine sensitiser. Figure 9.1(a) shows the absorption and photoluminescence spectra of undoped F8BT, and Fig. 9.1(b) shows the absorption spectra of Ls.Nd in a polymer film and of the Ls.Nd/F8BT blend. The latter shows contributions from both F8BT and Ls.Nd. As can be seen, there is considerable overlap between the emission

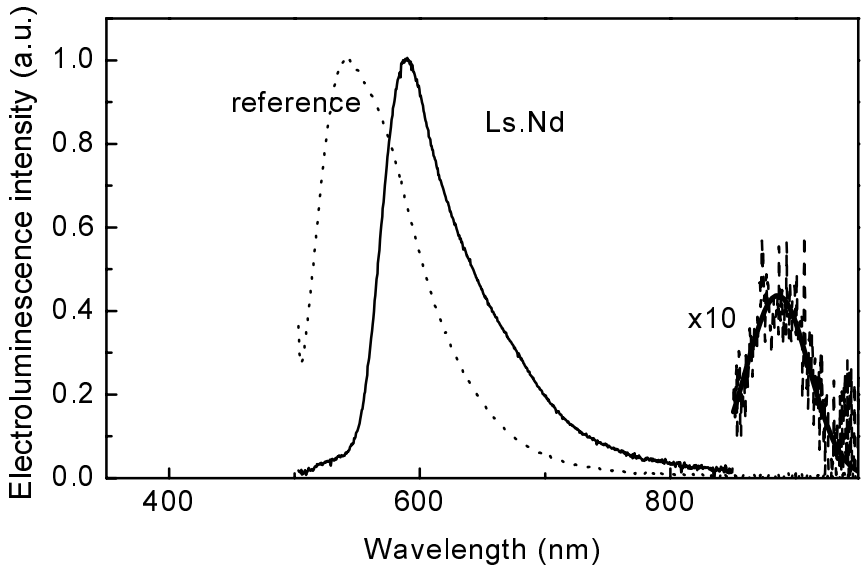

Figure 9.2 Electroluminescence spectrum of an ITO/PEDOT/F8BT:Ls.Nd/Ca/Al structure, biased at 31 V (~100 mA/cm^2) (solid line). The Nd signal around 890 nm has been multiplied by a factor 10. The noise is related to the low detector sensitivity in the near infrared. An EL spectrum from an ITO/PEDOT/F8BT/Ca/Al reference structure without the lissamine sensitiser, biased at 6 V (~1000 mA/cm^2), is also shown (dotted line).

spectrum of F8BT and the absorption spectrum of Ls.Nd, which makes Förster energy transfer from the conjugated polymer to the Ls.Nd complex possible.

Figure 9.2 displays the EL spectrum of the Ls.Nd doped LED (solid line). The luminescence around 600 nm originates from the lissamine sensitiser. Emission around 890 nm from the Nd^{3+} ions is also clearly detected, whereas emission from the F8BT is not. The integrated 890 nm emission intensity of Nd^{3+} amounts to ~3% of the total intensity. Nd^{3+} luminescence at 890, 1060, and 1340 nm results from transitions between the $^4F_{3/2} \rightarrow {}^4I_{9/2}$, $^4I_{11/2}$, and $^4I_{13/2}$ levels, respectively and thus stems from the same luminescence level. All three transitions have been observed previously for the Nd^{3+} complexes in a polycarbonate film. It is assumed that the polymer matrix does not have a large effect on the branching ratios of the transitions within the Nd^{3+} ion, as the ion is shielded from the polymer by the complex. So, if luminescence at 890 nm is observed, also luminescence at 1060, and 1340 nm will be present. We will concentrate on the 890 nm transition as this is more conveniently detected with our equipment. Typical integrated intensity ratios of the Nd^{3+} luminescence are 12:14:3 (890 nm:1060 nm:1340 nm) as measured on Ls.Nd doped polycarbonate waveguides.[4] Using these intensity ratios, and the estimated Nd luminescence quantum efficiency of 1 %, it can be estimated that the majority of the excitation on the sensitiser is transferred to the Nd^{3+} ion.

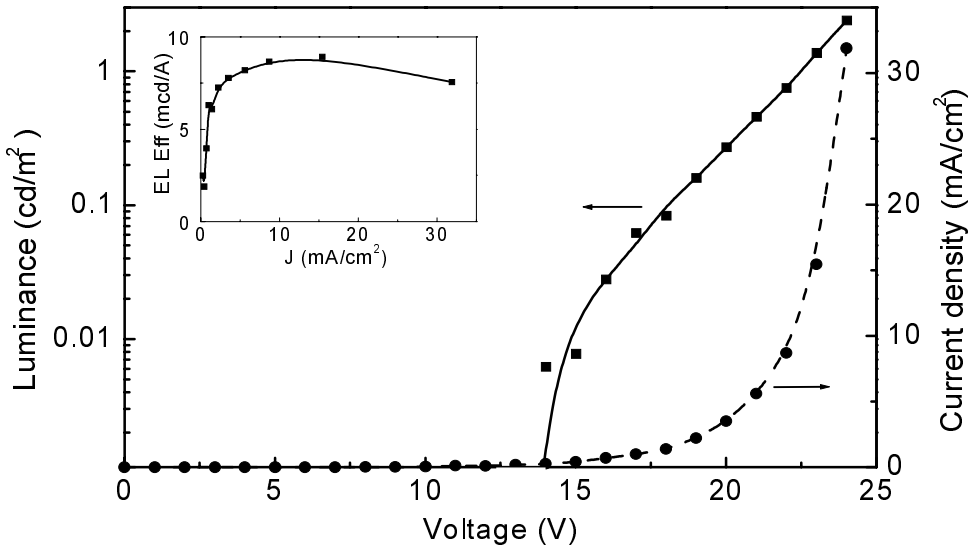

Figure 9.3 Current-voltage (closed circles) and luminance-voltage (squares) characteristics for an ITO/PEDOT/ F8BT:Ls.Nd/Ca/Al LED structure. Active area is ~2 mm^2, thickness of the active layer is ~80 nm. The inset shows the efficiency (luminance/current) as a function of the current density through the device.

We also note that although the presence of the lissamine luminescence is undesired for (near-) infrared applications, it provides a convenient (i.e. in the visible range) probe of exciton formation and recombination, and also a tool for discriminating singlet and triplet transfer from F8BT to the lissamine, as the 600 nm luminescence stems from the singlet state of lissamine, whereas the 890 nm Nd^{3+} luminescence is due to energy transfer from the triplet state of the lissamine.[10,11] The incomplete quenching of the lissamine luminescence is evidence that intersystem crossing (ISC), i.e. singlet-triplet transfer within the lissamine, is competing with the radiative decay from the singlet state of lissamine (η_{isc}~60%).[5] This shows that there is considerable scope for improvement. We are currently developing materials and devices aimed at achieving complete quenching of the sensitiser luminescence via optimised ISC and different bonding configurations between the sensitiser and the complex in order to reduce the distance between the sensitiser and the rare-earth emitter to improve the energy transfer. Interestingly, while the electroluminescence in 'pure' polymer LEDs is limited, as it originates only from the fraction that is excited into the singlet state, in the present Nd-doped structure the excitation of both the singlet and triplet states can be used. This is due to the fact that the Nd is excited via the triplet state of the lissamine, which is excited via triplet-triplet transfer from the polymer, or via intersystem crossing from the singlet state of the lissamine.

When measured relative to the lissamine emission, the Nd^{3+} PL emission around 890 nm is about 4 times higher than in PL experiments on Nd-doped polycarbonate waveguides (see dashed line in Fig. 9.1(b)). In PL experiments the optical excitation generates excitons in the singlet state. Only the fraction that transfers to the triplet manifold of the lissamine (via ISC) contributes to the Nd^{3+} luminescence. On the contrary, for electroluminescence we expect a larger proportion of triplet states to be formed on the F8BT and possibly on the lissamine, owing to the fact that charge injection is not spin-polarised. The measured ratio between the Nd- and lissamine-emission in EL and PL suggests that the relative triplet population on the lissamine is at least 4 times higher in EL than in PL.

Figure 9.2 also shows an electroluminescence spectrum of a reference device doped with a Nd complex without the lissamine sensitizer similar to that described in Chapter 3 (dotted line). This device shows clear luminescence from the F8BT, while no Nd^{3+}-related luminescence is observed. This implies that the lissamine sensitiser plays a crucial role in mediating the energy transfer from the F8BT host to the Nd^{3+} ion, either as an intermediate between the F8BT and lissamine, where both singlet-singlet and triplet-triplet transfer can occur, or as an antenna that captures excitons directly. More research must be done to resolve this issue.

Figure 9.3 displays the current and luminance vs. voltage characteristics for the Ls.Nd doped LED. The turn-on voltage for visible emission V_{on} (at 0.01 cd/m^2) is ~15 V, which is relatively high compared to that of pure F8BT structures (2.5 V or less).[12] This has to be related to the low efficiency which is ~ 8 mcd/A as can be seen in the inset of Fig. 9.3. This results from the substantial quenching of the lissamine luminescence via ISC to the triplet states, which is both desired and expected. However, even though the low PL efficiency of the lissamine (which is measured to be 3-7% depending on deposition conditions) might be expected to increase the threshold, we notice that the voltage dependence of the luminance is very steep close to the turn-on. We consider that this is an indication that the Ls.Nd complex acts as a trap and reduces electron and/or hole mobilities with respect to those of pure F8BT. A similar increase of turn-on voltage has been observed for sensitised visible-emitting lanthanide complexes with a sensitiser doped into conjugated polymers.[13] We finally note that the present devices showed significant degradation during operation, resulting in an operating lifetime of a few minutes.

9.5 Conclusions

We have shown electroluminescence at 580 nm and 890 nm from an F8BT layer doped with a lissamine-functionalised Nd^{3+} complex. The lissamine sensitiser plays a key role in mediating the energy transfer from the polymer to the Nd^{3+}

ion. From a comparison of the Nd/lissamine emission intensity ratios under electrical excitation and optical excitation, we conclude that electrical excitation leads to an enhanced generation of triplet states on the lissamine. The turn-on voltage of these Ls.Nd doped devices is much higher than for non-doped polymer LEDs, indicating that the Ls.Nd complex acts as a trap, reducing electron and/or hole mobilities. Further work will focus on developing materials with optimised intersystem crossing and energy transfer efficiency, and applications in electrically pumped polymer waveguide optical amplifiers operating in the near-infrared.

References

1 F. Cacialli, Current Opinion in Colloid & Interface Science **4**, 159 (1999)

2 see for a review: P. G. Kik, and A. Polman, MRS Bull. **23**, 48 (1998)

3 S. Lin, J. Feuerstein, and A. R. Mickelson, J. Appl. Phys. **79**, 2868 (1996)

4 L. H. Slooff, A. Polman, S. I. Klink, G. A. Hebbink, L. Grave, F. C. J. M. van Veggel, D. N. Reinhoudt, and J. W. Hofstraat, Opt. Mat. **14**, 101 (2000)

5 S. I. Klink, Ph.D. Thesis, University of Twente, Enschede, The Netherlands (2000), ISBN 90-3651436-3

6 R. J. Curry, and W. P. Gillin, Appl. Phys. Lett. **75**, 1380 (1999)

7 J. S. Kim, M. Grandström, R. H. Friend, N. Johansson, W. R. Salaneck, R. Daik, W. J. Feast, and F. Cacialli, J. Appl. Phys. **84**, 6859 (1998)

8 T. M. Brown, J. S. Kim, R. H. Friend, F. Cacialli, R. Daik, and W. J. Feast, Appl. Phys. Lett. **75**, 1679 (1999)

9 J. S. Kim, P. K. H. Ho, D. S. Thomas, R. H. Friend, F. Cacialli, G. W. Bao, and S. F. Y. Li, Chem. Phys. Lett. **315**, 307 (1999)

10 G. A. Crosby, R. E. Whan, and R. J. M. Alire, J. Chem. Phys. **34**, 743 (1961)

11 A. V. Hayes, and H. G. Drickamer, J. Chem. Phys. **76**, 114 (1982)

12 J. Morgada, and F. Cacialli, unpublished

13 M. D. McGehee, T. Bergstedt, C. Zhang, A. P. Saab, M. B. O'Regan, G. C. Bazan, V. I. Srdanov, and A. J. Heeger, Adv. Mater. **11**, 1349 (1999)

10 Optically and electrically pumped rare-earth doped polymer waveguide amplifiers: Outlook

In this final Chapter, we will discuss some issues that play a role in the fabrication of polymer-based optical waveguide amplifiers. First the use of rare-earth doped organic complexes is reviewed. Next, Er-doped silica colloids are discussed, that can overcome some of the intrinsic problems encountered for the rare-earth doped complexes. Possible solutions for some of the unsolved issues in the preparation of the Er-doped colloids are presented. Finally, the fabrication issues for an electrically pumped polymer-based optical waveguide amplifier are discussed. The standard optical waveguide configuration asks for new polymer materials that are transparent in the infrared and still have a reasonable conductivity.

10.1 Optically pumped rare-earth doped polymer amplifiers

Rare-earth doped organic complexes

As we have seen in Chapter 2 and 3, organic cage complexes can be used to encapsulate the rare-earth ion, thereby making it dissolvable into the polymer. In this way the rare-earth doping problem was solved. However, we also found that the optical transitions in the rare-earth ions are quenched due to coupling with vibrational overtones of C-H and O-H bonds in the complex or polymer.

Summary

Polymer-based optical waveguide amplifiers offer a low-cost alternative for inorganic waveguide amplifiers. Due to the fact that their refractive index is almost similar to that of standard optical fibers, they can be easily coupled with existing fibers at low coupling losses. Doping the polymer with rare-earth ions that can yield optical gain is not straightforward, as the rare-earth salts are poorly soluble in the polymer matrix.

This thesis studies two different approaches to dope a polymer waveguide with rare-earth ions. The first one is based on organic cage-like complexes that encapsulate the rare-earth ion and are designed to provide enough coordination sites to bind the rare-earth ion and to shield it from the surrounding matrix. Chapter 2 describes the optical properties of Er-doped organic polydentate cage complexes. The complexes show clear photoluminescence at 1.54 μm with a bandwidth of 70 nm, the highest reported for an erbium-doped material so far. The luminescence lifetime is very short (~1 μs) due to coupling to vibrational overtones of O-H and C-H bonds. Due to this short luminescence lifetime, high pump powers (~1 W) are needed for optical gain in a waveguide amplifier based on these complexes. The pump power can be reduced if the Er is excited via the aromatic part of the complex, which has a higher absorption cross section. In Chapter 3 a lissamine-functionalised neodymium complex is studied in which the highly absorbing lissamine acts as a sensitiser. The lissamine is first excited into the singlet state from which intersystem crossing to the triplet state can take place. From there it can transfer its energy to the Nd ion by a Dexter transfer mechanism. Room-temperature photoluminescence at 890, 1060, and 1340 nm from Nd is observed, together with luminescence from the lissamine sensitiser at 600 nm. Photodegradation of the lissamine sensitiser is observed, which is studied in more detail in Chapter 4. The observed change in time of the spectral shape of the lissamine luminescence can be explained by assuming that two types of complexes exist. One type in which energy transfer to the Nd^{3+} ion can take place, and one that is not coupled to Nd. The highly absorbing sensitiser makes the standard butt-end coupling of the pump light into a waveguide amplifier impractical. The pump power can be used more efficiently by using a novel coupled waveguide system as described in Chapter 5. This employs gradual evanescent field coupling between parallel pump and signal waveguides.

An alternative approach to make a rare-earth doped polymer waveguide is by combining the excellent properties of SiO_2 as a host for the rare-earth with the easy processing of polymers. The optical properties of Er-doped silica films made by an acid-catalysed sol-gel synthesis are reported in Chapter 6. The Er exhibits long luminescence lifetimes of 10-12 ms, which indicates that OH from the wet chemical synthesis is successfully removed during the vacuum anneal

treatment. Using a base-catalysed sol-gel synthesis, silica colloidal spheres with diameters of 175 and 340 nm were grown. Chapter 7 describes the luminescence properties of the 340 nm spheres, implanted with Er up to concentrations of 1.0 at.%. The Er shows a very long luminescence lifetime of 17 ms, and the radiative lifetime is estimated to be 20-22 ms, indicating a high quantum efficiency. This long luminescence lifetime is partly due to the low local optical density of states (DOS) in the free standing silica colloids. Optical gain calculations are made for the colloid/polymer waveguide that predicts a net gain of 8.7 dB at a pump power of 30 mW, for a 15 cm long waveguide. Such a length can be rolled up on an area of 16 mm^2. In Chapter 8, calculations of the DOS are described for thin films as well as the spherical colloids. By comparing the calculation with experimentally probed decay rates, radiative and non-radiative components in the decay of Er are determined.

Besides optical pumping of planar waveguide amplifiers it would be interesting if electrical pumping could be achieved. As a first step in this direction Chapter 9 reports 890 nm electroluminescence from lissamine-functionalised Nd complexes in a polymer light emitting diode. It is shown that the lissamine sensitiser plays a crucial role in mediating the energy transfer from the conjugated polymer to the Nd^{3+} ion, via singlet-singlet and triplet-triplet energy transfer. Finally, Chapter 10 gives an overview of important device considerations for the fabrication of optically and electrically pumped polymer-based planar optical amplifiers based on the novel materials concepts described in this thesis.

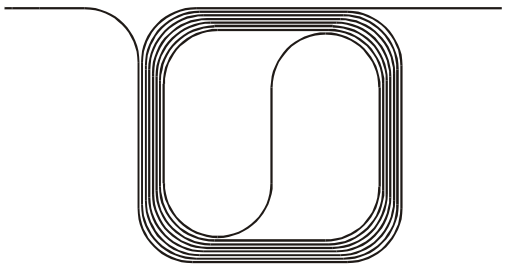

Figure 10.1 Planar 15-cm long optical waveguide amplifier rolled up on an area of ~ 16 mm^2. Due to the high index contrast that can be achieved using polymer technology a small bending radius can be made.

Deuteration of the complex reduces the quenching by a factor 2. Still, the quantum efficiency achieved is less than 1 %. It seems this is an intrinsic problem for the use of organic complexes and polymer hosts.

At the short luminescence lifetimes found, very high pump powers are required to achieve population inversion. This problem was solved by attaching a highly absorbing lissamine sensitiser to the complex. Population inversion can now be achieved at very low pump powers (~1 mW) in the waveguide. However, it should be noted that the gain efficiency is low, since that is determined by the internal quantum efficiency of the rare-earth ion. One problem found with the use of the lissamine sensitiser is that it exhibits photodegradation upon illumination (Chapter 4), which is thought to be the result of a photo-oxidation reaction. This problem might be solved by encapsulation of the devices, and fabrication under N_2 atmosphere to avoid O_2 contamination. Due to the high absorption of the lissamine, traditional butt-end coupling of the waveguide amplifier is not practical. The new coupling scheme using a pump waveguide parallel to the signal waveguide, introduced in Chapter 5, can be used to increase the pumping efficiency in the waveguide. A pump power of ~ 1 W is needed to achieve an optical gain of 3 dB in the waveguide. Given this power, photostability will be a key parameter in the final choice of the used polymer.

Rare-earth doped silica colloids

The problem of C-H quenching can be overcome by using Er-doped silica colloids. These silica colloids can be dissolved in a polymer to form the core layer of a planar polymer waveguide amplifier. This composite material enables high gain, provided the index of the polymer can be matched accurately with that of the colloids. Yoshimura *et al.*[1] have shown that by mixing fluorinated and deuterated PMMA, the refractive index of the mixed polymer can be tuned

around 1.45 with an accuracy < 0.001, and that the resulting material can be used to produce low-loss optical waveguides. This combination is a promising candidate as a polymer host for Er^{3+}-doped silica sphere/polymer nano-composite optical waveguides, and gain predictions (see Chapter 7) show a very low (several mW) pump threshold for optical gain. To reduce the effect of co-operative upconversion interactions between excited Er ions, the Er concentration in the colloid must be kept below ~0.8 at.%. As a result, a rather long waveguide (~15 cm) is required to achieve reasonable gain (8.7 dB at 30 mW). We note that due to the large index contrast between polymer core and cladding a rather small waveguide bending radius can be achieved. Fig. 10.1 shows a waveguide spiral geometry in which a 15 cm long waveguide is rolled up on an area of only 16 mm^2.

Alternative methods for Er incorporation

The Er ion implantation experiments have clearly demonstrated that silica colloids form an ideal host for Er. The next step would be to develop a method by which the Er could be incorporated directly using the wet chemical process used to form the colloids, thus avoiding the implantation step. We have tried several approaches to achieve this. These experiments were performed on silica films, rather than colloids, using a similar chemical process as discussed in Ref. [2].

First, we have grown a 65 nm thick silica film, that was then put in a solution of $Er(NO_3)_3 \cdot 5H_2O$ and afterwards annealed at 950 °C. RBS showed indications for a small amount of Er left at or near the surface, but no photoluminescence from Er at 1.5 μm was observed. Second, we tried the use of a 3-aminopropyltriethoxysilane (APS) coupling agent. A 75 nm thick oxide film was first grown, subsequently a 75 thick layer was grown using the coupling agent, and next the sample was put in a $Er(NO_3)_3 \cdot 5H_2O$ solution. Again, a small Er content was measured on the film surface using RBS but no PL was observed. Mixing the APS with the Er nitrite also did not lead to the desired result. Finally, we investigated the use of N-(trimethoxysilylpropyl)-ethylenediamine, triacetic acid, trisodium salt (EDTA), a method that has previously shown to lead to the incorporation of metal ions in an acid-catalysed sol-gel process.[3] Again, no Er-related PL was observed on these grown films.

As becomes clear from this summary, the task to find a novel process to incorporate Er during the wet chemical reaction remains. Two novel approaches come to mind: 1) a different Er precursor such as e.g. erbium methoxyethoxide or isopropoxide[4] may be used, or 2) an erbium(III)methacrylate/poly-methyl-methacrylate (PMMA) coating could be made around the silica colloids, that could then be covered with the pure oxide, whereupon the Er could be diffused into the colloid by thermal annealing.

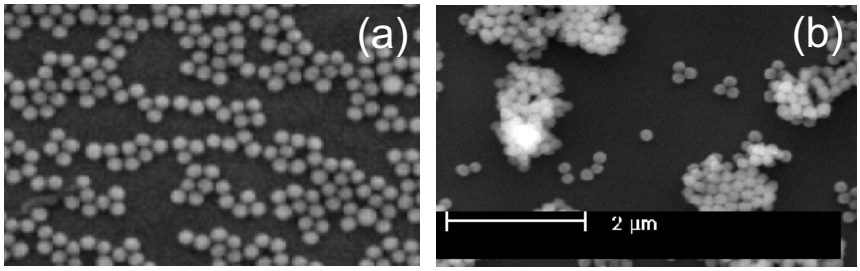

Figure 10.2 SEM Images of silica spheres on a Si substrate. The spheres were first deposited on a Si substrate coated with a carbon film, then one sample was used for reference (a) and one was annealed at 750 °C for 1 hour (b). Finally the spheres were dissolved in ethanol using an ultrasonic bath, and deposited again on a Si substrate.

Thermal annealing of Er colloids

As shown in Chapter 7, thermal annealing is essential to optically activate the Er in the ion-implanted colloids. Even if a successful wet chemical process to incorporate Er were developed, thermal annealing will likely be necessary. One important question is whether annealed colloids can actually be re-dispersed in solution, for later incorporation in the polymer waveguide. Figure 10.2(b) shows a SEM image of a surface covered with colloids that were first deposited on a carbon-coated Si wafer, then annealed in vacuum at 750 °C for one hour, ultrasonically lifted from the substrate, and then re-deposited. A reference sample that did not have the anneal treatment is shown in Fig. 10.2(a). Clearly, larger agglomerates of clusters are observed for the annealed material. At the present colloid size used, the size of these clusters is impractical for application in waveguides. To reduce the size of these clusters, smaller colloids could be used. Alternatively, core-shell particles could be used, that are composed of a shell that does not sinter at 750 °C or that evaporates during annealing thus isolating the colloids so that no sintering can occur.

10.2 Electrically pumped rare-earth doped polymer amplifiers

One of the great advantages of the sensitised rare-earth complexes is the possibility of electrical excitation. In this way it becomes possible to fabricate an electrically pumped polymer waveguide amplifier operating in the infrared. Note that there is no conjugated polymer known that emits at these wavelengths. We have shown (see Chapter 9) that an absorbing sensitiser group attached to a Nd complex, can transfer the excitation from the conjugated polymer to the Nd^{3+} ion. However, luminescence from the sensitiser itself was also observed. The

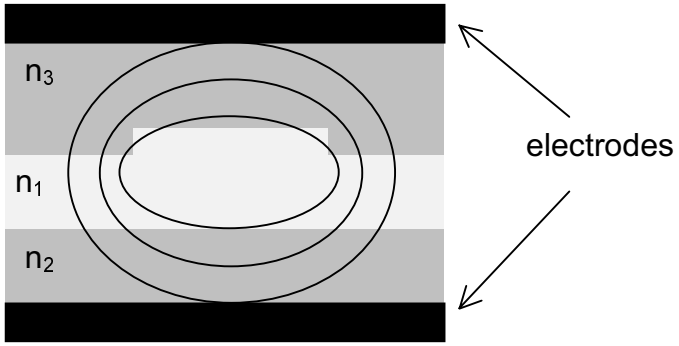

Figure 10.3 Schematic structure of an electrically pumped optical waveguide amplifier. An example of an optical mode profile is also indicated. Refractive indices of the rare-earth doped core (n_1) and electron- and hole- conducting layers (n_2, n_3) are such that $n_1 > n_2, n_3$.

device performance can be increased if a sensitiser can be found with optimised intersystem crossing. The sensitiser and conjugated polymer have to be chosen such that the emission of the polymer overlaps the absorption spectrum of the sensitiser.

It should be noted that the electrodes used in the LEDs in Chapter 9 were not optimised for the infrared emission wavelength. For example, the 130 nm thick indium-tin-oxide electrode (ITO) in that device absorbs 6 % of the light at 890 nm. At a wavelength of 1.5 μm more than 80 % of the light would be absorbed in such a film. Clearly, optimisation of the ITO composition, or the use of alternative materials that transmit better in the infrared but still have reasonable conductivity, such as $CuAlO_2$ and $CuGaO_2$,[5,6] must be considered to improve the infrared emission intensity in these novel sensitised rare-earth doped polymer LEDs. For the anode Al can be used, as it has a high reflection (~90 %) at 1500 nm.

The issue of transparent conducting electrodes becomes even more important when these sensitised rare-earth doped polymers are used in an electrically pumped optical waveguide amplifier, as the interaction length with the electrode in such a device is on the order of centimeters. Figure 10.3 shows a schematic of such a waveguide structure, with an active (rare-earth doped, high refractive index) waveguide core, embedded in an electrically conducting cladding layer with lower refractive index. An example of an optical mode profile is also indicated. In this geometry it would be desirable to use thick waveguide cladding layers to minimise the interaction between the optical mode and the electrodes. At the same time such cladding layers must be efficient electron and hole conductors, i.e. have high carrier mobilities. A hole conducting layer that may suit this requirement is N,N'-diphenyl-N,N'-bis(3-methylphenyl)-1,1'-biphenyl-4,4'-diamine (TPD) which has a hole drift mobility of $10^{-3}cm^2/Vs$.[7] It is more difficult to find a good electron conducting polymer,

although some promising results have been reported for 1,2,3-oxadiazole derivative (PBD)[8,9] and poly(phenyl quinoxaline) (PPQ).[10] However, all these materials have been used in very thin layers of ~100 nm. For a typical cladding layer thickness of 1 μm the operating voltage of an electrically pumped waveguide amplifier will be higher than that for the LED. Therefore more detailed studies of the optical properties of electron- and hole conducting layers are required to further optimise the polymer waveguide amplifier device design.

References

1 R. Yishimura, M. Hikita, S. Tomaru, and S. Imamura, J. Lightw. Techn. **16**, 1030 (1998)

2 D. L. J. Vossen, M. J. A. de Dood, T. van Dillen, L. H. Slooff, C. M. van Kats, T. Zijlstra, E. van der Drift, A. Polman, and A. van Blaaderen, Adv. Mat. **12**, (October 1, 2000), in press

3 P. Tien, and L.-K. Chau, Chem. Mater. **11**, 2141 (1999)

4 G. Milova, S. I. Najafi, A. Skirtach, D. Simkin, and M. P. Andrews, Proc. Soc. Photo-Optical Instrumentation **2997**, 90 (1997)

5 . E. Stauber, J. D. Perkins, P. A. Parilla, and D. S. Ginley, Electrochem. Solid-State Lett. **2**, 654 (1999)

6 H. Kawazoe, H. Yanagi, K. Ueda, and H. Hosono, MRS Bull. **25**, 28 (2000)

7 J. Kido, H. Hayase, K. Hongawa, and K. Nagai, Appl. Phys. Lett. **65**, 2124 (1994)

8 C. Adachi, K. Nagai, and S. Saito, Appl. Phys. Lett. **55**, 1489 (1989)

9 C. Adachi, K. Nagai, and S. Saito, Appl. Phys. Lett. **57**, 531 (1990)

10 D. O'Brien, M. S. Weaver, D. G. Lidzey, and D. C. Bradley, Appl. Phys. Lett. **69**, 881 (1996)

Samenvatting

Planaire optische versterkers gemaakt op basis van polymeertechnologie bieden een goedkoop alternatief voor anorganische versterkers. Doordat the brekingsindex van polymeren ongeveer gelijk is aan die van standaard optische glasvezelkabels, kunnen deze versterkers met lage koppelverliezen worden gekoppeld met bestaande glasvezelkabels. Het doteren van het polymeer met zeldzaam-aard ionen is niet eenvoudig, omdat de zeldzaam-aard zouten slecht oplosbaar zijn in het polymeer.

Dit proefschrift beschrijft twee verschillende manieren om een polymeer te doteren met zeldzaam-aard ionen. De eerste is gebaseerd op organische kooivormige complexen die het zeldzaam-aard ion omgeven. Ze zijn ontworpen om genoeg coördinatieplaatsen te leveren om het zeldzaam-aard ion te binden en het af te schermen van de omgeving. Hoofdstuk 2 beschrijft de optische eigenschappen van een erbium-gedoteerd kooivormig complex. De complexes laten duidelijke fotoluminescentie zien rond 1.54 μm met een bandbreedte van 70 nm. Dit is tot nu toe de hoogste gerapporteerde bandbreedte voor Er-gedoteerde materialen. De luminescentie-levensduur is kort (< 1 μs). Dit komt doordat de Er overgang koppelt met vibrationele boventonen van O-H en C-H bindingen. Als gevolg van deze korte levensduur zijn hoge pomp vermogens nodig (~1 W) om versterking te krijgen in een optische versterker gemaakt op basis van deze complexen. Het pompvermogen kan worden gereduceerd als het Er wordt geëxciteerd via de aromatische ringen in het complex. Deze hebben een hogere werkzame doorsnede voor absorptie dan het Er zelf. In Hoofdstuk 3 wordt een lissamine-gefunctionaliseerd neodymium complex bestudeerd waarin het lissamine werkt als een antenne. Het lissamine wordt eerst geëxciteerd in het singlet niveau waar vandaan het via een interne overgang naar de triplet toestand kan gaan. Van daar uit kan het door middel van Dexter overdracht zijn energie overdragen aan het Nd ion. Fotoluminescentie van Nd bij 890, 1060 en 1340 nm is bij kamertemperatuur gemeten, alsmede de luminescentie van het lissamine rond 600 nm. Het lissamine vertoont fotodegradatie, die in meer detail wordt beschreven in hoofdstuk 4. De gemeten verandering van het luminescentie spectrum in de tijd kan worden verklaard met de aanwezigheid van twee typen complexen. Eén type dat energie overdracht geeft naar het Nd^{3+} ion en één dat niet met het Nd gekoppeld is. De sterke absorptie van de lissamine antenne maakt de standaard methode van inkoppelen van het pomplicht in de lichtgeleider minder praktisch. Het pompvermogen kan efficiënter worden gebruikt door middel van een nieuw systeem van gekoppelde lichtgeleiders dat wordt beschreven in Hoofdstuk 5. Dit systeem maakt gebruik van de koppeling tussen de evanescente velden van twee parallelle pomp en signaallichtgeleiders.

Een alternatieve aanpak om een zeldzaam-aard gedoteerde polymere lichtgeleider te maken, is de uitstekende eigenschappen van SiO_2 als gastmateriaal voor Er te combineren met de makkelijke verwerkbaarheid van polymeren. Als eerste aanzet worden in hoofdstuk 6 de optische eigenschappen beschreven van Er-gedoteerde SiO_2 lagen die zijn gemaakt door middel van een zuur-gekataliseerde sol-gel synthese. Het erbium heeft een lange luminescentie levensduur van 10-12 ms, wat aantoont dat OH uit de chemische synthese succesvol is verwijderd tijdens het uitstoken van het materiaal in vacuum. Silica ballen met een diameter van 175 en 340 nm werden gegroeid in een base-gecataliseerde sol-gel synthese. Hoofdstuk 7 beschrijft de luminescentie eigenschappen van de 340 nm ballen geïmplanteerd met Er tot een concentratie van 1.0 at.%. Het erbium heeft een zeer lange luminscentie-levensduur van 17 ms en de geschatte stralende levensduur is 20-22 ms. Dit wijst op een hoge quantum efficiciëntie. De lange luminescentie levensduren worden gedeeltelijk veroorzaakt door de lage lokale optische toestandsdichtheid in de vrij-liggende silica ballen. Berekingen van de optische versterking van een colloïd/polymeer versterker voorspellen een netto versterking van 8.7 dB voor een pomp vermogen van 30 mW in een 15 cm lange lichtgeleider. Een lichtgeleider van deze lengte kan worden opgerold op een oppervlak van 16 mm^2. In Hoofdstuk 8 wordt de lokale optische toestandsdichtheid beschreven voor dunne SiO_2 lagen en colloïden. Door de resultaten van de berekening te vergelijken met gemeten vervalsnelheden kunnen de stralende- en de niet-stralende vervalcomponenten van het Er worden bepaald.

Naast de mogelijkheid van optisch pompen is het ook interessant om te onderzoeken of het mogelijk is de lichtversterker elektrisch te pompen. In Hoofdstuk 9 wordt de 890 nm electroluminescentie beschreven van lissamine-gefunctionaliseerde Nd complexen in een polymere licht-emitterende diode. De metingen laten zien dat de lissamine antenne een cruciale rol speelt in de energieoverdracht van het geconjugeerde polymeer naar het Nd^{3+} ion door middel van singlet-singlet en triplet-triplet energieoverdracht. Tot slot geeft Hoofdstuk 10 een overzicht van de aandachtspunten die van belang zijn bij de fabricage van planaire polymere optische versterkers, gebaseerd op de nieuwe materialen zoals die in dit proefschrift worden beschreven.

Dankwoord

Aan alles komt een eind en zo ook aan dit proefschrift. Wat nu nog rest is een ode aan alle personen die hebben bijgedragen aan de totstandkoming van dit boekje.

Allereerst natuurlijk aan mijn promotor Albert Polman, die de afgelopen jaren altijd voor me klaar stond en met name de afgelopen maanden ontzettend veel heeft moeten lezen. Albert, dit zijn echt de laatste bladzijden. Ik wil je van harte bedanken voor de leerzame tijd die ik op het Amolf heb mogen doorbrengen.

De opto-electronic materials groep met Gerlas van den Hoven, Jan van der Elsken, Edwin Snoeks, Mark Brongersma, Pieter Kik, Michiel de Dood, Christof Stohhöfer, Teun van Dillen, Mariëlle Ladevèze, Nicolas Hamelin, José dos Santos, Stefania Acco, Freek Suyver, Daniel Peters, Michael Hensen, en Basjan Berkhout was voor mij de thuisbasis gedurende mijn onderzoek. Buiten de vele nuttige discussies hadden we ook altijd een hoop lol. Speciale herinneringen heb ik aan de 'Varenna-gangers' Pieter, Michiel, Christof en Mark. Een flesje wijn, een gitaar en het kattenstrandje, ik zal het nooit vergeten. Onmisbaar waren ook de groepstechnici Johan Derks en Jan ter Beek die ons 'machinepark' in topconditie hielden. Goed gereedschap is het halve werk, ook in het onderzoek! Daarnaast wil ik Alfons van Blaaderen en Adriaan Tip van harte bedanken voor hun bijdrage. Ook de ondersteunende afdelingen wil ik hierbij bedanken.

Gedurende de afgelopen twee jaar heb ik deel uitgemaakt van de instituutsraadcommissie. Een hele leerzame periode, waarvoor ik de IRC-leden van harte wil bedanken. En dan natuurlijk de leden van de Impuls-redactie. De gezellige vergaderingen zorgden altijd voor welkome afwisseling. Bedankt!

Verder was daar de zes-wekelijkse werkbespreking bij de Universiteit Twente, Akzo Nobel, en later Philips, die altijd zeer de moeite waard was. De chemische inbreng van Hans Hofstraat, Frank van Veggel, Manon Oude Wolbers, Steve Klink, Lennard Grave en Gerald Hebbink werkte altijd inspirerend. Daarnaast wil ik Benno Hams bedanken voor het maken van de waveguides en Frank Geurts en Martijn Werts voor hun hulp bij een aantal metingen.

Special thanks are due to Richard Friend and Franco Cacialli from Cambridge University. Their enthusiastic reaction to our idea resulted in quick results and a beautiful Chapter in my thesis.

Tot slot wil ik mijn familie bedanken en speciaal mijn ouders. Zij hebben me door dik en dun gesteund en waren altijd geïnteresseerd, ook al begrepen ze lang niet altijd waar ik het over had. En natuurlijk Léon. Met je nuchtere kijk op zaken wist je me altijd weer de juiste richting te wijzen. Iets waar ik toch zo af en toe behoefte aan had.

Curriculum Vitae

Lenneke Hendrika Slooff werd op 18 augustus 1972 in Uithoorn geboren. In 1990 behaalde zij haar VWO diploma aan de openbare scholengemeenschap “het Snellius”, in Amstelveen. In september van dat jaar begon ze aan de studie Lucht- en Ruimtevaarttechniek aan de Technische Universiteit Delft. In april 1991 begon zij de opleiding tot luchtverkeersleider op Schiphol, die ze in 1992 afbrak om natuurkunde te gaan studeren in Utrecht. Haar afstudeeronderzoek verrichtte ze in de groep van Prof. Dr. A. Polman aan het FOM-Instituut voor Atoom- en Molecuulfysica in Amsterdam. In augustus 1996 behaalde ze het doctoraalexamen experimentele natuurkunde. Het afstudeeronderzoek op het gebied van organische optisch materialen zette ze voort als promovendus. De resultaten van dat onderzoek worden in dit proefschrift beschreven. Op 1 januari 2001 treedt ze in dienst van het Energieonderzoek Centrum Nederland (ECN) in Petten, alwaar ze onderzoek gaat doen aan materialen voor polymere zonnecellen.

List of publications

This thesis is based on the following publications:

Optical properties of erbium-doped organic polydentate cage complexes
L. H. Slooff, A. Polman, M. P. Oude Wolbers, F. C. J. M. van Veggel, D. N. Reinhoudt, and J. W. Hofstraat
J. Appl. Phys. **83**, 497 (1998)

Optical properties of lissamine functionalized Nd^{3+} complexes in polymer waveguides and solution
L. H. Slooff, A. Polman, S. I. Klink, G. A. Klink, G. A. Hebbink, L. Grave, F. C. J. M. van Veggel, D. N. Reinhoudt, and J. W. Hofstraat
Opt. Mat. **14**, 101 (2000)

Concentration effects in the photo-degradation of lissamine-functionalized Nd complexes in polymer waveguides
L. H. Slooff, A. Polman, S. I. Klink, G. A. Hebbink, F. C. J. M. van Veggel, D. N. Reinhoudt, and J. W. Hofstraat
Submitted to J. Opt. Soc. Am. B

Pumping planar waveguide amplifiers using a coupled waveguide system
L. H. Slooff, P. G. Kik, A. Tip, and A. Polman
Submitted to J. Lightwave Techn.

Effects of heat treatment and concentration on the luminescence properties of erbium-doped silica sol-gel films
L. H. Slooff, M. J. A. de Dood, A. van Blaaderen, and A. Polman
Submitted to J. Non-Cryst. Sol.

Erbium-implanted silica colloids with 80% luminescence quantum efficiency
L. H. Slooff, M. J. A. de Dood, A. van Blaaderen and A. Polman
Appl. Phys. Lett. **76**, 3682 (2000)

Local optical density of states in SiO_2 colloidal spheres
L. H. Slooff, M. J. A. de Dood, A. Polman, A. Moroz, A. Tip, and A. van Blaaderen
To be submitted

Near-infrared electroluminesce of polymer light emitting diodes doped with a lissamine-sensitized Nd^{3+} complex
L. H. Slooff, A. Polman, F. Cacialli, R. H. Friend, G. A. Hebbink, and F. C. J. M. van Veggel
Submitted to Appl. Phys. Lett.

Related publications:

Sensitized near-infrared luminescence from polendentate triphenylene-functionalized Nd^{3+}, Yb^{3+}, and Er^{3+} complexes
S. I. Klink, G. A. Hebbink, L. Grave, F. C. J. M. van Veggel, and
D. N. Reinhoudt, L. H. Slooff, A. Polman, and J. W. Hofstraat
J. Appl. Phys. **86**, 1181 (1999)

1, 2 and 3 dimensional photonic materials made using ion beams: Fabrication and optical density of states
M. J. A. de Dood, L. H. Slooff, T. M. Hensen, D. L. J. Vossen, E. van der Drift, A. van Blaaderen and A. Polman
Submitted to proceedings of NATO ASI on Photonic crystals and light localization (2000)